2011

Cofactors in Coronavirus Entry

Ana Shulla
Loyola University Chicago

LOYOLA UNIVERSITY CHICAGO

COFACTORS IN CORONAVIRUS ENTRY

A DISSERTATION SUBMITTED TO

THE FACULTY OF THE GRADUATE SCHOOL

IN CANDIDACY FOR THE DEGREE OF

DOCTOR OF PHILOSOPHY

PROGRAM IN MICROBIOLOGY AND IMMUNOLOGY

BY

ANA SHULLA

CHICAGO, IL

AUGUST 2011

ACKNOWLEDGEMENTS

I would like to thank my mentor, Dr. Tom Gallagher, for training me to become an independent scientist. His dedication to science has been a true inspiration to me. I would also like to thank present and past members of the Gallagher lab, especially Taylor Heald-Sargent, Heidi Olivares and Snawar Hussein Ph.D., for their support and contributions to my dissertation project.

I would also like to thank everyone in the Department of Microbiology and Immunology, especially Dr. Katherine Knight, for her dedication and contribution to mentoring graduate students. I feel fortunate to have been part of such an enriching environment.

Finally, I would like to thank all my family members, especially my husband, my parents and my sister, for their unconditional love and support.

To Genti

TABLE OF CONTENTS

LIST OF TABLES

LIST OF FIGURES

LIST OF ABBREVIATIONS

^{o}C	degrees Celcius (centigrade)
α	anti
h	hour
μL	microliter
μM	micromolar
Ab	antibody
APN	aminopeptidase N
CoV	coronavirus
CPM	scintillation counts per minute
CRM	cysteine rich motif
CTB-HRP	cholera toxin subunit B peroxidase conjugate
CYTO	cytoplasmic
DMEM	Dulbecco's Modified Eagle Medium
DOC	deoxycholate
DRM	detergent resistant membrane
E	coronavirus small E protein
EM	electron microscopy
ENDO	endodomain

ER	endoplasmic reticulum
ERGIC	endoplasmic reticulum Golgi intermediate compartment
FCS	fetal calf serum
FL	firefly luciferase
fMHV	feline mouse hepatitis virus
FP	fusion peptide
GP	glycoprotein
GPI	glycosylphosphatidylinositol
HA	hemagglutinin
hACE2	human angiotensin converting enzyme 2
HB	helix bundle
HR	heptad repeat
HIV-1	human immunodeficiency virus type 1
HSV-1	herpes simplex virus 1
IB	immunoblot
IBV	infectious bronchitis virus
IP	immunoprecipitation
kb	kilobase
kDa	kilodalton
L	liter
M	coronavirus membrane protein
mAb	monoclonal antibody

MHV	mouse hepatitis virus
N	coronavirus nucleocapsid protein
NP-40	nonidet P-40
ORF	open reading frame
PAGE	polyacrylamide gel electrophoresis
PFU	plaque forming unit
rA59	recombinant mouse hepatitis virus strain A59
RBD	receptor binding domain
RL	renilla luciferase
S	spike
SARS	severe acute respiratory syndrome
SDS	sodium dodecyl sulfate
siRNA	short interfering ribonucleic acid
TM	transmembrane
TMPRSS2	transmembrane protease serine subfamily member 2
TTSP	type II transmembrane serine protease
TX	triton X
VSV	vesicular stomatitis virus
w/v	weight/volume
wt	wild type

ABSTRACT

Viruses are obligate intracellular parasites that use the machineries inside living cells to replicate and disseminate. Although relatively simple in structure and composition, viruses have evolved complex ways to penetrate barriers and cause disease. These barriers include the virus shells themselves and the host cell membrane. Enveloped viruses accomplish this task by viral glycoprotein-mediated binding to host cells and fusion of virus and host cell membranes. For the coronaviruses, viral spike (S) proteins execute these cell entry functions. After binding cellular receptors, S proteins undergo a series of conformational changes that drive virus and cellular membrane coalescence. Despite extensive research, there is still limited knowledge on the intermediates of the fusion reaction and the factors controlling their refolding kinetics. Further understanding of these processes can reveal new ways to inhibit protein refolding and ultimately virus entry.

One potential determinant of refolding rate is in the S fusion protein endodomain. The S proteins are set apart from other viral and cellular membrane fusion proteins by their extensively palmitoylated membrane-associated tails. Palmitate adducts are generally required for protein-mediated fusions but their precise roles in the process are unclear. To obtain additional insights into the S-mediated membrane fusion process, we focused on these carboxy-terminal intravirion tails. Substituting alanines for the cysteines that are subject to palmitoylation had effects on both S incorporation into virions and S-

mediated membrane fusions. In specifically dissecting the effects of endodomain mutations on the fusion process, we used antiviral heptad repeat peptides that bind only to folding intermediates in the S-mediated fusion process, and found that mutants lacking three palmitoylated cysteines remained in transitional folding states nearly ten times longer than native S proteins. This slower refolding was also reflected in the paucity of post-fusion six-helix bundle configurations amongst the mutant S proteins. Viruses with fewer palmitoylated S protein cysteines entered cells slowly and had reduced specific infectivities. These findings indicate that lipid adducts anchoring S proteins into virus membranes are necessary for the rapid, productive S protein refolding events that culminate in membrane fusions. These studies reveal a previously unappreciated role for covalently-attached lipids on the endodomains of viral proteins eliciting membrane fusion reactions.

The membrane fusion process also requires an S protein conformational flexibility that is facilitated by proteolytic cleavages. Most coronavirus S proteins are cleaved in their ectodomains, between their S1 and S2 domains, by a furin-like protease in virus-producing cells. Other coronavirus S proteins, such as those of severe acute respiratory syndrome (SARS) coronavirus, lack furin recognition motifs and virions exit cells bearing uncleaved spikes. The SARS S proteins rely on host cell proteases in virus-target cells for fusion activation. We hypothesized that the most relevant cellular proteases in this process are those closely linked to host cell receptors. The primary receptor for the human SARS coronavirus is angiotensin-converting enzyme 2 (ACE2). ACE2 immunoprecipitation captured transmembrane protease / serine subfamily member 2

(TMPRSS2), a known human airway and alveolar protease. ACE2 and TMPRSS2 colocalized on cell surfaces and enhanced the cell entry of both SARS S – pseudotyped HIV and authentic SARS-CoV. Enhanced entry correlated with TMPRSS2-mediated proteolysis of both S and ACE2. These findings indicate that a cell-surface complex comprising a primary receptor and a separate endoprotease operate as portals for activation of SARS coronavirus cell entry.

Many viruses enter cells through specialized lipid microdomains or "lipid rafts". Virus receptors, coreceptors and other cellular factors important for virus entry often concentrate within lipid rafts, thereby setting the stage for high affinity interactions during entry. The receptor for SARS coronavirus, ACE2, has been shown to localize in lipid rafts. Furthermore, it is known that the integrity of lipid rafts is important for efficient SARS-CoV entry into cells. We wanted to determine whether the entry-activating protease, TMPRSS2, also localized into membrane rafts together with ACE2 and whether the lipid raft localization was important to augment virus entry. We isolated detergent resistant membranes (DRMs), the *in vitro* equivalents of lipid rafts, and determined that ACE2 completely partitioned into lipid raft fractions, while only a portion of TMPRSS2 did so. However, when cells were incubated with HIV particles displaying SARS-CoV S on the surface, almost all TMPRSS2 partitioned into lipid rafts, indicating that multivalent virus binding relocalizes cell entry cofactors into lipid rafts on the target cell membrane.

Collectively, my results indicate that multiple factors, including spike lipidation, proteolysis and lipid rafts, operate to facilitate coronavirus entry into cells. These results

obtained using coronaviruses as models likely apply generally to influenza, paramyxo- and other pathogenic viruses and may serve as the basis for a general appreciation of viral surface protein refolding during entry. These results also lay the groundwork for future evaluation of viral entry determinants.

CHAPTER I

INTRODUCTION

Some of the most devastating diseases in human history, such as smallpox, yellow fever, poliomyelitis, influenza and AIDS, are caused by viruses. Viral diseases, ranging from the common cold to immunodeficiency and cancer, continue to be a burden in our society. An estimated 15-20% of human cancers (Butel, 2000; Talbot and Crawford, 2004) as well as many other chronic disorders are initiated by viral infections (Gern, 2010; Grau, Urbanek, and Palm, 2010; Rao, 1991). In addition to pathogenesis in humans, viruses cause serious disease in plants and livestock, thus greatly impacting the agricultural and veterinary industry (Fraile and Garcia-Arenal, 2010; Hanssen, Lapidot, and Thomma, 2010).

The need to prevent viral diseases, and find cures for ongoing viral infections, has fueled decades of scientific research studying viruses and their interactions with host organisms. These studies have helped us understand mechanisms of virus-induced disease in molecular detail. The knowledge gained has been applied to the development of vaccines and antiviral agents that have saved millions of lives. The vaccine against smallpox has led to eradication of the disease worldwide (Parrino and Graham, 2006; Wehrle, 1980). Other vaccination programs have led to prevention of diseases such as poliomyelitis, measles, mumps, rubella fever, adenovirus and influenza respiratory syndromes, hepatitis B, chicken pox, and cervical cancer (Bart, Orenstein, and

Hinman, 1986; Jacobson and Dienstag, 1985; Romanowski et al., 2009). Antiviral therapies for several viral diseases are in place, such as acyclovir therapy for serious herpes virus infections (Elion, 1993), as well as highly active antiretroviral therapy (HAART) for treatment of HIV-1 induced AIDS (Mitsuya and Broder, 1987).

Studies of the interactions between viruses and their hosts have not only led to the development of vaccines and antiviral treatments, but also provided numerous insights into cell and structural biology, immunology and biochemistry. For example, cellular RNA splicing mechanisms were elucidated by studying adenoviruses (Berget, Moore, and Sharp, 1977; Chow et al., 1977) and translational controls were demonstrated through the study of picornaviruses (Pelletier and Sonenberg, 1988). Crystallization of tobacco mosaic virus in 1935 (Stanley, 1935) and more importantly the 2.9 Å atomic resolution of tomato bushy stunt virus crystal structure in 1978 (Harrison et al., 1978) were huge leaps for structural biology. In the field of immunology, several discoveries were made by studying virus-host cell interactions. Such were the discoveries of interferon in 1957 (Isaacs and Lindenmann, 1957) and major histocompatibility (MHC) locus restriction in 1974 (Zinkernagel and Doherty, 1974). In the field of cellular biochemistry, the landmark discovery that single-stranded RNA can be transcribed into double-stranded DNA by the enzyme reverse transcriptase came through studying RNA-containing retroviruses (Baltimore, 1970; Temin and Mizutani, 1970).

Studies of virus-host interactions will certainly continue to open new paths in understanding disease mechanisms as well as basic cellular biology. The complex set of interactions between a virus and a host organism starts off with the virus breaching

physical cellular barriers and gaining entry into cells. This virus-cell entry process is the primary topic of my dissertation research and is the focus of this introduction.

Virus Entry into Animal Cells

Viruses are obligate intracellular parasites that use the machineries inside living cells to replicate and disseminate. Even though relatively simple in structure and composition, viruses have evolved complex ways to penetrate hosts, move through the bloodstream and disperse in the body via motile cells (Smith and Helenius, 2004). Many viruses can breach physical barriers in the body, including the tight endothelial cell lining such as the blood-brain barrier that restricts access to the central nervous system (Salinas, Schiavo, and Kremer, 2010).

One of the most important barriers the virus has to cross is the target cell membrane, and this is achieved in various ways depending on the virus type. In this respect, there are two virus types, enveloped and nonenveloped. Nonenveloped viruses have distinct cell entry programs that involve membrane lysis or pore formation in the target cell membrane to deliver their genomes into cells (Dimitrov, 2004). Enveloped viruses, which will be the focus of my dissertation work, have their capsids surrounded by a lipid bilayer. As such, they can fuse their membrane envelope with the host cell membrane, thereby releasing their capsids into the cell interior.

A subset of enveloped viruses can fuse their outer envelope directly with the plasma membrane of target cells, a process mediated by the viral surface proteins. While providing a quick access to the host cytoplasm (Anderson and Hope, 2005), this route of entry may not be as efficient as the one involving the cellular endocytic network, because

delivered viral capsids have to travel considerable distances through the cortical cytoskeleton and the highly structured cytoplasm to reach sites of replication (Marsh and Bron, 1997). Furthermore, direct fusion with the plasma membrane leaves residual viral glycoproteins on the cell surface, which may "mark" the infected cell and contribute to its detection by the immune system (Smith and Helenius, 2004).

The more commonly observed entry route for most viruses, both nonenveloped and enveloped, is internalization via the different cellular endocytic mechanisms, which allow viruses to get close to the site of replication while still protected in a membrane vesicle. There are several endocytic routes by which viruses can be internalized, such as clathrin-mediated endocytosis, caveolar endocytosis, and clathrin-and caveolae-independent endocytosis. Most viruses are internalized via the well-studied clathrin-mediated endocytosis (Marsh and Helenius, 1989; Mercer, Schelhaas, and Helenius, 2010; Smith and Helenius, 2004). This endocytic process is driven by the formation of a clathrin coat on the cytoplasmic leaflet of the plasma membrane (Mercer, Schelhaas, and Helenius, 2010). Following invagination and pinching of the clathrin-coated pits, the clathrin-coated vesicles fuse with early endosomes and the clathrin coat is lost (Maxfield and McGraw, 2004). The lumen of early endosomes is slightly acidic (pH 6.5-pH 6.0) as a result of proton pumps that transport protons into the endosome lumen (Casey, Grinstein, and Orlowski, 2010). The pH changes in the maturing endocytic vesicle prime the virus for membrane fusion (Skehel and Wiley, 2000), while the resident acid-dependent proteases assist in partial uncoating (Ebert et al., 2002). Recent studies suggest that even herpes simplex virus 1 (HSV-1) and HIV-1, which can penetrate into

cells directly from the plasma membrane, nonetheless are typically endocytosed before they fuse with cell membranes and deliver their internal capsids to the cytosol (Mercer, Schelhaas, and Helenius, 2010; Miyauchi et al., 2009; Nicola, McEvoy, and Straus, 2003).

One possible downside of endocytic entry is that viruses failing to deliver their capsids in a relatively short time frame would be transported to lysosomal degradative compartments, a dead end for lumenal contents. To escape endocytic vesicles and reach the site of replication, viruses have different mechanisms in place. In the next section, I will explain in detail how enveloped viruses escape endosomes via a membrane fusion event mediated by virus surface proteins.

Virus Membrane Fusion

Enveloped viruses have their genomic material surrounded by a lipid bilayer membrane that is derived during budding from host cells. Besides having structural and protective roles, the envelope provides the virus with the ability to fuse with cellular membranes. The fusion process is mediated by transmembrane glycoproteins anchored on the virus membrane. These viral proteins drive the coalescence of virus and cell membranes by undergoing a series of refolding events that release the energy needed to overcome barriers to membrane fusion.

Based on their structural features, the virus fusion proteins can be divided into three classes, I, II and III (Harrison, 2008; White et al., 2008) (Table 1). The most common class I viral fusion proteins, which are central to my dissertation work, include the influenza virus hemagglutinin (HA) (Bullough et al., 1994; Wilson, Skehel, and

Wiley, 1981), HIV-1 gp41 (Chan et al., 1997; Weissenhorn et al., 1997), Ebola virus GP2 (Malashkevich et al., 1999), human respiratory syncytial virus (HRSV) F1 (Zhao et al., 2000), and the coronavirus (CoV) spike (S) protein (Bosch et al., 2003).

	Class I	Class II	Class III
Examples	Influenza virus HA Human immunodeficiency virus-1 (HIV-1) gp41 Ebola virus GP2 Human respiratory syncytial virus (HRSV) F1 Coronavirus S	Tick-born encephalitis virus (TBEV) E Semliki forest virus (SFV) E1	Vesicular stomatitis virus (VSV) G Herpes simplex virus-1 (HSV-1) gB Baculovirus gp64
Type of integral membrane protein	Type I	Type I	Type I
Major secondary structure	α-helix	β-sheet	α-helix and β-sheet
Oligomeric structure of pre-fusion protein	Trimer	Dimer	Trimer
Requirement for proteolytic processing	Yes (of viral fusion protein)	Yes (of companion protein)	No
Oligomeric structure of fusion active form	Trimer	Trimer	Trimer
Structure of the post-fusion form	Trimer of hairpins	Trimer of hairpins	Trimer of hairpins

Table 1. Properties of Class I, II, and III Fusion Proteins. (Modified from (White et al., 2008))

Class I fusion proteins are synthesized within the endoplasmic reticulum of infected cells as single-chain precursors, which then assemble into trimeric complexes. They are primed for fusion through a proteolytic cleavage event which gives rise to an N-terminal receptor binding subunit and a C-terminal membrane anchored subunit. The two subunits are held together via hydrophobic interactions, disulfide linkages and / or salt bridges. Upon receptor engagement (White et al., 2008) or encounter with the acidic and proteolytic endosomal environment (Chandran et al., 2005; Mothes et al., 2000; Simmons et al., 2004), the subunits dissociate and structural refolding of the C-terminal subunit

ensues. This latter subunit contains the fusion machinery composed of a fusion peptide (FP) and two alpha-helical heptad repeat (HR) regions, HR1 and HR2, with HR2-being the helices closest to the virion membranes (Fig. 1).

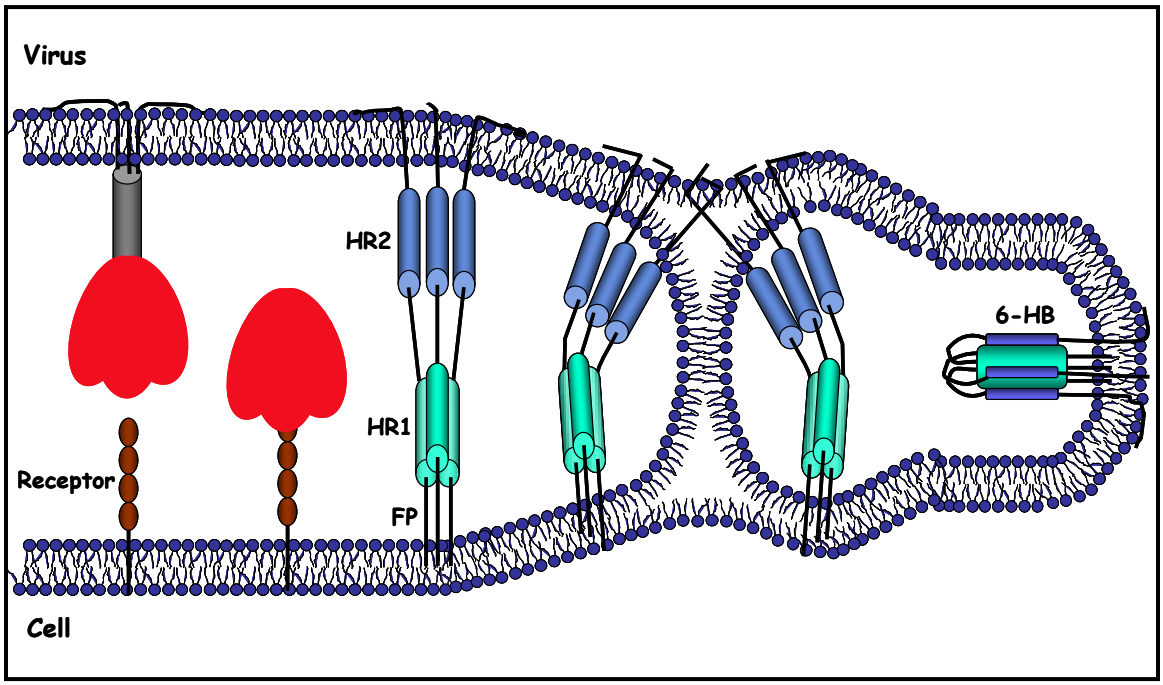

Fig. 1. Class I Protein-Mediated Membrane Fusion Model. A hypothetical depiction of the native pre-fusion viral protein (left) is depicted binding to cellular receptor. The viral protein is composed of two subunits generated by proteolysis of the single chain precursor. The N-terminal subunit dissociation and the C-terminal subunit unfolding generates prehairpin structures (middle) depicted with cell membrane-intercalated fusion peptides (FP) and exposed heptad repeat regions (HR1 and 2). Pre-hairpin closure through a lipid stalk intermediate generates a highly stable, rod-like 6-helix bundle (6-HB), in which HR2 helices are positioned antiparallel to an interior HR1 trimer, and in which the viral transmembrane spans surround the FPs in an antiparallel trimeric arrangement within the fused membrane.

The fusion peptide is generally an apolar stretch of 15-25 amino acids, rich in glycine and alanine residues, and containing several bulky hydrophobic residues (Tamm and Han, 2000). Several studies have shown that the fusion peptide becomes associated with the target membrane during the fusion process. The fusion peptide sequences are well-conserved among members of a virus family; however, it is not always clear which stretch of hydrophobic residues serves as a fusion peptide in each virus case (Martin and Ruysschaert, 2000). Many enveloped virus surface glycoproteins have more than one stretch of residues that are consistent with a fusion peptide motif; however, not all of these residues are involved in interacting with target membrane during the fusion reaction. The fusion peptide gains the conformational flexibility required for inserting into target membranes through a proteolytic cleavage at its N-terminus (Klenk and Garten, 1994). In the case of influenza HA, proteolysis permits a normally buried hydrophobic fusion peptide to propel away from the virion membrane and into the apposed target cell membrane during low pH-induced HA conformational change (Bentz and Mittal, 2000).

Daggering of the fusion peptides into cellular membranes is followed by a refolding process that, in analogy to a closing hairpin, brings fusion peptides and associated cellular membranes toward the virion membranes, driving formation of a lipid stalk connecting the opposing outer membrane leaflets (Chernomordik and Kozlov, 2008) and culminating in complete cell-virion membrane coalescence (Melikyan et al., 2000; Skehel and Wiley, 2000) (see Fig. 1). This allows for virus particle-cell content mixing and delivery of viral genetic material into the cell.

For class I fusion proteins, the arms of the pre-hairpin intermediates are the HR1 tri-helical bundles and HR2 helices. The HR1 and HR2 domains consist of seven residue repeats (where the positions are labeled "abcdefg") and are characterized by the occurrence of hydrophobic residues in the "a" and "d" positions comprising the interface of two interlocking helices. These domains have high propensity to form α-helices that interact as coiled-coils (Burkhard, Stetefeld, and Strelkov, 2001). The presence of coiled-coils is widespread in fusion proteins, including the SNARE proteins which operate in cellular vesicular fusion (Rothman and Warren, 1994; Skehel and Wiley, 1998; Sollner and Rothman, 1996).

Due to the high affinity of HR2 helices for HR1, the pre-hairpin intermediate collapses and the HR2 helices fold back onto the central trimeric coiled-coil of HR1 helices to form a highly stable rod-like structure otherwise known as a 6-helix bundle (6-HB) (Colman and Lawrence, 2003; Skehel and Wiley, 2000) (Fig. 1). In the 6-HB, there are no contacts between the HR2 monomers. Instead, each HR2 instead associates with the HR1 grooves through hydrophobic interactions. The formation of the 6-HB post-fusion structure arrives temporally concomitant with coalescence of the viral and cellular membranes (Melikyan et al., 2000; Russell, Jardetzky, and Lamb, 2001). 6-HB complexes are resolved crystallographically for many virus fusion proteins, and extensive biochemical data indicate that the complexes are extremely stable, resistant to chemical denaturation, proteolytic digestion and high temperatures. The stability of the post-fusion conformations is much higher than that of the pre-fusion states, and the energy released

from the refolding into 6-HBs is what drives membrane coalescence. A schematic illustration of this process is provided in Fig. 1.

Class II fusion proteins include the tick-borne encephalitis (TBE) E protein and the Semliki forest virus (SFV) E1 protein (Kielian and Rey, 2006; Lescar et al., 2001). They differ from class I fusion proteins in several aspects as outlined in Table 1. While class I fusion proteins are trimeric both in pre-fusion and post-fusion conformations, class II fusion proteins start as dimers and rearrange into a more stable trimeric post-fusion conformation (Kielian and Rey, 2006) (Fig. 2). Class II fusion proteins are not themselves cleaved for fusion activation, instead a tightly associated viral protein, acting as a chaperone, is cleaved to release the fusion protein from its metastable state, thus activating the membrane fusion process. For example, in the case of alphaviruses, cleavage and release of partner protein E2 protein provides the activation trigger for the fusogenic E1 protein (Harrison, 2008).

The recently classified class III virus glycoproteins (Backovic and Jardetzky, 2009) include the herpesvirus gB protein (Heldwein et al., 2006), the vesicular stomatitis virus glycoprotein (VSV G) (Roche et al., 2006; Roche et al., 2007) and the baculovirus gp64 protein (Kadlec et al., 2008). Class III fusion proteins seem to combine features of both class I and class II proteins. They contain two fusion loops that are rich in hydrophobic amino acids and thought to insert into the target membrane in the same manner that the class II viral fusion loops do (Heldwein et al., 2006). In contrast to class I and class II fusion proteins, there is no proteolytic cleavage involved in activation of class III fusion proteins.

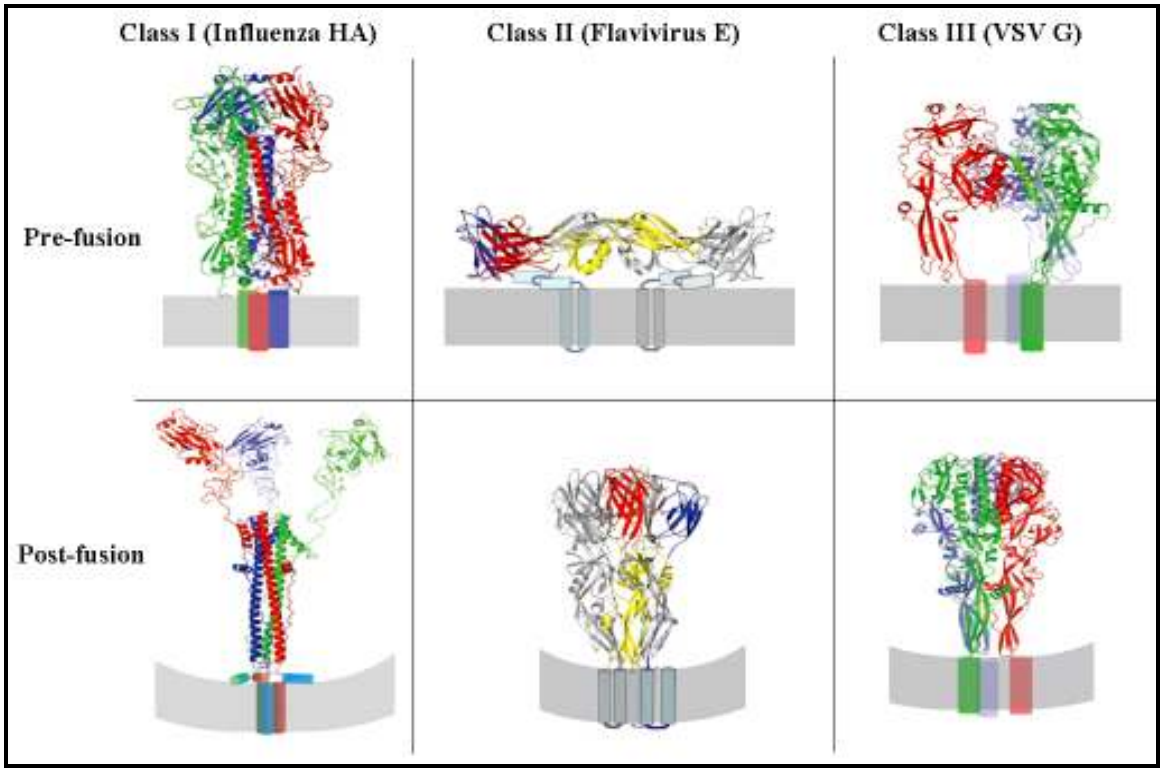

Fig. 2. Pre-and Post-Fusion Structures from Class I, II, and III Viral Fusion Proteins. Crystal structures of the indicated viral proteins were modified from (Harrison, 2008). The crystallographically determined components are depicted in ribbon representation, while the transmembrane segments, which are not structurally resolved, are shown as cylinders. Each viral protein monomer is shown in a different color.

The viral fusion proteins undergo dramatic conformational changes during the fusion process (Fig. 1 and 2). Detailed structural data have revealed the pre- and post-fusion structures of several virus fusion proteins (Bullough et al., 1994; Heldwein et al., 2006; Lescar et al., 2001; Roche et al., 2006; Roche et al., 2007; Wilson, Skehel, and Wiley, 1981; Yin et al., 2006), however there is no structural information yet on any of the intermediate conformations (Fig. 1), except a very recent early intermediate influenza

HA structure (Xu and Wilson, 2011). Most of the work to date, therefore, has involved functional characterizations, which provides only inferential insights on possible structural intermediates. For example, synthetic peptides derived from the HR2 region of gp41, such as the currently prescribed antiviral T20/enfuvertide (Eckert, 2001; Kilby et al., 1998; Wild, 1993), inhibit the fusion process by binding to the prehairpin intermediate folded states of gp41 that have exposed HR1 coils, thus interfering with the collapse of the HR1 and HR2 helices into the post-fusion 6-HB (Chan and Kim, 1998; Furuta et al., 1998). These type of experiments revealed that for HIV-1 gp41 the half-life of pre-hairpin intermediates is several minutes, while for other viral glycoproteins such as influenza HA, the half-life is in seconds (Harrison, 2008). These sorts of functional analyses, similar to the ones that I have pursued in my dissertation research, have been filling the current knowledge gaps related to viral glycoprotein-mediated membrane fusion reaction and its intermediates.

Fusion Triggers

The triggering events that initiate membrane fusion vary significantly among different viruses. These triggers force dramatic structural changes to occur at the right time (when virus is entering cells) and place (in organelles of the endocytic network) so that the fusion event is productive. Depending on the particular virus, one or a combination of cell receptor bindings (Feng et al., 1996), protonations in the endosome (Skehel et al., 1982; White and Helenius, 1980), disulfide reductions (Barbouche et al., 2003; Wallin, Ekstrom, and Garoff, 2004), and proteolytic cleavages (Chandran et al., 2005; Simmons et al., 2005) triggers surface protein refolding and virus opening. For

example, influenza HA is in metastable state and upon encountering the acidic endosomal environment is triggered to refold into a low energy conformation (Carr, Chaudhry, and Kim, 1997). HIV-1 gp41, on the other hand, is triggered at neutral pH via binding to the receptor CD4 and chemokine coreceptor CCR5 (Furuta et al., 1998; Moore et al., 1990). For herpesviruses and paramyxoviruses, the trigger consists in changing the contact with another viral protein, which has altered conformation due to binding a cellular receptor.

I will focus on proteolytic processing as a fusion trigger, because this trigger relates closely to my dissertation work. Proteolytic processing of viral proteins prior to cell entry is a common theme in virus biology. This principle applies to nonenveloped viruses (Chandran and Nibert, 1998; Duncan, 1996; Greber et al., 1996; Lee, Monroe, and Rueckert, 1993) and to enveloped viruses as well, most notably in the surface glycoproteins extending from virion membranes (Chandran et al., 2005; Hallenberger et al., 1992; Lazarowitz and Choppin, 1975). Surface glycoproteins facilitating virus-cell membrane fusions are synthesized and often maintained in precursor intermediate folding states, and proteolysis allows these proteins to refold into lower energy states, with virus entry then achieved by coupling this refolding energy to stable virus-cell linkages and membrane coalescence (see Fig.1).

Such proteolysis is usually executed in virus producer cells by Golgi resident furin and furin-like proteases as fusion proteins flow from the endoplasmic reticulum to to the infected cell surfaces. Once cleaved, the viral fusion proteins are metastable and can be triggered to refold upon binding to cellular receptor and/or encountering acidic endosomal environments (White et al., 2008). Typically the proteolytic cleavage occurs

immediately N-terminal to the hydrophobic fusion peptide, so that the fusion peptide can become exposed and insert in the target membrane upon trigger activation (White et al., 2008).

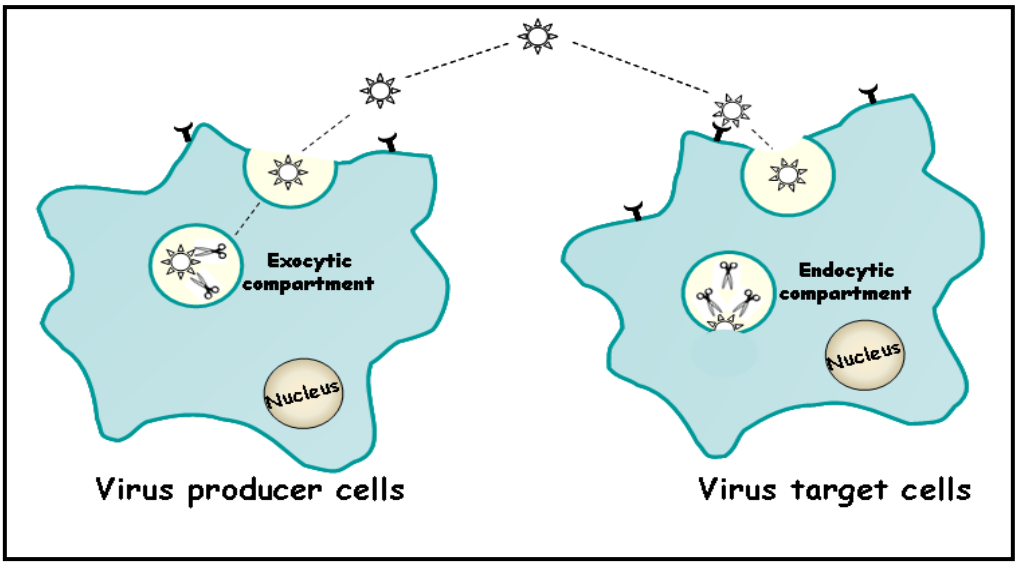

Fig. 3. Schematic Depiction of Two Fusion Protein Activation Pathways. Proteolytic processing of virus glycoproteins can occur in the exocytic (assembly) route by furin and furin-like proteases (traditional activation pathway) or in the endocytic (entry) route by endosomal proteases (novel target-cell activation pathway), as indicated by the scissors in each panel.

Notably some fusion glycoproteins do not get cleaved in virus-producing cells during assembly, but instead undergo cleavage in target cells during entry (Fig. 3). More viruses use this latter route of activation than was previously assumed, including important pathogens such as SARS-CoV and Ebola viruses (Chandran et al., 2005; Simmons et al., 2004). This diversity among viruses with respect to the place and timing

of proteolytic fusion activation is interesting and generates many ideas on the advantages that each activation route offers. One such idea is that viruses exiting cells with primed spikes have the advantage of successfully infecting a large range of target cells without any protease requirement, but suffer from the disadvantage of short-term maintenance in the extracellular milieu due to the propensity for primed proteins prematurely progressing into post-fusion conformations. On the other hand, viruses with uncleaved glycoproteins may retain infectivity in extracellular environments but could be restricted in their host range to tissues and cells enriched in activating proteases (Fig. 3). I will address these ideas later in my manuscript, using coronaviruses as models.

Coronaviruses and Disease

Coronaviruses belong to the order Nidovirales, family Coronaviridae and genus Coronavirus. Members of the Coronaviridae family are important pathogens that infect a wide variety of hosts including birds, domesticated animals and humans. As such, they are of great clinical, veterinary, agricultural and economic importance. The ensuing disease ranges from respiratory and enteric to neurologic and hepatic. The disease in humans is mainly respiratory and to a lesser extent gastrointestinal (Lai and Cavanagh, 1997). Coronavirus disease, once considered to be routinely quite mild and inconsequential in humans, was dramatically reconsidered during and after the SARS coroanvirus epidemic of 2002-2003, in which ~ 10% of infected individuals died from severe coronavirus – induced respiratory disease (Cherry, 2004; Lee et al., 2003; Rota et al., 2003).

CORONAVIRUSES		
Group I	**Group II**	**Group III**
TGEV (Pig)	MHV (Mouse)	IBV (Chicken)
PRCoV (Pig)	BCoV (Cow)	TCoV (Turkey)
FIPV (Cat)	RCoV (Rat)	PhCoV (Pheasant)
FCoV (Cat)	SDaV (Rat)	GCoV (Goose)
CCoV (Dog)	HCoV-OC43 (Human)	PCoV (Pigeon)
HCoV-229E (Human)	HEV (Pig)	DCoV (Mallard
PEDV (Pig)	PCoV (Puffin)	
HCoV-NL63 (Human)	ECoV (Horse)	
Bat-CoV-61 (Bat)	CRCoV (Dog)	
Bat-CoV-HKU2 (Bat)	SARS-CoV (Human)	
	HCoV-HKU1 (Human)	
	Bat-SARS-CoV (Bat)	

Table 2. Coronaviruses and Their Hosts.

Coronaviruses are divided into three groups (I, II and III) initially based on immunological characteristics and more recently on sequence comparisons (Gonzalez et al., 2003). Almost all viruses in groups I and II have mammalian hosts, while group III viruses have been isolated solely from avian hosts. The human coronaviruses are distributed between groups I and II. Table 2 lists all members of the Coronavirus family and their respective animal hosts.

The first two identified human coronaviruses, HCoV-229E and HCoV-OC43, were isolated in the mid-1960s from people with common cold symptoms (Hamre and Procknow, 1966; McIntosh, Becker, and Chanock, 1967). They cause mild upper and sometimes lower respiratory infections that get efficiently cleared in normal healthy

individuals, or severe pneumonia in immunocompromised people (McIntosh, 2005). About one third of all common colds and upper respiratory tract infections can be attributed to HCoV-229E and HCoV-OC43 (Tyrrell, Cohen, and Schlarb, 1993; Vabret et al., 2003). No new human coronaviruses were identified until 40 years later, when severe acute respiratory syndrome (SARS) coronavirus was discovered. The SARS-CoV was responsible for the 2002-2003 epidemic that emerged from the Guangdong province in China, and quickly spread to infect circa 8000 individuals (Drosten et al., 2003; Rota et al., 2003). Nearly 10% of infected individuals succumbed to death (Cherry, 2004; Lee et al., 2003). It was confirmed that SARS-CoV was the etiologic agent of the disease, when macaques inoculated with the virus displayed disease symptoms almost identical to the ones observed in the human cases of SARS (Fouchier et al., 2003). Notably, SARS-like coronaviruses are abundant in nature, infecting several bat species, civet cats and raccoon dogs (Kan et al., 2005; Poon et al., 2005). The large number of species in which the virus can replicate indicates that SARS-CoV is capable of efficient zoonotic transmission. Indeed, SARS-CoV transmission into the human population was a result of zoonosis from bats and civet cats (Guan et al., 2003; Lau et al., 2005; Li et al., 2005b).

Since the emergence of SARS-CoV, two new human coronaviruses were identified, HCoV-NL63 isolated in 2004 (van der Hoek et al., 2004) and HKU1 isolated in 2005 (Woo et al., 2005). Almost all children encounter their first NL63 infection during early childhood, resulting in conjunctivitis, croup, and sometimes serious infection that may lead to hospitalization (Esper et al., 2005; van der Hoek et al., 2004). Unlike SARS-CoV being a novel pathogen, the two coronaviruses HCoV-NL63 and HKU1 were

already present in the human population. It is likely that previously unidentified coronaviruses are circulating amongst us, and they may be discovered in the future due to the development of sensitive viral detection techniques.

While zoonotic potential and pathogenicity in humans is a complex function of many if not all viral genes and gene products, the viral spike (S) protein receives the greatest attention in the field. This is because S proteins dictate cell entry events. Spikes bind cell receptors and also mediate virus-cell membrane fusions. Evolution of spike proteins thus correlates with virus "jumps" from animal to human cell receptors (Li et al., 2005c; Sheahan et al., 2008) and also with increases in virus penetration into cells, spread through tissues, tropism and virulence (Casais et al., 2003; Haijema, Volders, and Rottier, 2003; Kuo et al., 2000; Leparc-Goffart et al., 1998; Schickli et al., 2004). For these reasons, our incentives are to increase understanding of the coronavirus spike proteins as well as other cofactors required for S-mediated entry into cells.

The S Glycoprotein

The coronavirus S protein is the sole mediator of virus entry into cells as well as a determinant of host-range, tissue tropism, pathogenesis and virulence. It is the largest known viral transmembrane fusion protein, ranging from 1162-1481 residues in length (~ three times larger than influenza HA), with an N-exo, C-endo orientation on the viral membrane. The ectodomain constitutes the majority of the molecule, with only a small carboxy-terminal segment of ~71 amino acids comprising the endodomain. The spike proteins occur as homotrimers and they protrude ~ 11-20 nm from the virion envelope (Davies and Macnaughton, 1979).

The S protein contains a cleavable N-terminal signal sequence that allows for cotranslational insertion in the endoplasmic reticulum (ER). Folding of the protein in the ER is a slow process, mainly due to the formation and rearrangement of several intramolecular disulfide bonds (de Haan and Rottier, 2005). The S protein is heavily glycosylated; there are 21 potential N-glycosylation sites in MHV and 23 in SARS-CoV S. At least 12 out of the 23 putative consensus sites in SARS-CoV are indeed glycosylated as determined by mass spectroscopy (Krokhin et al., 2003). As with other integral membrane glycoproteins, initial N-glycosylation occurs cotranslationally, followed by trimerization of the spike monomers and further de-and re-glycosylations in the Golgi (Delmas and Laude, 1990).

.

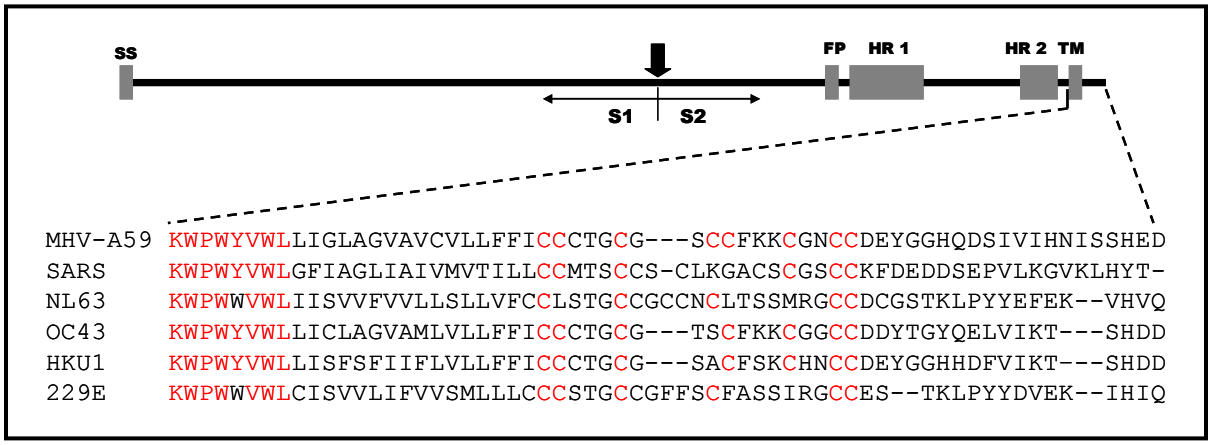

Fig. 4. Structural Features of the Coronavirus S Protein. The MHV-A59 spike protein is depicted in linear fashion. SS = signal sequence. S1= Peripheral spike proteolytic subunit 1. S2 = Transmembrane spike proteolytic subunit 2. FP= fusion peptide. HR1=heptad repeat 1. HR2= heptad repeat 2. TM= transmembrane span. An expanded view of the transmembrane span and proximal cytoplasmic residues reveals the highly conserved cysteine rich motif.

The S protein is synthesized as a single-chain precursor which in some cases gets cleaved in the Golgi by furin-like enzymes to generate an amino-terminal S1 subunit and a membrane-anchored S2 subunit, of roughly equal sizes (Sturman and Holmes, 1984; Sturman, Ricard, and Holmes, 1985) (Fig. 4). The S1 subunit (or the equivalent in those viruses that do not get cleaved) is responsible for binding the cellular receptor and the S2 subunit contains the fusion machinery necessary for mediating virus-cell membrane fusion. The two subunits are held together via non-covalent interactions and they easily dissociate from each other upon encountering a fusion trigger (Sturman, Ricard, and Holmes, 1990)

The cleavage between the S1 and S2 subunits occurs after the last residue in a highly basic site, RRARR in mouse hepatitis virus (MHV) strain JHM, RRAHR in MHV strain A59 (Luytjes et al., 1987) and RRFRR in infectious bronchitis virus (IBV) S protein (Cavanagh et al., 1986). Notably, several human coronaviruses such as SARS-CoV, HCoV-NL63, and HCoV-OC43 S proteins do not have a basic furin recognition motif and thus do not get cleaved in virus producer cells. The importance of S1/S2 cleavage and how it relates to the S protein function will be discussed in more detail later in this dissertation.

The S1 subunit is the most divergent region when comparing coronavirus spikes within and across groups, and even among isolates of a single species (Gallagher, Parker, and Buchmeier, 1990; Wang et al., 1994). The hypervariability of this region could be due to natural recombination, which is very common for coronaviruses. Due to their

replication strategy, coronaviruses exhibit high frequency of recombination and strain variability (Lai et al., 1994; Makino et al., 1986).

The receptor binding domains (RBD) in the S1 subunit have been mapped for many coronaviruses, and both the sequences and their positions within the S1 subunit vary among the different coronaviruses (Fig. 5). The SARS-CoV S RBD has been defined at residues 318-510 of the S1 domain, and it was shown to bind the angiotensin converting enzyme 2 (ACE2) receptor with higher affinity than the full S1 domain (Wong et al., 2004). The first 330 residues in the S1 subunit of MHV are sufficient to bind the carcinoembryonic antigen-cell adhesion molecule 1 (CEACAM1) receptor (Kubo, Yamada, and Taguchi, 1994). A different region in the S1 subunit of HCoV-229E comprising residues 407-547 is sufficient to associate with the aminopeptidase N (APN, CD13) receptor (Bonavia et al., 2003; Breslin et al., 2003).

The S2 subunit contains two heptad repeat (HR) regions (de Groot et al., 1987) that have similar characteristics with other class I fusion protein coiled coil domains. Condensed 6-HB of antiparallel HR1 and HR2 have been crystallographically resolved (Supekar et al., 2004; Xu et al., 2004). The location of the fusion peptide is still unknown, despite several predictions (Bosch et al., 2004; Chambers, Pringle, and Easton, 1990; Luo, Matthews, and Weiss, 1999). Recently, residues 798-815 in SARS-CoV S were shown to have the ability to interact with membranes in vitro and they were also important for the membrane fusion process, thus implying that these residues might comprise a fusion peptide (Madu et al., 2009) (Fig. 4).

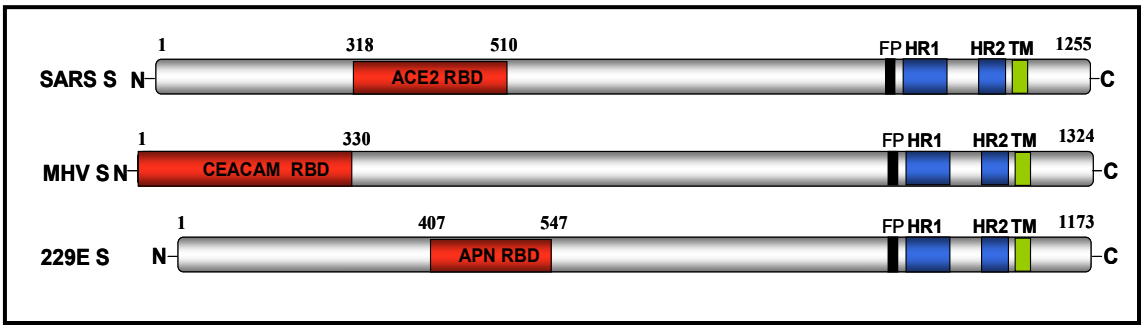

Fig. 5. Receptor Binding Domains in Coronavirus Spikes. Shown here are linear depictions of three coronavirus spike glycoproteins. The receptor binding domains (RBD) are depicted in red and their positions along each spike glycoprotein are indicated by numbers. FP= fusion peptide. HR1=heptad repeat 1. HR2= heptad repeat 2. TM= transmembrane span.

Besides the HR regions and the fusion peptide, other parts of the S2 subunit may be important for mediating the fusion process. For example, downstream of HR2 there is a region comprised of mainly aromatic residues (KWPWYVWL), which are highly conserved among all coronaviruses (Fig. 4). Substitution of the aromatic residues in this region of SARS-CoV S protein results in potent inhibition of fusion and virus entry (Howard et al., 2008). This region may be the start of the transmembrane portion of the S protein, and transmembrane domains of several viral fusion proteins are shown to be important for fusion, even though a detailed mechanism is not yet elucidated (Langosch, Hofmann, and Ungermann, 2007). A similar region in HIV-1 Env protein was shown to be important for Env-mediated membrane fusion (Salzwedel, West, and Hunter, 1999).

Immediately downstream of the transmembrane domain, there is another well-conserved region among coronaviruses: the cysteine rich motif (CRM) (Fig. 4). In the

prototype murine coronavirus, strain A59, the CRM spans 17 amino acids, 9 of which are cysteines. A helical wheel depiction of this region, predicted to have alpha-helical structure, reveals that all 9 cysteines lie on one face of the putative helical rod (Fig. 6). Many of these cysteines are post-translationally modified with palmitic acids, suggesting that one face is markedly hydrophobic and likely intercalated into the cytoplasmic leaflets of intracellular membranes. The functional role of the cysteine-rich domain is investigated later in this report.

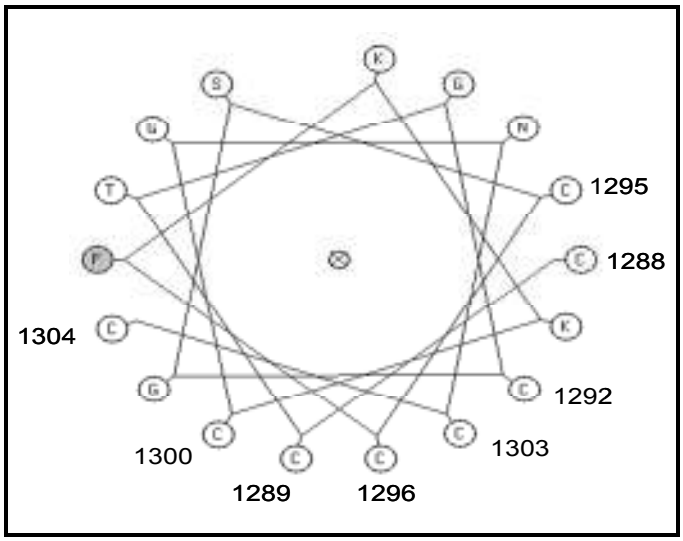

Fig. 6. Hypothetical Helical Wheel Depiction of MHV-A59 S Cysteine Rich Motif. The 'wheel' is a view along the long axis of an alpha helix, with numbered positions and residues indicated. MHV A59 S contains a cysteine rich motif in which 9 of 17 residues are cysteines. A helical wheel depiction of this region reveals that all 9 cysteines lie on one face of the putative helical rod.

Only a proportion of the available S protein pool gets assembled into nascent virions through interactions with M proteins. The remaining S proteins travel through the

exocytic pathway to reach cell surfaces where they can interact with receptors on adjacent cells to mediate cell-cell fusions. Cell-cell fusion leads to formation of multinucleated cells, otherwise known as syncytia, and rapid spread of infections.

Coronavirus Architecture

Coronaviruses are enveloped viruses with the largest known single-stranded positive sense RNA genome of ~30 kb (Lee et al., 1991). The 5' ~ two thirds of the genome encodes polyproteins that get cleaved into nonstructural proteins (nsps) 1-16 that operate in RNA-dependent RNA replication, polyprotein processing and host immune evasion. The 3' ~one third part of the genome encodes the structural proteins, S, E, M and N, needed to generate infectious viral particles.

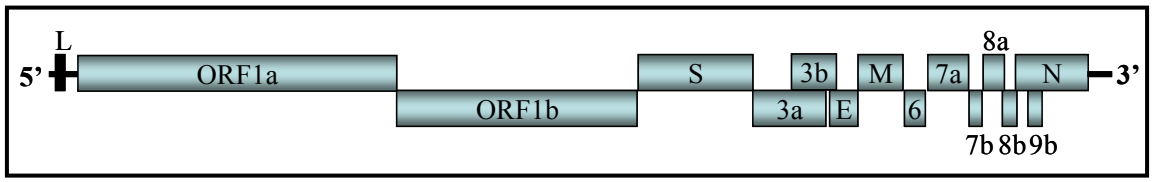

Fig. 7. Coronavirus Genome Organization. Depiction of the human SARS coronavirus (GenBank accession number AY278741) positive strand RNA genome. There is a leader (L) sequence in the 5' end of the genome. Open reading frames (ORF1a and ORF1b), encoding for the polymerase and protease polyprotein complex, are translated via a ribosomal frameshifting mechanism. Besides the main structural proteins (sequentially S, E, M, and N) the SARS-CoV genome contains additional accessory genes (3a, 3b, 6, 7a, 7b, 8a, 8b and 9b) that might be important during *in vivo* infections.

In between the structural genes in the coronavirus genome are several other genes called “accessory genes”, because many studies have shown that these genes and their products are not required for virus growth *in vitro* (de Haan et al., 2002; Yount et al., 2005). However, many of the accessory genes are maintained in coronavirus genomes, suggesting that they might be important for *in vivo* virus infections. The severe acute respiratory syndrome coronavirus (SARS-CoV) genome organization is depicted in Fig. 7. SARS-CoV has a genome of 29 kb, encoding for 9 open reading frames (ORFs) (Marra et al., 2003).

The virions are pleimorphic in structure with a diameter of about 80-120 nm (Neuman et al., 2006a). The transmembrane spike glycoprotein trimers protrude circa 20 nm from the virion membrane giving the appearance of a crown or “corona”-like arrangement under the electron microscope. The major protein species in the membrane is the triple-pass membrane glycoprotein (M) that mediates interactions of the genome structure with the viral envelope. Recent cryoelectron tomographic 3D reconstructions of the mouse hepatitis virus (MHV) indicate that the C-termini of M proteins are organized as a proteinacious shell between the membrane and the virion interior (Barcena et al., 2009). The small envelope (E) protein is a minor component of the virion membrane and, in contrast to the M protein, it does not have a structural role in the virion. The ribonucleoprotein (RNP) core contains a single copy of the positive strand genomic RNA wrapped into helical structures by multiple copies of the nucleocapsid protein (N) (Masters, 2006; Risco et al., 1998). The virion architecture is illustrated in Fig. 8.

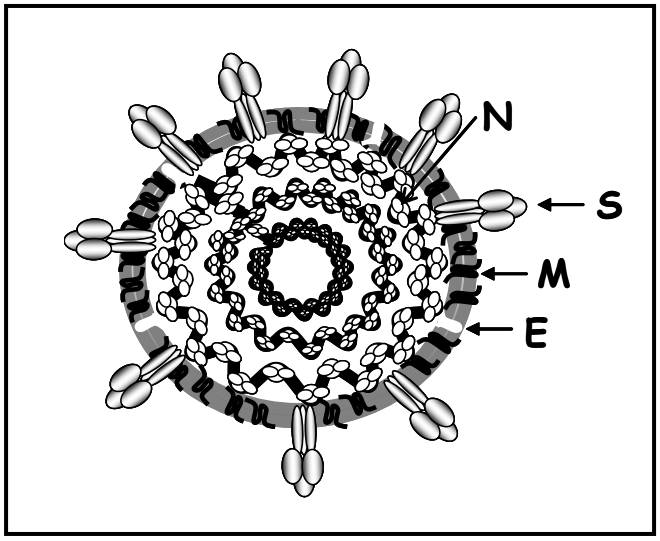

Fig. 8. Model of Coronavirus Architecture. S: spike glycoprotein trimers, M: triple-pass membrane spanning glycoprotein**,** E: small envelope glycoprotein, N: nucleocapsid protein. The positive strand RNA genome is depicted wrapped around N proteins forming helical arrays inside the virion.

Coronavirus Assembly

Part of my dissertation research focuses on coronavirus assembly. Most of the work on assembly has been concentrated on specific viral components and the coordinated interplay between them, while very little is known about the cellular factors involved in the process. The development of virus-like particle (VLP) system for coronaviruses was central to understanding the molecular interactions involved in assembly. In this system, expression of only M and E proteins was sufficient to generate VLPs with the same morphology as authentic coronavirions (Bos et al., 1996; Vennema et al., 1996). M protein is the key player mediating virion assembly through homotypic interactions with each other (de Haan, Vennema, and Rottier, 2000), with RNP complexes (Kuo and Masters, 2002; Narayanan et al., 2000), and with the E and S

proteins (de Haan et al., 1999; Godeke et al., 2000). The E protein may act to induce the membrane curvature required for viral assembly (Raamsman et al., 2000). Intracellular targeting signals in S, E and M ensure localization of these proteins at the site of assembly (Corse and Machamer, 2002; Lontok, Corse, and Machamer, 2004; McBride, Li, and Machamer, 2007), which for coronaviruses occurs intracellularly on the membranes of the endoplasmic reticulum Golgi intermediate complex (ERGIC) (Krijnse-Locker et al., 1994).

As mentioned above, the spike glycoproteins are dispensable for virion particle formation, which requires only the action of M and E proteins (Vennema et al., 1996). Only a proportion of the available S protein pool gets assembled into nascent virions through interactions with M proteins. The remaining S proteins travel through the exocytic pathway to reach cell surfaces and mediate cell-cell fusions and spread of infection. The number of spike glycoprotein trimers per virion varies from 50 to 100 (Neuman et al., 2006b), and spikeless virions do form under specified conditions, indicating that the S protein is not an active participant in assembly (Holmes, Doller, and Sturman, 1981; Rottier, Horzinek, and van der Zeijst, 1981).

Coronavirus Entry: Involvement of Viral and Cellular Cofactors

Successful virus entry and subsequent infection requires the coordinated interplay between viral, cellular proteins and the environment in which these factors reside. Understanding these interactions will provide insights into the mechanism by which viruses gain access into susceptible cells.

Coronaviruses provide a good model in which one can study mechanisms of virus entry. For many coronaviruses the fusion reaction takes place at cell surfaces, which makes them accessible to extracellular probes such as antibodies and peptides. Also, assays to evaluate coronavirus fusion and entry reactions are in place and the assays are very robust with high sensitivity and broad >10,000-fold range. Most importantly, a coronavirus reverse genetics system is in place to evaluate various mutations in the context of authentic virions. In my dissertation research, I focused on identifying viral and cellular cofactors required for coronavirus entry. I found that multiple factors, including coreceptors, proteolysis, lipid rafts and spike lipidation, operate to facilitate coronavirus entry into cells.

Receptors on Susceptible Cells

Cellular receptors are of central importance to virus infectivity and understanding virus-receptor interactions can make significant contributions to the development of vaccines and antiviral therapies. Typically, receptors provide a high-affinity docking site that enriches virus particles on the surface of target cells. Upon binding, the receptor then induces conformational changes in the virus structure that are important for entry. In the case of nonenveloped viruses, the structural changes in the capsid upon receptor binding at the cell surface lead to limited disassembly, which is a prerequisite for complete opening of the virus at later stages (He et al., 2000; Nakano et al., 2000; Tsang et al., 2001). Due to their ability to recycle between the surface of a cell and its interior compartments, receptors actively assist in virus internalization. In addition to shuttling viruses inside cells, receptors may bring viruses in close proximity to additional factors

required for entry, such as coreceptors (Moore, Trkola, and Dragic, 1997) and proteases. Some receptors may also contain signaling modules (Barton et al., 2001; Brojatsch et al., 1996; Hofer et al., 1994) that can get triggered upon virus binding to activate downstream effectors assisting in multiple aspects of virus entry and lifecycle.

Coronaviruses S proteins have a wide variety of receptor specificities as listed in Table 3. Members of the CEACAM family, immunoglobulin-like type I-oriented membrane glycoproteins, serve as receptors for MHV (Dveksler et al., 1991; Williams, Jiang, and Holmes, 1991). ACE2, present on the apical surfaces of pulmonary and gastrointestinal epithelial cells (Hamming et al., 2007), is a functional receptor for two human respiratory pathogens, SARS-CoV (Li et al., 2003) and HCoV-NL63 (Hofmann et al., 2005). APN, a type II-oriented membrane glycoprotein abundant in respiratory epithelia, was shown to be a receptor for multiple group I coronaviruses including canine coronavirus (Benbacer et al., 1997), feline infectious peritonitis virus (Tresnan, Levis, and Holmes, 1996), HCoV-229E (Yeager et al., 1992) and transmissible gastroenteritis virus (Delmas et al., 1992). To date, no receptors have been unambiguously identified for group III coronaviruses, although candidates include heparan sulfate (Madu et al., 2007) and sialic acid (Winter et al., 2006).

For several coronavirus S proteins, binding to the primary cell surface receptor leads to conformational changes in the S protein. For example, MHV S binds to the CEACAM receptor with an affinity of ~ 0.5 nM (Krueger et al., 2001). This binding leads to structural changes in the S protein, namely the dissociation of S1 and S2 subunits and the refolding of spike into a post-fusion conformation (Gallagher, 1997; Matsuyama

and Taguchi, 2002; Zelus et al., 2003). Similarly, SARS-CoV S binds the ACE2 receptor with a high affinity of ~ 2nM (Li et al., 2003), and this binding leads to structural rearrangements in the SARS-CoV S that can be visualized by cryo-electron microscopy reconstruction techniques (Beniac et al., 2007; Li et al., 2006).

Group	Virus species	Receptor
1	TGEV	Porcine aminopeptidase N (pAPN)
	FIPV	Feline aminopeptidase N (fAPN)
	CCoV	Canine aminopeptidase N (cAPN)
	HCoV-229E	Human aminopeptidase N (hAPN)
	HCoV-NL63	Angiotensin converting enzyme 2 (ACE2)
2	MHV	Murine carcinoembryonic adhesion molecule 1 (mCEACAM)
	SARS-CoV	Angiotensin converting enzyme 2 (ACE2)
	OC43	Sialic acid
	BCoV	9-*O*-acetyl sialic acid

Table 3. Coronavirus Receptors. Listed are the known cellular receptors for group 1 and 2 coronaviruses. No receptors have been identified for group 3 coronaviruses.

Besides the primary cell surface receptor, other protein cofactors might be required for coronavirus S-mediated entry. For example, even though HCoV-NL63 can bind ACE2, not all cell lines expressing ACE2 are able to support NL63 replication, suggesting that HCoV-NL63 may bind molecules on the host cell surface in addition to ACE2. Indeed, many viruses interact with more than one cell surface molecule to mediate the process of attachment and internalization thereafter, such as Coxsackie B and HIV-1 viruses (Greber, 2002).

Integrins and their Roles as Virus Entry Cofactors

We hypothesized that β1 integrins might serve as coreceptors for HCoV-NL63 entry. Recently, Schornberg *et al*. described a new and interesting role for β1 integrins in Ebola virus entry (Schornberg et al., 2009). Their findings indicated that β1 integrins regulated the activities of endosomal cathepsins required to render Ebola virus competent for cell entry (Schornberg et al., 2009). Knowing that the HCoV-NL63 S proteins are uncleaved (van der Hoek et al., 2004), and that they might require endosomal proteases for fusion activation, led us to the hypothesis that β1 integrins may be operating as coreceptors to guide HCoV-NL63 into the appropriate endosomal environments. Several coronaviruses are dependent on endosomal cathepsin proteases for entry into cells (Qiu et al., 2006; Simmons et al., 2005); however, it is currently unknown whether integrins are involved.

Integrins are expressed on the cell surface as heterodimeric glycoproteins composed of α and β subunits. The large integrin family is comprised of 18 α and 8 β units that can form 24 different α/β heterodimeric complexes (Hynes, 2002). These complexes are involved in many aspects of cellular life, including cell adhesion, migration, growth, survival and differentiation (Giancotti, 2000). In addition to these roles, integrins serve as portals of entry for a variety of viral and bacterial pathogens (Triantafilou, Takada, and Triantafilou, 2001). Both enveloped and non-enveloped viruses utilize integrins for entry, including members of the adeno-, herpes- (Akula et al., 2002; Feire, Koss, and Compton, 2004; Wickham et al., 1993), hanta-, picorna- (Bergelson et al., 1992; Jackson et al., 2002), reo- (Graham et al., 2003; Maginnis et al.,

2006) and paramyxo-viridae (Cseke et al., 2009).

The integrin contributions during the course of viral infections are multifold and include virus attachment, entry as well as signaling events (Stewart and Nemerow, 2007). Virus binding to integrins is often enough to trigger cellular signaling pathways. The cytoplasmic domains of integrins interact with a variety of intracellular factors that mediate the signaling events important for subsequent virus entry. For example, Kaposi's sarcoma-related herpesvirus and cytomegalovirus binding to β1 integrins activates focal adhesion kinase (FAK), which is critical for virus entry post-receptor binding (Krishnan et al., 2006). Besides its well-known role in cell motility, FAK also impacts downstream molecules such as ERK1/ERK2 mitogen-activated protein (MAP) kinases (Eblen et al., 2002; Schlaepfer et al., 1994).

There are several integrin recognition motifs (Plow et al., 2000) and all viruses known to use integrins as entry receptors have one or more of these sequences in their surface proteins. Notably, the human coronavirus HCoV-NL63 contains the well-defined integrin recognition motif Asn-Gly-Arg (NGR) in its S sequence (Koivunen, Gay, and Ruoslahti, 1993). The presence of this integrin recognition motif has probably gone unnoticed due to the fact that HCoV-NL63 uses the primary protein receptor ACE2 for entry (Hofmann et al., 2005). My experimental results argue for a role of β1 integrins in HCoV-NL63 entry.

Cellular Proteases and their Roles as Virus Entry Factors

During the course of identifying and characterizing cofactors for coronavirus entry, we discovered TMPRSS2 as a novel SARS-CoV activating protease. Class I

fusion proteins, such as coronavirus S, require proteolysis for fusion activation. Coronavirus spikes vary in their mode of proteolytic priming. Most of the group II and all of the group III coronavirus S proteins are cleaved between their S1 and S2 domains by a furin-like protease in the producer cells (Jackwood et al., 2001; Sturman, Ricard, and Holmes, 1985). This cleavage correlates well with the ability of S proteins to mediate cell-cell fusion and formation of syncytia. For example, MHV-A59 S proteins with mutations in their multibasic cleavage motif, cannot execute cell-cell fusion and formation of syncytia (Bos et al., 1995; Gombold, Hingley, and Weiss, 1993). Also, inhibition of the furin protease correlates with inhibition of S protein cleavage and ability to mediate cell-cell fusion (de Haan et al., 2004).

Notably, some coronavirus S proteins, such as those of SARS-CoV, lack furin recognition motifs and nascent virions exit cells harboring uncleaved spikes (Song et al., 2004; Xiao et al., 2003; Yao et al., 2004), thus relying on target cell proteases for activation (Simmons et al., 2004). Therefore, the host cell proteases that cleave and activate SARS-CoV S are central entry determinants.

SARS-CoV binds to its ectopeptidase receptor, angiotensin converting enzyme 2 (ACE2), with very high affinity (Sui et al., 2004). ACE2 without ectopeptidase activity is also an efficient SARS-CoV receptor (Li et al., 2005c) and S proteins bind at a distance from the ACE2 enzyme pocket (Li et al., 2005a), making it clear that ACE2 is not a direct S-activating protease. There are, however, several proteases that can cleave SARS-CoV S including trypsin, cathepsin L, elastase, factor Xa, thermolysin, and plasmin (Belouzard, Madu, and Whittaker, 2010; Du et al., 2007; Matsuyama et al., 2005;

Simmons et al., 2005). The most prominent proteases in this group, trypsin and cathepsin L, are discussed in more detail below.

Trypsin is a well-characterized member of the serine protease family of proteins that gets secreted in the extracellular space. Addition of exogenous trypsin protease induces SARS-CoV S-mediated syncytia formation in infected cell cultures (Matsuyama et al., 2005; Simmons et al., 2004). The trypsin cleavage site maps to a position that aligns precisely with the furin cleavage site in MHV (Li et al., 2006). Indeed, introduction of a furin cleavage site at this position in SARS-CoV S allows for cleavage of the protein into S1 and S2 fragments and the ability to induce cell-cell fusion and syncytia (Follis, York, and Nunberg, 2006; Watanabe et al., 2008). As trypsin activity is tightly regulated in humans, it is not clear whether trypsin contributes to activation of SARS-CoV infections *in vivo*.

Cathepsin L is a member of the cathepsin family of proteins, which includes serine proteases (cathepsins A and G), aspartic proteases (cathepsins D and E), and the more numerous cysteine proteases (cathepsins B, C, F, H, K, L, O, S, W, V, and Z) (Reiser, Adair, and Reinheckel, 2010). In general, the cysteine proteases are stable in acidic cellular compartments, such as endosomes and lysosomes. Thus, unlike trypsin protease that is secreted into the extracellular space, cathepsin L protease remains cell-associated, residing mainly in endo-lysosomal compartments. The initial evidence for involvement of cathepsin L in activating SARS-CoV S proteins came from studies using protease inhibitors. Thus, specific inhibitors of the cathepsins L endosomal protease greatly inhibit SARS-CoV S-mediated entry into target cells (Huang et al., 2006;

Simmons et al., 2005). Recently, the cathepsin L proteolytic target site in SARS-CoV S was mapped only 11 residues downstream of the trypsin cleavage site (Bosch, Bartelink, and Rottier, 2008).

Trypsin, cathepsin L and the other proteases known to activate S-mediated fusion *in vitro* are mostly soluble proteases and it is not obvious how they might be retained in the vicinity of the ACE2 receptor. These questions of protease subcellular location and the timing of enzyme action are relevant because activating S protein cleavages take place only after ACE2 engagement. Indeed, without prior ACE2 binding, these soluble proteases excessively cleave and inactivate virus spikes (Matsuyama et al., 2005; Simmons et al., 2005). Given that the productive sequence is for S proteins to bind ACE2, then undergo activating proteolysis, it is reasonable to suspect that the relevant proteases activating SARS-CoV entry might be anchored into the plasma membrane and juxtaposed near the ACE2 receptors.

Amongst the candidates for membrane-anchored virus-activating proteases are the type II transmembrane serine proteases (TTSPs), a family of serine proteases whose physiologic functions are just beginning to be discerned (Bugge, Antalis, and Wu, 2009). TTSPs belong to the same serine protease family as the well-studied trypsin, chymotrypsin, elastase, thrombin and plasmin proteases. The main difference between TTSPs and the rest of serine proteases is the presence of an N-terminal transmembrane domain, which allows TTSPs to be membrane-associated. The human TTSP family comprises 19 members that can be further grouped into four subfamilies: the HAT/DESC (human airway trypsin-like protease/differentially expressed in squamous cell

carcinoma), the Hepsin/TMPRSS (transmembrane protease/serine), the Matriptase and the Corin subfamily (Antalis et al., 2010).

As it is true for all serine proteases, TTSPs are synthesized as inactive single-chain precursors or zymogens. They undergo autocatalytic cleavage to generate a mature form containing the serine protease domain and a sister transmembrane fragment, connected together via a disulfide linkage (Hooper et al., 2001). At least for one member of the family, matriptase, it has been shown that the autocatalytic cleavage occurs at the plasma membrane (Miyake et al., 2009).

The physiologic roles of the TTSPs are quite diverse and they may be key regulators of signaling events at the plasma membrane. The TTSPs are involved in activating zymogen cascades, cleaving protease-activated receptors (PARs), processing growth factors, activating epithelial sodium channels as well as processing viral proteins and thus promoting virus spread and infectivity (Choi et al., 2009).

Three TTSPs (TMPRSS2, TMPRSS11a and TMPRSS11d) are expressed in the surface of airway epithelial cells (Donaldson et al., 2002; Kam et al., 2009; Yasuoka et al., 1997), and thus can potentially be positioned appropriately at virus-cell junctions. Importantly, TTSPs are known to activate entry of some respiratory viruses including both seasonal and pathogenic human influenzae as well as human metapneumoviruses (Bottcher et al., 2006; Chaipan et al., 2009; Shirogane et al., 2008). A recent report has implicated TMPRSS11a in the proteolysis of SARS-CoV S proteins (Kam et al., 2009). This valuable contribution stimulated our interest in cell entry cofactors and prompted questions concerning the transmembrane proteases, their substrate preferences and their

potential localization with the primary ACE2 receptors. In considering these questions, we made discoveries that relate to SARS-CoV and potentially other virus entry events. These discoveries are described in section 3-2 of this dissertation document.

Localization of Receptors and Proteases in Lipid Rafts: Roles for Lipid Rafts as Virus Entry Factors

Many viruses enter cells through specialized lipid microdomains or "lipid rafts". Virus receptors, coreceptors and other cellular factors important for virus entry often concentrate within lipid rafts, thereby setting the stage for high affinity interactions during entry. Both the receptor and coreceptor for HIV-1, CD4 and CCR5 respectively, are associated with lipid rafts (Campbell, Crowe, and Mak, 2001; Popik, Alce, and Au, 2002). Following virus-receptor/coreceptor engagement, membrane rafts continue to influence the entry process by assisting in shaping membrane invaginations and subsequent uptake of viruses into cells (Chazal and Gerlier, 2003). In some cases, the cholesterol and sphingolipid moieties in rafts are crucial to virus entry and infectivities, such as Semliki Forest and Sindbis (Kielian and Helenius, 1984; Smit, Bittman, and Wilschut, 1999); however, the exact mechanisms of these lipid requirements remain unknown.

Lipid rafts can be operationally defined as nonionic detergent – insoluble, and thus are frequently referred to as detergent-resistant membranes (DRMs) (Brown, 2006). They are enriched in cholesterol and sphingolipids, and are readily isolated from the majority of cellular material by floatation in sucrose density gradients. This biochemical cell fractionation process may arguably create low density lipid-protein assemblages that

are not present in intact cells; however, numerous immunofluorescence and electron mcroscopic investigations of living cells have revealed striking membrane heterogeneities, with distinct (~ 50 nm in diameter) “lipid rafts” present in the plasma membrane, apical transport vesicles, as well as Golgi and *trans* Golgi membranes (Brown, 2006; Simons and Ikonen, 1997). The *in vivo* existence of bona-fide lipid rafts still remains debatable, even though multiple techniques independent of detergent extraction have been used to visualize lipid rafts in living cells (Schutz et al., 2000).

Even though detergent-resistant membranes can form in vitro solely by mixing cholesterol and sphingolipids in the absence of any proteins, certain proteins do associate with these special lipid microdomains (Simons and Ikonen, 1997). Most proteins that associate with lipid raft membrane domains have post-translational lipid modifications that include glycophosphatidylinositol (GPI) anchors, N-terminal myristic acid tails, cysteine acylation, and the addition of C-terminal sterol moieties (Levental, Grzybek, and Simons). Proteins that reside in less ordered membrane domains can move to lipid rafts through interaction with a raft associated protein. Such is the case of influenza virus M1 protein, which by interaction with the glycoprotein HA becomes incorporated into lipid rafts (Ali et al., 2000). In many cases, virus binding relocalizes receptor from non-raft to raft microdomains. This is in line with the documented, dynamic and rapid association/dissociation of lipid microdomains to form smaller or larger rafts (Kusumi and Sako, 1996).

Multiple studies have implicated lipid rafts in coronavirus entry. CD13 and ACE2, which serve as receptors for human coronaviruses 229E and SARS respectively,

have been shown to localize in detergent-resistant membranes (Lu, Liu, and Tam, 2008; Nomura et al., 2004). Furthermore, cholesterol depletion by pharmacological agents results in disruption of virus infection, implicating the importance of cholesterol in virus entry (Thorp and Gallagher, 2004). The presence of ACE2 in lipid rafts could be a cell-type specific phenomenon; ACE2 localizes to DRMs in Vero E6 cells (Lu, Liu, and Tam, 2008), but not CHO cells stably expressing ACE2 (Warner et al., 2005).

We recently identified the transmembrane serine protease, TMPRSS2, as an important factor for SARS coronavirus entry (Shulla et al., 2011). TMPRSS2 localizes on the cell surface and might be closely associated with the SARS coronavirus receptor, ACE2. It is not known whether TMPRSS2 or any of the other 19 members of the type II transmembrane serine protease family are associated with raft membrane domains. Interestingly, all known cell surface substrates for these proteases are lipid raft resident proteins. We wanted to determine whether ACE2 and TMPRSS2 were associated with lipid rafts and whether this association was important for virus entry.

Spike Protein Palmitoylations as Virus Entry Factors

Palmitoylation is one of several post-translational modifications that influence protein stability, trafficking and interactions with lipid raft membranes. Palmitate is a 16-carbon saturated fatty acid that is attached to cysteine residues through a reversible thioester linkage catalyzed by protein acyltransferases (PATs) (Linder and Deschenes, 2007). Several viral membrane glycoproteins are palmitoylated at sites near the cytoplasmic face of the membrane shortly after synthesis (Schmidt and Schlesinger, 1980; Veit and Schmidt, 1993).

The S protein endodomains comprising the carboxy-termini are set apart by their abundance of cysteine residues (see Fig. 4). Many, if not all of these cysteines, are well-known to be post-translationally acylated with palmitate and / or stearate adducts (Bos et al., 1995; Chang, Sheng, and Gombold, 2000; Petit et al., 2007; Thorp et al., 2006); these posttranslational modifications add considerable lipophilicity to the endodomains and likely position the cytoplasmic tails against the inner face of virion membranes. Indeed, the S proteins are set apart from other enveloped virus glycoproteins in having very richly acylated endodomains. For example, there are nine acylated cysteines in coronavirus S, while there are only three in influenza HA (Veit et al., 1991) and two in HIV gp160 (Yang, Spies, and Compans, 1995). Interference with S endodomain palmitoylation, either by engineered mutations or by pharmacologic agents, diminishes or eliminates S-mediated membrane fusion activities (Bos et al., 1995; Chang and Gombold, 2001; Chang, Sheng, and Gombold, 2000; Thorp et al., 2006), but the mechanisms by which these endodomain alterations influence membrane fusion activities are unknown. My dissertation document will address the question of how endodomains and more specifically how palmitoylated cysteine residues influence membrane fusion reactions (Shulla and Gallagher, 2009).

CHAPTER II

MATERIALS AND METHODS

Materials

Cells

Murine 17cl1 fibroblasts (Sturman and Takemoto, 1972) were grown in Dulbecco's modified Eagle medium (DMEM) containing 5% tryptose phosphate broth (Difco Laboratories) and 5% heat-inactivated fetal bovine serum (FBS). 293T, FCWF (Pedersen et al., 1981) and HeLa-CEACAM (carcino embryonic antigen cell adhesion molecule isoform 1a, cell line no. 3) cells (Rao and Gallagher, 1998) were grown in DMEM supplemented with 10% FBS. hACE2-293 cells, obtained from Shibo Yang (New York Blood Center, NY), were grown in DMEM-10% FBS supplemented with 10 μg/ml puromycin. All growth media were buffered with 0.01M sodium HEPES (pH 7.4).

Plasmid DNAs

Unless otherwise stated, all plasmids were propagated in *E. coli* strain DH5α and purified using Qiagen Maxiprep Kit (catalog no.12662)

- pMH54.A59 (for targeted recombination reverse genetics) was obtained from Paul Masters, Wadsworth Center for Laboratories and Research, NY. This vector, ~ 13 kb in size, is a donor RNA transcription vector containing a 5' genomic fragment attached to a synthetic linker which is fused to the rest of 3' end of the MHV-A59 genome. This original vector was modified (Mai Nguyen) to encode for firefly luciferase

positioned between E and M genes and the new pMH54-E-FL-M construct was generated (Boscarino et al., 2008).

- MHV-A59 S and M cDNAs were PCR amplified using template pMH54-A59 (Kuo et al., 2000; Masters and Rottier, 2005) and cloned into pCAGGS.MCS (Niwa, Yamamura, and Miyazaki, 1991) between SacI and XmaI restriction sites.
- Mutations in the pCAGGS-A59 S construct were created using mutagenic primers and a site-directed mutagenesis protocol (QuikChange® XL; catalog no. 200519-5; Stratagene). The pCAGGS-A59 S C1304A and pCAGGS-A59 S C1303A/C1304A constructs were generated by Hillary Logan in the Gallagher lab. I used the following primers to introduce the C1300A mutation in pCAGGS-S C1303A/C1304A construct: forward 5'-GTTTTAAGAAGGCTGGAAATGCTGCTGATGAGTATGG -3' and reverse 5'-CAGCAGCATTTCCAGCCTTCTTAAAACAACATGAGCC-3'. All plasmid constructs were sequenced to confirm the presence of desired mutations.
- The S cDNAs containing C1304A, C1303A/C1304A, and C1300A/C1303A/C1304A were subcloned into pMH54-E-FL-M plasmid between XhoI and SbfI restriction sites using pCAGGS-A59 S C1304A, pCAGGS-A59 S C1303A/C1304A and pCAGGS-A59 S C1300A/C1303A/C1304A respectively, as templates. The same primers were used for all three subclonings: forward 5'-GGTGTTACTATAAGCTCGAGACTGCCAGACGG-3' and reverse 5'-CTGTCTTTCCTGCAGGGGCTGTGATAGTCAATCC- 3'.
- pcDNA3.1 SARS S_{C9} and pcDNA3.1 $ACE2_{C9}$ plasmids were obtained from Michael Farzan, Harvard Medical School, Boston, MA. Both SARS S (codon optimized version of strain Urbani) and ACE2 contain a C9 tag (GGTETSQVAPA) at their C-termini.

- pCDM8-NL63 S_{C9} plasmid was obtained from Hyeryun Choe, Harvard Medical School, Boston, MA. NL63 S contains a C9 tag (GGTETSQVAPA) at its C-terminus. This plasmid required propagation in *E. coli* strain MC1061/P3.
- pCDM8-NL63 S_{C9}-cl was generated by first synthesizing a 427bp stretch of DNA at GenScript Corporation. The synthetic DNA contained the mutations (NSS to RSR and IAG to RAR) and it was between unique restriction enzymes NotI and BstE2 sites. The synthetic DNA was cut out of pUC57 using NotI and BstE2 and ligated into pCDM8-NL63 S_{C9} that was already digested with NotI and BstE2.
- The pCDM8-NL63 S_{C9} R199K mutant was derived from pCDM8-NL63 S_{C9} using mutagenic primers and a site-directed mutagenesis protocol. (QuikChange® XL; catalog no. 200519-5; Stratagene). The following primers were used to introduce the R119K mutation in pCDM8-NL63 S_{C9} construct: forward 5'GACCACCCACAACGGCAAGGT GGTGAATTACACCG 3' and reverse 5'CGGTGTAATTCACCACCTTGCCGTTGTG GGTGGTC 3'.
- pcDNA 3.1 Ebola Zaire glycoprotein (Ebo GP) and pHEF-VSV G (VSV G) were obtained from Lijun Rong, University of Illinois Chicago, Chicago, IL.
- pNL4.3-Luc R-E- was obtained from the NIH AIDS Research and Reference Program # 3418.
- pRL-TK plasmid encoding renilla luciferase was purchased from Promega.
- pCAGT7 and pT7EMC-Luc plasmids (Okuma et al., 1999) were obtained from Richard Longnecker, Northwestern University Feinberg School of Medicine, Chicago, IL.

- pEGFP-N1 encoding a "red-shifted" variant of wild-type GFP for brighter fluorescence was purchased from Clontech. This plasmid was used routinely to measure transfection efficiencies in various cell types.
- TMPRSS2 cDNA containing a C-terminal FLAG epitope tag (DYKDDDDK) was PCR amplified using template pCMV-Sport6- TMPRSS2 (Open Biosystems) and primers: forward 5'-GGAGAGCTCCACCATGGCTTTGAACTCAGGGTC-3' and reverse 5'- CGACTCGAGCTACTTGTCATCGTCATCCTTGTAGTCTCCGCCG TCTGCCCTCAT – 3'. Subsequently, TMPRSS2 cDNA was cloned into pCAGGS.MCS between SacI and XhoI restriction sites.
- TMPRSS11a cDNA containing a C-terminal FLAG epitope tag (DYKDDDDK) was PCR amplified using template pCR-BluntII-TOPO-TMPRSS11a (Open Biosystems) and primers: forward 5'-GGAGAATTCCACCATGATGTATCGGACAGTAGG -3' and reverse 5'CGACCCGGGCTACTTGTCATCGTCATCCTTGTAGTCTCCGAT GCCTGTTTTTGAAG - 3'. Subsequently, TMPRSS11a cDNA was cloned into pCAGGS.MCS between EcoRI and XmaI restriction sites.
- TMPRSS11d cDNA containing a C-terminal FLAG epitope tag (DYKDDDDK) was PCR amplified using template pCR-BluntII-TOPO-TMPRSS11d (Open Biosystems) and primers: forward 5'- GGAGAATTCCACCATGTATAGGCCAGCACG -3' and reverse 5'CGACCCGGGCTACTTGTCATCGTCATCCTTGTAGTCTCCGATCCC AGTTTGTTGC – 3'. Subsequently, TMPRSS11d cDNA was cloned into pCAGGS.MCS between EcoRI and XmaI restriction sites.

- The catalytically inactive, pCAGGS-TMPRSS2(S441A)$_{FLAG}$ mutant was derived from pCAGGS-TMPRSS2$_{FLAG}$ using mutagenic primers and a site-directed mutagenesis protocol. (QuikChange® XL; catalog no. 200519-5; Stratagene). The following primers were used to introduce the S441A mutation in pCAGGS-TMPRSS2$_{FLAG}$ construct: forward 5' GCCAGGGTGACGCTGGAGGGCCTCTGG TC 3' and reverse 5' GACCAGAGGCCCTCCAGCGTCACCCTGGC 3'.

Methods

Virus Propagation, Harvesting, Storage, and Titer

MHV-A59 viruses were produced in murine 17cl1 cell cultures. Cells were infected when ~ 80% confluent with virus multiplicities of 0.01 to 1 plaque forming unit (PFU)/cell. Viruses were adsorbed on the cells for 1 hour at 37^{o}C in serum-free DMEM. Subsequently, the inoculums were replaced with complete DMEM-5% FBS and cell supernatants containing progeny viruses were collected 17-20 hours post-infection (hpi). Cellular debris was removed by centrifugation at 2000 x g for 10 minutes, and subsequently the viruses were aliquoted and stored at -80^{o}C.

Viral infectivities were determined by standard plaque assay using 17cl1 as indicator cells. Briefly, cells seeded in 6-well cluster plates at ~ 80% confluency were overlaid with serial dilutions of virus in serum-free DMEM. Virus was adsorbed for 1 hour at 37^{o}C and subsequently the inocolum removed and replaced with DMEM-2% FBS, 0.5% Noble Agar. Following incubation for 2-3 days, the cells were fixed in 37% w/w formaldehyde solution in saline for a minimum of 1 hour. Agar plugs were removed

by extensive rinsing and cells stained with 0.1% crystal violet in saline for a minimum of 30 minutes. Following rinsing of the crystal violet, individual plaques were counted. When viruses required plaque purification, following the 2-3 incubation, individual plaques were picked by punching out the agar plugs with a sterile pipette p200 tip and diluting the agar in 1 mL of DMEM-10% FBS.

Generation of Recombinant Viruses

Recombinant (r) MHVs were created via targeted RNA recombination (Kuo et al., 2000). Mutations in the pMH54-E-FL-M construct (Boscarino et al., 2008) were created using site directed mutagenesis, as described above. The plasmid DNAs were linearized by digestion with PacI enzyme and used as templates for in vitro transcription reactions using T7 RNA polymerase and reagents from Ambion (mMESSAGE mMACHINE®; catalog no. AM1344). Transcripts were electroporated into ~10^7 feline FCWF cells that were infected 4 h earlier with recombinant coronavirus feline MHV-A59 (Kuo et al., 2000) using a Bio-Rad Gene Pulser II. The electroporated FCWF cells were added to a monolayer of ~10^6 17cl1 cells. Recombinant viruses, identified by syncytia development on 17cl1 cells, were then collected from media and isolated by three cycles of plaque purification on 17cl1 cells.

Sequencing of recombinant viruses

Mutations fixed into the rMHVs were confirmed by reverse transcription PCR and sequencing. Briefly, cytoplasmic RNA was harvested from infected 17cl1 cells at 20 h post-infection, using an RNeasy Mini Kit (Qiagen; catalog no. 7414). Then, reverse transcription of the RNA was performed using the Ambion retroscript kit (catalog no.

AM1710) and oligo(dT) primers. PCR amplification of a 380 bp fragment spanning the intended site-directed mutations was performed using the following primers: forward 5'GAATCAAGACGTCTATTGCGCC 3' and reverse 5'CTGTCTTTCCTGCAGGGGC TGTGATAGTCAATCC 3'. The PCR fragment was subsequently sequenced to confirm mutations.

Radiolabeling and Virus Purification

Viruses were adsorbed to 17cl1 cells at a multiplicity of infection of 1 PFU/cell for 1 h at 37^{o}C in serum-free DMEM, then aspirated and replaced with DMEM supplemented with 5% FBS. At 12 hpi, media were removed and cells rinsed extensively with saline (0.9% NaCl). For radiolabeling with ^{35}S amino acids, cells were first incubated for 30 min at 37^{o}C in labeling medium (methionine- and cysteine-free DMEM containing 1% dialyzed FBS). The cells were then replenished with labeling medium containing 60 μCi per ml ^{35}S translabel (MP Biomedicals, Irvine, CA) and incubated for 4 h at 37^{o}C. Media collected from infected cell cultures were centrifuged for 10 min at 2,000 x g, then for 20 min at 20,000 x g and then overlaid on top of discontinuous sucrose gradients consisting of 5 ml 30% and 2 ml 50% (wt/wt) sucrose in HNB buffer (50mM HEPES [pH 7.4], 100mM NaCl, 0.01% BSA). Virions were equilibrated at the 30%-50% sucrose interface, using a Beckman Spinco SW41 rotor at 40,000 rpm for 2 h at 4^{o}C, and recovered by fractionation from air-gradient interfaces.

Determination of Virus Specific Infectivity

^{35}S-radiolabeled viruses were purified and banded between 30%-50% sucrose as described above. Following centrifugation, I collected 1 ml fractions starting from the

air-liquid interface. 30 μL from each fraction was evaluated biochemically by SDS-PAGE followed by autoradiography. Briefly, following electrophoresis of proteins present in each fraction, the SDS gel was fixed in fixing solution (10% glacial acetic acid, 25% methyl alcohol) for 1 h at room temperature. The fixed gel was allowed to dry before exposing to blue ultra autorad film (BioExpress F-9029). Typically 2 days at -80^{o}C were allowed for film exposure. To determine the amount of radioactivity in each fraction, 4 μl from each fraction was subjected to scintillation counting. The fraction containing the highest counts per minute (CPM) and the highest amount of viral proteins, was selected to be tittered on 17cl1 cells, as described above. Virus specific infectivity was determined as the ratio of plaque forming units (PFU) to CPM.

Generation of Viral-Like Particles

To produce viral-like particles (VLPs), 293T cells were co-transfected via calcium phosphate (Graham and van der Eb, 1973; Wigler et al., 1978) with equal DNA amounts of pCAGGS-A59 M, pCAGGS-A59 E, pCAGGS-A59 S, and pCAGGS-A59 N constructs. At 40 h post-transfection, the media above cells were collected and subjected to centrifugation at 2000 x g for 10 minutes to remove cellular debris. To concentrate VLPs for biochemical analysis, the media were overlaid on top of a 30% sucrose cushion in HNB buffer and centrifuged at 70,000 rpm for 20 min at 4^{o}C using a TLA 100.3 rotor. Pelleted particles were resuspended in electrophoresis sample buffer and processed by immunoblotting as described below. MHV-A59 S proteins were detected with murine monoclonal antibody (MAb) 10G (Grosse and Siddell, 1994) (1:2000 in TBS-T). MHV-

A59 M proteins were detected with murine MAb J.3.1 (Fleming et al., 1983) (1:500 in TBS-T). MHV-A59 N proteins were detected with murine MAb J1.3 (1:300 in TBS-T).

Immunoprecipitations and Immunoblotting

To evaluate S-M associations, 293T cells were co-transfected via calcium phosphate with pCAGGS-M and pCAGGS-S constructs. At 40 h post-transfection the cell monolayers were lysed in HNB buffer containing 0.5% NP-40, 0.5% sodium deoxycholate (DOC) and 0.1% protease inhibitor (Sigma P2714). Cell lysates were first clarified by centrifugation at 2,000 x g for 5 min then 160'000 cell equivalents were mixed with 0.01 ml of 1 mg/ml N-CEACAM-Fc (Gallagher, 1997) and 0.06 ml protein G magnetic beads (NEB Corporation, Inc.) for 2 h at 25^{o}C. Beads were rinsed three times with HNB buffer containing 0.5% NP-40, 0.5% sodium deoxycholate (DOC). Proteins were eluted from beads by addition of electrophoresis sample buffer (0.125 M Tris [pH 6.8], 10% dithiothreitol, 2% sodium dodecyl sulfate [SDS], 10% sucrose, 0.004% bromophenol blue) and heating to 95^{o}C for 5 min and subsequently subjected to SDS-polyacrylamide gel electrophoresis (SDS-PAGE). SDS gels were transferred to polyvinylidene difluoride membranes that were subsequently blocked for 1 h with 5% nonfat milk powder in TBS-T (25mM Tris-HCl [pH 7.5], 140mM NaCl, 2.7 mM KCl, 0.05% Tween 20). MHV-A59 S proteins were detected with murine monoclonal antibody (MAb) 10G (Grosse and Siddell, 1994) (1:2000 in TBS-T). MHV-A59 M proteins were detected with murine MAb J.3.1 (Fleming et al., 1983) (1:500 in TBS-T).

To evaluate ACE2-TMPRSS2 associations, 293T cells were co-transfected via calcium phosphate with pcDNA3.1-ACE2$_{C9}$, pcDNA3.1 empty vector, pCAGGS.MCS

empty vector, pCAGGS-TMPRSS2$_{FLAG}$, and pCAGGS-TMPRSS2(S441A)$_{FLAG}$ in the indicated combinations. At 35 h post-transfection the cell monolayers were lysed in HNB buffer containing 0.5% NP-40, 0.5% DOC and 0.1% protease inhibitor (Sigma P2714). Cell lysates were first clarified by centrifugation at 2,000 x g for 5 min then 150'000 cell equivalents were mixed with either 0.9 μg anti-FLAG antibody (Sigma, catalog no. F7425), 0.9 μg 1D4 antibody, or 0.9 μg mouse IgG and 0.06 ml protein G magnetic beads (NEB Corporation, Inc.) for 14 h at 4^{o}C. Beads were rinsed three times with HNB buffer containing 0.5% NP-40, 0.5% DOC. Proteins were eluted from beads by addition of electrophoresis sample buffer and heating at 95^{o}C for 5 min. ACE2$_{C9}$ proteins were detected with 1D4 antibody (1:5000 in TBS-T). TMPRSS2$_{FLAG}$ and TMPRSS2(S441A)$_{FLAG}$ proteins were detected with rabbit anti-FLAG antibody (1:1000 in TBS-T).

Pseudotyped Virions and Transductions

To generate pseudotyped HIV particles, 293T cells were co-transfected via calcium phosphate (Graham and van der Eb, 1973; Wigler et al., 1978) with pNL4.3-Luc R-E- (NIH AIDS Research and Reference Program # 3418) and the various envelope constructs. For a 10 cm dish containing ~ 6 x 10^6 cells, 5 μg of pNL4.3-Luc R-E and 5 μg of plasmid encoding the spike of interest were used. When producing HIV-bald particles, 5 μg of pCAGGS.MCS was used in place of spike encoding vector. After 2 days, media were collected, clarified for 10 min at 2,000 x g, then overlaid on top of a 30% sucrose cushion in HNB buffer and centrifuged at 40,000 rpm for 2 h at 4^{o}C using a Beckman SW41 rotor. Pelleted particles were resuspended in HNB buffer and stored at -80^{o}C.

Alternatively, the media containing pseudoparticles were collected, clarified for 10 min at 2,000 x g, and then stored at -20^{o}C.

For biochemical analysis, pelleted HIV pseudoparticles were resuspended in electrophoresis sample buffer and processed by immunoblotting as described above. MHV-A59 S proteins were detected with murine monoclonal antibody (MAb) 10G (Grosse and Siddell, 1994) (1:2000 in TBS-T). SARS-CoV S and HCoV-NL63 S proteins were detected using anti-C9 tag (1D4) antibody (1:5000 in TBST-T) obtained from Hyeryun Choe, Harvard Medical School, MA HIV capsid protein (p24) was detected with murine MAb α-p24 (NIH AIDS Research and Reference Program) (1:5000 in TBS-T).

For transductions, HIV particles, normalized to p24 levels, were adsorbed to HeLa-CEACAM cells in serum-free DMEM for 2 h. Subsequently, the inoculum was removed and replaced with DMEM supplemented with 10% FBS. At 2 d post-transduction, the cells were rinsed with saline and dissolved in luciferase lysis buffer (Promega E397A). Luminescence was measured upon addition of luciferase substrate (Promega E1501) using a Veritas microplate luminometer (Turner BioSystems). In other experiments, HIV particles were concentrated into 293T cells by centrifugation at 1600 x g for 2 h at 25^{o}C, a process known as spinoculation. Subsequently, the inoculum was removed and replaced with DMEM supplemented with 10% FBS. Luminescence was assayed as described above.

Protease Digestion Assay

For the protease digestion assay (Matsuyama and Taguchi, 2002), 10^4 PFU of rA59 coronavirus in 20 μL DMEM supplemented with 5% FBS or HIV pseudoparticles in 20 μL HNB buffer, were incubated with N-CEACAM-Fc (2μM) for various times at 37^{o}C. After samples were placed on ice for 10 min, proteinase K (Sigma) was added at a final concentration of 10 μg/ml and digestion was carried out at 4^{o}C for 20 min. Reactions were terminated by addition of electrophoresis sample buffer and subjected to SDS-PAGE and immunoblotting as described above.

Cell-Cell Fusion Assay

Cell-cell fusion was performed as described previously (McShane and Longnecker, 2005). Briefly, effector cells (HeLa) were transiently transfected with pCAG-T7 polymerase and the various pCAGGS-S constructs using Lipofectamine 2000 reagent (Invitrogen). Target cells were generated by Lipofectamine-transfection of HeLa-CEACAM cells with pT7pro-EMC-luc which encodes firefly luciferase under T7 promoter control (Aoki et al., 1998). At ~6 h post-transfection the target cells were quickly trypsinized and added to adherent effector cells in a 1:1 effector: target cell ratio. After a ~4 h co-cultivation period, luciferase levels were quantified as described above.

In other experiments, effector cells (293T) were transiently transfected with pCAG-T7 pol and pcDNA3.1-SARS S via calcium phosphate. Target cells were generated by co-transfection of 293T cells with pT7EMC-luc which encodes firefly luciferase under T7 promoter control, pcDNA3.1-ACE2$_{C9}$ and pCAGGS-TMPRSS2$_{FLAG}$. At ~24 h post-transfection the target cells were quickly trypsinized and added to adherent

effector cells in a 1:1 effector: target cell ratio. After a ~3 h co-cultivation period, luciferase was read as described above.

Transductions in the Presence of HR2 Peptides

The HR2 peptide (NVTFLDLTYEMNRIWDAIKKLNESYINLKE) was synthesized from GenScript Corporation at a 90.0% purity. The lyophilized powder was dissolved in ddH_2O to a final 2mM concentration and stored at -20^oC. In our experiments, the stock HR2 peptide was diluted to a final concentration of 25 μM in serum-free DMEM.

Drug Treatments during Transductions

Target 293T cells seeded in 6-well plates were co-transfected with pcDNA3.1-$ACE2_{C9}$ and pRL-TK along with pCAGGS-$TMPRSS2_{FLAG}$ or pCAGGS.MCS via calcium phosphate. Two days post-transfection the cells were incubated with Bafilomycin A1 (Sigma) at 300 nM or NH_4Cl (Sigma) at 25 mM concentrations in complete DMEM media for 1 hour at 37^oC. Parallel cultures were incubated in DMSO and water, the vehicle controls for stock Bafilomycin A1 and NH_4Cl, respectively. After the 1 hour incubation, HIV-SARS S particles in complete media were spinoculated onto the target cells in presence of endosomotropic agents. Following spinoculation, the cells were incubated at 37^oC for another 27 h until lysis and evaluation of both renilla and firefly luciferase accumulations (E1910, Promega).

Integrin β1 siRNA Knockdown

The integrin β1 custom siRNA with the following sequence: sense strand (GCG CAUAUCUGGAAAUUUGtt) and antisense strand (CAAAUUUCCAGAUAUGCGC

tt) was purchased from Ambion (catalog no. AM16100). I resuspended the individual siRNAs (sense and antisense) in nuclease free water and annealed the two strands together to a final siRNA concentration of 20 μM. The negative control non-target siRNA (50 μM) was also purchased from Ambion (catalog no. AM4642). To transfect siRNA duplexes into cells, I used Lipofectamine RNAiMax reagent (Invitrogen, catalog no. 13778) following Invitrogen's guidelines. A final RNAi concentration of 10 nM was used for each transfection. The efficiency of RNAi knockdown was evaluated by immunoblotting with anti-integrin β1 monoclonal antibody (MAb 1965, Millipore) at 1:1000 in TBS-T.

Immunofluorescence Microscopy

Immunofluorescence microscopy was performed by Taylor Heald-Sargent as described below. 293T cells seeded onto fibronectin coated coverslips were co-transfected via Polyethylenimine (PEI) with a constant amount of pcDNA3.1-ACE2$_{C9}$ and varying doses of pCAGGS-TMPRSS2$_{FLAG}$. At 24 hours post-transfection the cells were fixed with 3.7% formaldehyde (Polysciences) in 0.1 M PIPES [piperazine –N,N'-bis(2-ethanesulfonic acid)], pH 6.8. Following blocking with 10% donkey serum the coverslips were incubated with primary antibodies in PBS containing donkey serum. Cell surface ACE2 was detected using SARS-RBDFc while TMPRSS2 was detected using rabbit anti-FLAG antibody (Sigma, catalog no. F1804). The SARS-RBD$_{Fc}$ protein contained a 15 amino acid CD5 signal sequence and residues 318 to 510 of SARS spike in a modified pCEP4 vector. SARS-RBD$_{Fc}$ protein was produced in 293-EBNA cells, harvested in serum free media, and purified using protein A sepharose beads (GE

Healthcare). After thorough washing in PBS the coverslips were incubated with secondary antibodies goat anti-human conjugated to AlexaFluor488 (Molecular Probes) and goat anti-mouse conjugated to Cy5 (Jackson Immunoresearch). Nuclei were visualized with DAPI stain (Invitrogen). Coverslips were mounted on slides with Fluoro-Gel (EMS) and visualized using a Deltavision deconvolution microscope.

SARS-CoV Infections

For authentic SARS virus infections 293T cells were transfected in duplicate via calcium phosphate with pcDNA3.1-ACE2C9 and each of the indicated pCAGGS-$TTSP_{FLAG}$ plasmids. At 20 hours post-transfection cells were infected with HCoV-SARS (Urbani) at a multiplicity of infection of 0.1. Subsequently, at 6 hpi one set of infected samples was dissolved in Trizol (Invitrogen) and total cellular RNA was harvested. SARS CoV N and human GAPDH-gene specific RNAs were quantified by real-time PCR using an ABI Prism7700 thermocycler and software. The following primers were used: for SARS-CoV nucleocapsid (N) gene, forward primer 5'ATATTAGGTTTTTACC CAGG-3' and reverse primer 5'-CTTGCCCCATTGCGTCCTCC-3'; for human GAPDH gene, forward primer 5'- CCACTCCTCCACCTTTGAC-3' and reverse primer 5'-ACCC TGTTGCTGTAGCCA-3'. The levels of SARS N gene amplicons were normalized to that of GAPDH amplicons. The other set of infected cell cultures were harvested at 24 hpi and protein lysates in electrophoresis sample buffer were evaluated by western blotting for SARS N using rabbit anti-SARS N antibody (Imgenex, IMG-549), SARS S using anti-SARS S antibody (Imgenex, IMG-541) and mouse anti-beta actin antibody

(Sigma). All work with infectious SARS-CoV was performed in a BSL3 laboratory at the University of Iowa.

Preparation, Isolation and Detection of DRMs

293T cells were transiently transfected via PEI with pCDNA3.1-$ACE2_{C9}$ (8 µg/7 x 10^6 cells) and pCAGGS-$TMPRSS2_{FLAG}$ (4 µg/7x10^6 cells). At 27 hours post-transfection the cells were incubated with 2 ml of media containing HIV-SARS S or HIV-bald particles for 1 h at 37°C. Subsequently the cells were thoroughly rinsed with ice-cold PBS and chilled to 4°C. To biotinylate surface proteins, the cells were incubated with Sulfo-NHS-LC-Biotin (Pierce Cat no. 21335) (1mg/ml in PBS), a membrane impermeable reagent with a spacer arm of 22.4 Å. Following rinsing twice in ice-cold PBS, the cells were lysed in 1 ml of cold TNE (50 mM Tris-HCl [pH 7.4], 100 mM NaCl, 1 mM EDTA) containing 0.2% Triton X-100 for 30 min at 4°C. Cell extracts were passed five times through a 27-gauge needle and subsequently pelleted (700 x g for 5 min). Postnuclear supernatants were mixed with equal volumes of 80% w/v sucrose in TNE-0.2% TX-100 containing protease inhibitors. Samples were placed into Beckman SW41 ultracentrifuge tubes, overlaid sequentially with 7 ml of 30% w/v and 2.5 ml of 5% w/v sucrose in TNE-0.2% TX-100. Following centrifugation at 4°C for 17 h at 32'000 x rpm in a Beckman SW41 rotor, 1.3 ml fractions were taken starting from the air-liquid interface. Fractions 3, 4, 8 and 9 were incubated with 10 µl Streptavidin magnetic beads in the presence of protease inhibitors for 8 h at 4°C. Following three washes with HN buffer containing 0.5% NP-40 and 0.5% DOC, the biotinylated proteins were eluted off beads by addition of electrophoresis loading buffer and heating at 95°C

for 5 min. $ACE2_{C9}$ proteins were detected with 1D4 antibody (1:5000 in TBS-T). $TMPRSS2_{FLAG}$ proteins were detected with rabbit anti-FLAG antibody (1:1000 in TBS-T).

Use of Cholera Toxin as a Marker for Lipid Rafts

The cholera toxin subunit B peroxidase conjugate (CTB-HRP) (Sigma C3741) was used as a marker of lipid rafts, since it is known to bind to ganglioside GM1, a known resident of lipid raft membrane domains. Prior to lysing in cold detergent, the cells were incubated with 580 µg conjugate of CTB-HRP in PBS for 1 h at 4°C. Subsequently the cells were rinsed with ice-cold PBS and subjected to lysing and further processing as described above. To detect CTB-HRP, I spotted 3 µl from each fraction into nitrocellulose membrane, rinsed the membrane with PBS and after addition of chemiluminescence reagents, the membrane was exposed to film.

Silver Staining of Lipid Raft Gradient Fractions

Analysis of the protein content in each fraction was done by silver staining (Pierce, catalog no. 24612). Briefly, after ~ 1/100 of each fraction was subjected to SDS-PAGE, the gel was rinsed in water and subsequently fixed in 30% ethanol/10% acetic acid for 30 min. Following two washes in 10% ethanol and incubation in sensitizer solution, the gel was silver stained for 30 minutes. Subsequently, the gel was developed and once the protein bands were distinct, the reaction was stopped using 5% acetic acid solution.

CHAPTER III

RESULTS

Spike Protein Palmitoylations as Virus Entry Factors

While the current view of viral protein-mediated membrane fusion is satisfying in many ways, important details are missing. For example, the importance of the TM and endodomain (ENDO) portions of the surface proteins demand more prominent attention in the membrane fusion models. Because these TM and ENDO regions are not structurally resolved, it can be difficult to accurately add them into the models. However, abundant literature indicates that TM-ENDO portions of many different virus fusion proteins do operate to control virus-cell and cell-cell fusion (Abrahamyan et al., 2005; Cathomen, Naim, and Cattaneo, 1998; Langosch, Hofmann, and Ungermann, 2007; Sakai, Ohuchi, and Ohuchi, 2002). For example, an influenza hemagglutinin fusion protein with a glycosylphosphatidylinositol (GPI) anchor replacing its TM-ENDO domains was able to mediate outer membrane leaflet fusions, i.e., hemifusion, but could not create full membrane fusions (Kemble, Danieli, and White, 1994). Moreover, the animal retrovirus envelope proteins contain long ENDO domains that include the "R peptides" that, once removed by proteolysis, facilitate the fusion reaction (Green et al., 1981; Yang and Compans, 1996). Furthermore, truncation of the human immunodeficiency virus (HIV) envelope ENDO tail modulates its fusogenicity (Wyss et al., 2005). Finally, it is notable that many viral fusion protein ectodomain fragments

lacking TM and ENDO domains fold spontaneously into post-fusion states (Markosyan, Cohen, and Melikyan, 2003; Yin et al., 2005), suggesting that membrane-anchoring parts help maintain functional metastable high-energy conformations.

It is not entirely clear how the intra-virion parts of the fusion protein influence reactions that are carried out by the much larger exterior portion of the protein. We and others consider it plausible that changes in the fusion protein endodomain impact refolding rates, which in turn control the route and timing of virus entry. This is because the transitions from pre-hairpin intermediate to post-fusion states requires large-scale transit of TM-ENDO domains across lipid stalks (Chernomordik and Kozlov, 2003) (see also Fig. 1 in INTRODUCTION), which may be a rate-limiting step in the process.

Coronaviruses provide a good model in which one can study the relationship between endodomain changes and fusion reaction kinetics. The spike protein endodomains are rich in cysteine residues, most or all of which are known to be stably thioacylated with palmitic acids (Bos et al., 1995; Chang, Sheng, and Gombold, 2000; Petit et al., 2007; Thorp et al., 2006). Interference with S endodomain palmitoylation diminishes or eliminates S-mediated membrane fusion activities (Bos et al., 1995; Chang and Gombold, 2001; Chang, Sheng, and Gombold, 2000; Thorp et al., 2006), but the mechanisms by which these endodomain alterations influence membrane fusion activities are unknown. In my dissertation research, I explored the mechanistic basis for these observations and further discovered that the endodomain cysteines and palmitoylations also influence S incorporation into virions. I will first describe the effect of endodomain cysteines on S incorporation into coronavirus particles.

Effect of Endodomain Mutations on S Incorporation into Virions

The MHV strain A59 S protein has nine cytoplasmic (endodomain) cysteines (Fig. 4). We mutated those cysteines most distal from the transmembrane span, the carboxy-terminal C1300, C1303 and C1304, to alanines, with the expectation that these changes would prevent S palmitoylation at these positions and thus untether the ends of the S tails from cytosolic membrane faces (Fig. 9).

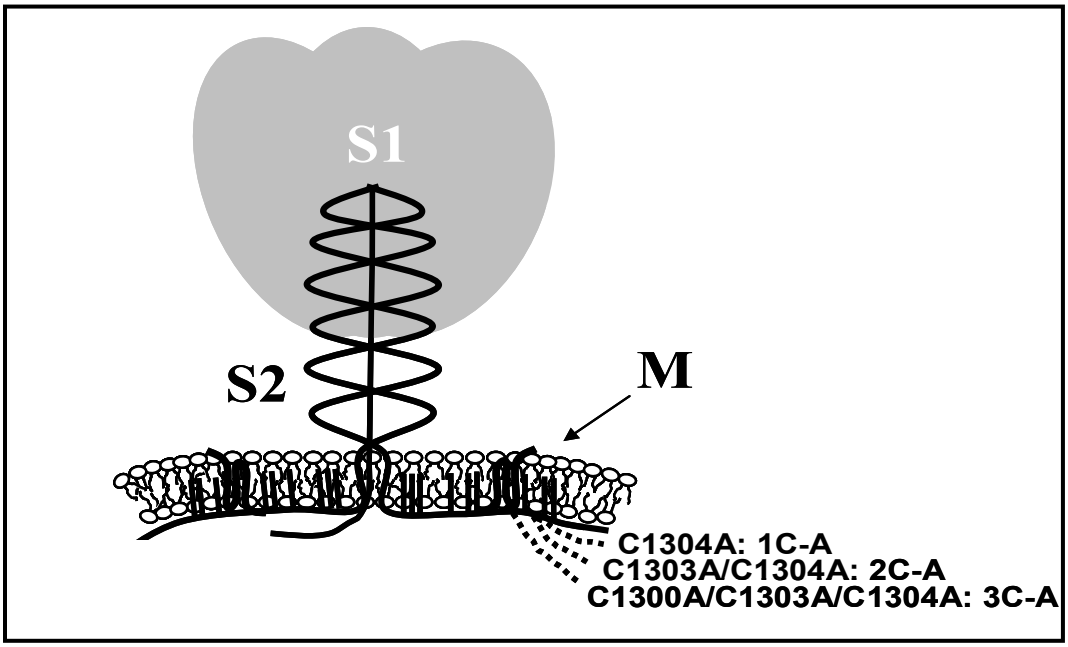

Fig. 9. Schematic Representation of the MHV-A59 S protein. The spike (S) trimer is depicted as peripheral S1 and integral-membrane S2 subunits. The S2 subunits are drawn in the context of a virion membrane and in association with membrane (M) proteins. Endodomain mutations preventing S acylation are illustrated on one S2 monomer. Loss of palmitoylation (black lines) and the hypothetical untethering of cytoplasmic tails from intravirion membrane leaflets are depicted by the dotted lines.

We discerned the functional consequences of these changes by first using our established corona virus-like particle (VLP) system (Boscarino et al., 2008). In this experimental design, 293T cells were co-transfected with pCAGGS plasmids encoding S, E, M and N proteins and subsequently radiolabeled with ^{35}S cysteine and ^{35}S methionine. Secreted ^{35}S-labeled VLPs were harvested from culture media, purified by density gradient ultracentrifugation and evaluated for radioactive protein content by SDS-PAGE and autoradiography.

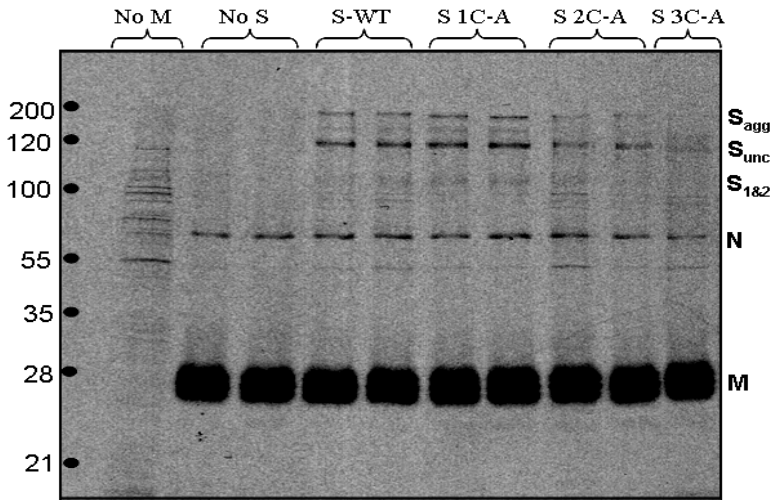

Fig. 10. Effect of S endodomain cysteine mutations on VLP incorporation. VLPs were metabolically radiolabeled with ^{35}S amino acids and purified by sucrose density gradient ultracentrifugation. Equal ^{35}S radioactivities were collected from each purified VLP preparation, electrophoresed on 10% SDS gel, and detected by autoradiography. S agg, S aggregates; S unc, uncleaved S; N, nucleocapsid protein; M, membrane protein. Molecular weights are shown in kilodaltons.

Our results (Fig. 10) reveal that substitution of endodomain cysteines with alanines reduced the levels of S incorporation into VLPs. Relative to standard VLPs,

those with C1304A (1C-A), C1303A/C1304A (2C-A) and C1300A/C1303A/C1304A (3C-A) had <5%, ~50%, and ~80% fewer spikes, respectively. No VLPs were assembled in the absence of M protein given that coronavirus assembly is fully dependent on M proteins (de Haan et al., 1998). On the contrary, normal levels of VLPs were synthesized in the absence of S protein, concurrent with the view that S protein is dispensable for assembly (Holmes, Doller, and Sturman, 1981; Rottier, Horzinek, and van der Zeijst, 1981).

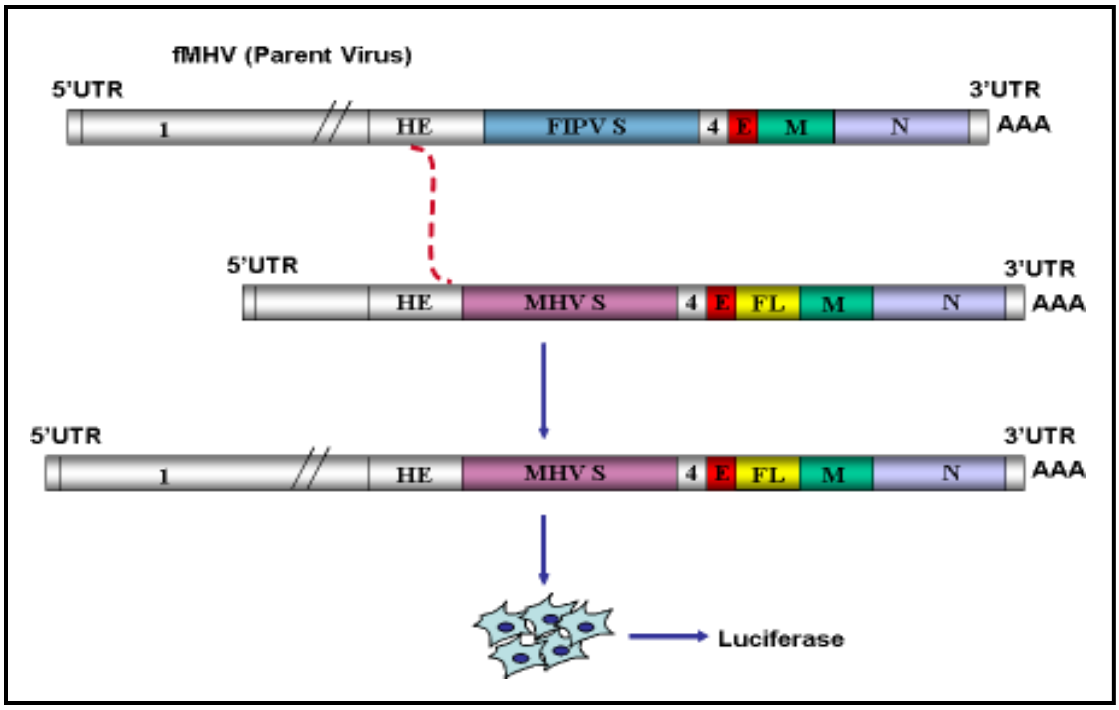

Fig. 11. Generation of Recombinant Reporter Viruses. This technique takes advantage of the high rate of homologous recombination by coronaviruses. The synthetic donor RNA containing the firefly luciferase (FL) gene was introduced into cells that were infected with the parent virus, fMHV. fMHV is a variant MHV virus in which the spike (S) is replaced by the FIPV S, so that the virus has lost the ability to grow in murine cells. Recombinant viruses containing the FL gene also reacquire the MHV S and thus can be selected by their ability to grow in murine cells.

Next, we wanted to assess whether endodomain mutant virions were depleted in S proteins, in accordance with the findings from VLPs. To this end, we used targeted RNA recombination to direct mutations into the MHV genome, thus creating a series of recombinant (r) MHV viruses harboring cysteine-to-alanine substitutions. The parent virus we used is a recombinant MHV- A59 strain engineered to produce firefly luciferase (FL) identical to that developed by de Haan and others (de Haan et al., 2003) (Fig. 11).

Biochemical evaluation of the newly generated recombinant viruses involved [^{35}S] radiolabeling of infected 17cl1 cell monolayers. [^{35}S]-virions were harvested from culture media, purified by density gradient ultracentrifugation, and evaluated for radioactive protein content by SDS-PAGE and autoradiography. Fig. 12 depicts the virion proteins associated with wild-type (WT) rA59 in comparison with C1304A (1C-A) and C1303A/C1304A (2C-A) rA59. The single mutant C1304A (1C-A) recombinant virions were indistinguishable from WT rA59 in these electrophoretic analyses (Fig. 12A). The 2C-A mutant virions were noticeably depleted in S protein content (11-fold relative to WT), as depicted in Fig. 12B. The triple mutant C1300A/C1303A/C1304A (3C-A) recombinant viruses were never isolated despite several attempts, suggesting that a threshold of spike density is required for virus viability.

An explanation for the reduced incorporation of endodomain mutant spikes into virions appeals to disruption of S protein interaction with M proteins, the M proteins being the key orchestrating agents in the virion assembly process (de Haan et al., 1999; Masters et al., 2006). Thus, we co-expressed the various spike constructs individually with M protein in 293T cells and subsequently dissolved cell monolayers in a buffer

containing both NP-40 and sodium deoxycholate, a detergent formulation known to preserve association between S and M proteins (Opstelten et al., 1995). S-M complexes were captured using the S-binding immunoadhesin N-CEACAM-Fc (Gallagher, 1997) and magnetic protein G beads. Eluted proteins were detected by Western blot using anti-S and anti-M antibodies and the results (Fig. 13) revealed that the poor incorporation of endodomain mutant spikes into recombinant virions correlated with their failure to efficiently associate with M proteins.

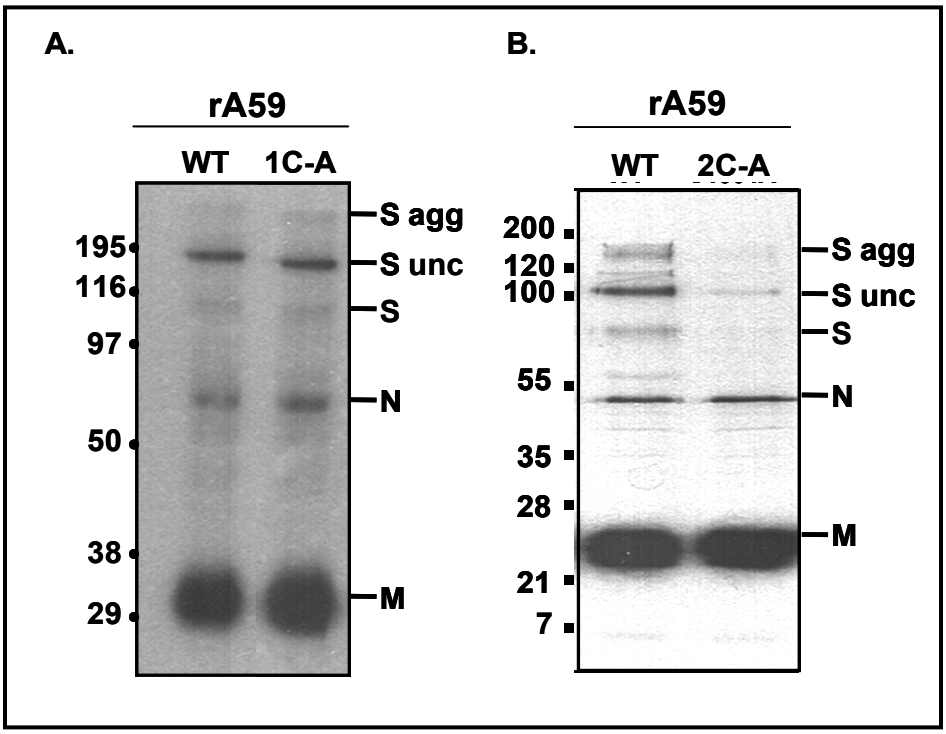

Fig. 12. Effect of S Endodomain Cysteine Mutations on Virion Incorporation. Recombinant virions were metabolically radiolabeled with ^{35}S amino acids and purified by sucrose density gradient ultracentrifugation. Equal ^{35}S radioactivities were collected from each purified virion preparation, electrophoresed on SDS gels, and detected by autoradiography. S agg, S aggregates; S unc, uncleaved S; N, nucleocapsid protein; M, membrane protein. Molecular weights are shown in kilodaltons.

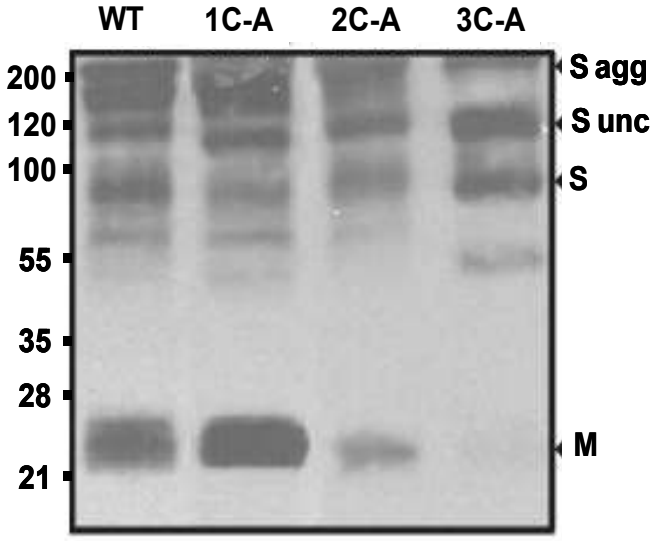

Fig. 13. Effect of S Endodomain Cysteine Mutations on Association with M Proteins. 293T cells co-expressing the indicated S constructs with M proteins were dissolved in NP-40/DOC buffer and S-M complexes were captured using an MHV soluble receptor immunoadhesin (nCEACAM-Fc) bound to magnetic protein G beads. Eluted proteins were detected by Western immunoblotting using S- and M-specific MAbs. S agg, S aggregates; S unc, uncleaved S. Molecular weights are shown in kilodaltons.

Further characterization of the recombinant viruses revealed that they had reduced specific infectivities (Table 4). Recombinant viruses with double, but not single, cysteine substitutions displayed significantly reduced specific infectivities, which could be attributed to the low abundance of S proteins on mutant virions, intrinsic defects on S protein fusogenic activity, or a combination of the two.

The reduced specific infectivities of the double cysteine mutant recombinant viruses correlated with their delayed entry kinetics into 17cl1 cells. We first assessed the entry kinetics of WT and 2C-A rA59 viruses by an endpoint dilution assay (Fig. 14A). Briefly, WT and 2C-A rA59 viruses at equal multiplicities of infection were bound to

17cl1 cells. Following removal of the unbound virus population, fresh culture media were added onto the cell monolayers and bound virus infections were allowed to proceed.

Mutant	Specific Infectivity (PFU/CPM)
S Standard	5.1
S C1300A	4.7
S C1303A	3.7
S C1304A	2.8
S C1300A/C1304A	0.66
S C1303A/C1304A	0.63
S C1300A/C1303A/C1304A	*

Table 4. Specific Infectivities of rA59 Viruses. Relative specific infectivities were determined for the indicated rA59 viruses by performing endpoint dilution plaque assays and relating infectivities to the ^{35}S content of the purified virion preparations. * not recoverable.

At different times post-infection, the media containing newly assembled virions were collected and titered onto 17cl1 cells. Despite the fact that the 2C-A mutant viruses bound to target cells with the same efficiency as WT rA59 viruses, they were unable to yield progeny virions in a timely fashion (Fig 14A). These data suggested that a post-binding entry event was delayed for 2C-A virions.

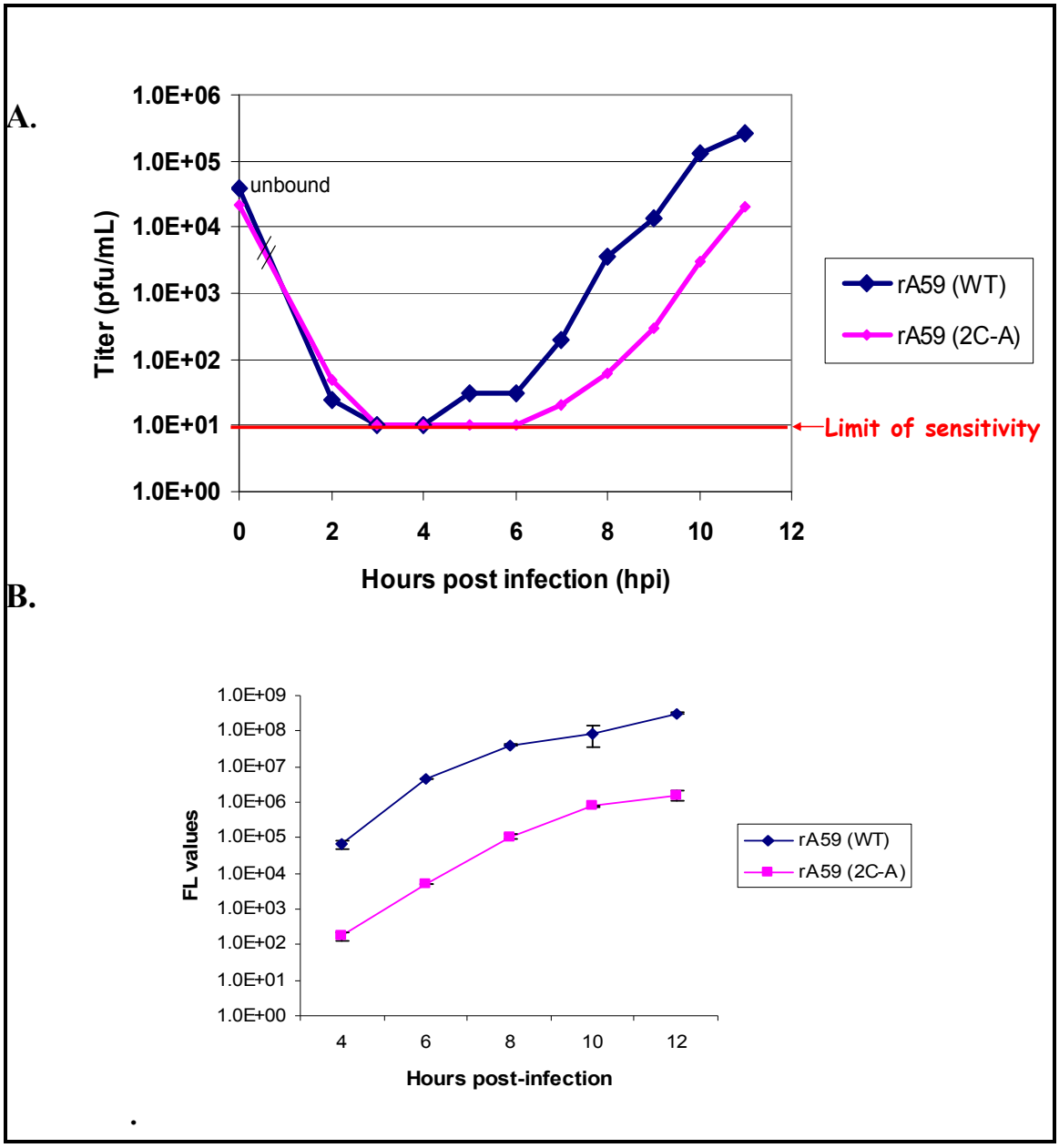

Fig. 14. Entry Kinetics of rA59 Viruses. A. The entry kinetics of rA59 (WT) and (2C-A) viruses was evaluated by assessing virus elution profiles. Briefly, virus particles were allowed to bind to 17cl1 cells for 1 hour at 4°C. Subsequently media containing unbound particles were removed and replaced with fresh media. At each time point the media containing newly released virions were collected and titered on fresh 17cl1 cells. **B.** The entry kinetics of rA59 (WT) and (2C-A) viruses was evaluated by measuring the accumulation of the luciferase reporter gene product that comes from a viral subgenomic RNA. At various times post infection the cells are lysed and luciferase activity is measured.

We also evaluated entry of WT and 2C-A rA59 viruses by a method that monitors viral RNA replication as early as 4 hours post-infection. Viral RNA replication was determined by measuring the accumulation of a luciferase reporter gene product, which is part of the recombinant virus genome (Fig. 11), at different times post-infection. The data revealed that the double cysteine mutant viruses were delayed in their entry kinetics compared to wild-type viruses despite equal input multiplicities (Fig. 14B).

Effect of Endodomain Mutations on S-Mediated Membrane Fusion

To investigate the role of endodomain cysteines on the membrane fusion reaction, we first performed cell-cell fusion assays. To this end, cells transfected with various pCAGGS-spike constructs were co-cultivated with target cells containing murine CEACAMs, the primary MHV receptors. Spike-bearing cells contained phage T7 polymerase and CEACAM cells harbored luciferase genes whose transcription required the T7 polymerases, making it so that luciferase enzyme activities increased in response to spike-induced cell-cell fusions. From these assays, we found that all spikes induced similar luciferase accumulations (Fig. 15). Thus, at least within a 4 h cell co-cultivation period, the various endodomain mutant spikes were equivalent in cell-cell fusion activities.

An inference from the results of cell-cell fusion assays is that the various spike proteins accumulate equivalently on cell surfaces. If so, then the spike proteins might incorporate equivalently onto HIV virus cores budding from plasma membrane sites (Cadd, Skoging, and Liljestrom, 1997), making HIV-coronavirus S pseudoparticles appropriate for virus-cell fusion assays. Such HIV-S pseudoviruses could replace

authentic rA59 coronaviruses for use in virus-cell fusion assays, the rA59 viruses being unsuitable for correlating endodomain changes with virus-cell fusion because of the confounding effect that these endodomain changes have on assembly of spikes into virions (Fig. 12).

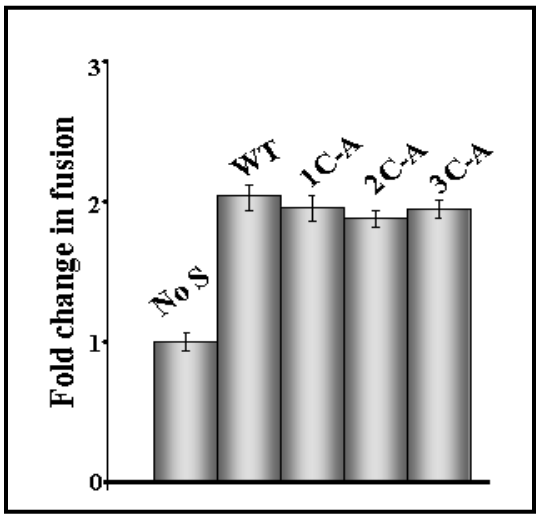

Fig. 15. Analysis of Coronavirus S-mediated Cell-Cell Fusion. The indicated S proteins were evaluated using assays involving luciferase reporter gene expressions as readouts of cell-cell fusion. Luciferase readings made 4 h after co-cultivation with fusion targets are plotted as fold change in fusion over the negative control lacking spike proteins.

HIV-CoV S pseudotype virions were produced by co-transfecting 293 cells with an envelope deficient HIV vector (pNL4-3-Luc-R-E) along with pCAGGS-S constructs. Released pseudoparticles were harvested from culture media, purified by sucrose gradient ultracentrifugation, and subjected to SDS-PAGE. The data (Fig. 16A) revealed that WT and endodomain mutant spikes did indeed incorporate into HIV particles with equal

efficiencies. However, when the HIV – S particles were used to transduce CEACAM receptor-bearing target cells, the single (1C-A) double (2C-A) and triple (3C-A) cysteine mutants were about 2, 20 and 40 times less efficient at delivering the HIV cores into cells, as measured by a luciferase reporter that is part of the recombinant HIV genome (Fig. 16B). These data indicate that endodomain cysteines, and most likely their palmitate adducts, are specifically needed to facilitate effective virus-cell fusion.

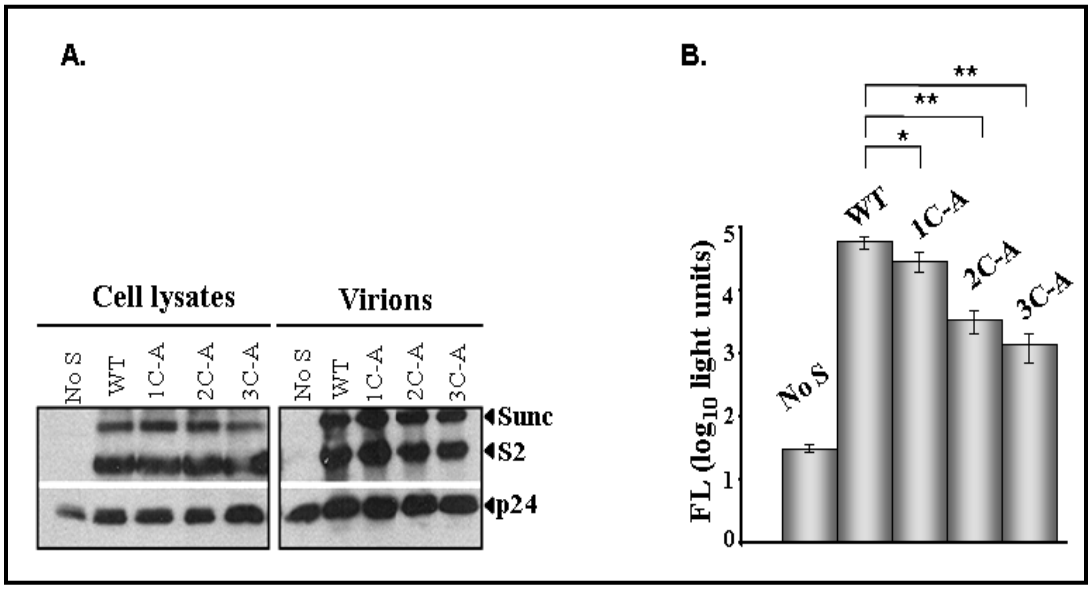

Fig. 16. Analysis of Coronavirus S-mediated Transduction Potentials. A. Pseudotyped HIV particles were produced in 293T cells by co-transfection of plasmid DNAs encoding the indicatesd spikes together with the HIV vector (pNL4.3-Luc R-E-). Released particles were harvested from culture media and concentrated by pelleting through 30% sucrose. Proteins present in cell lysates and in virion particles were detected by immunoblotting using S- and p24-specific MAbs. **B**. HIV particles normalized to p24 content were used to transduce HeLa-CEACAM cells. Two days post-transduction, the cells were lysed and luciferase activities assayed as described in Materials and Methods. *, $p<0.05$; **, $p<0.002$ (Student's t-test for independent samples).

I decided to investigate the mechanism by which these endodomain mutations suppressed virus entry. One possibility is that S-mediated entry was impaired because endodomain mutations reduced the affinity of S ectodomains for CEACAM receptors. To address this speculation, I produced highly-purified [^{35}S] WT and 2C-A rA59 virions and assessed their immunoprecipitation with N-CEACAM-Fc. In 1 h, 4^{o}C incubation periods, the ^{35}S radioactivities that were captured varied by <10% between WT and 2C-A virions. Furthermore, I observed no significant differences in the association of [^{35}S]-labeled WT and nC-A pseudovirions to CEACAM-bearing host cells (data not shown).

Given that the endodomain mutations had no obvious effect on receptor interactions, their suppression of virus entry was likely at the level of membrane fusion. To address this possibility and to evaluate S-mediated fusion in detail, I monitored S protein refolding events with an HR2 peptide that was previously shown to be a potent fusion inhibitor (Bosch et al., 2003). The HR2 peptide used (NVTFLDLTYEMNRIQ DAIKKLNESYINLKE) corresponds to residues 1225-1254 of the MHV strain A59 spike. The view is that HR2 peptides bind exposed HR1 trimers, thereby occluding the *cis* refolding of endogenous HR2 helices onto HR1, preventing 6-HB formation, membrane fusion, and virus entry (Chan and Kim, 1998; Furuta et al., 1998). These exposed HR1 trimers are present only in transitional S protein folding states; in support of this statement, I found that HR2 peptides could be incubated indefinitely with virions at 50 μM (50 x EC50) (Bosch et al., 2004) at 37^{o}C, and after diluting to 0.5 nM (0.0005 x EC50) exert no inhibition on plaque development.

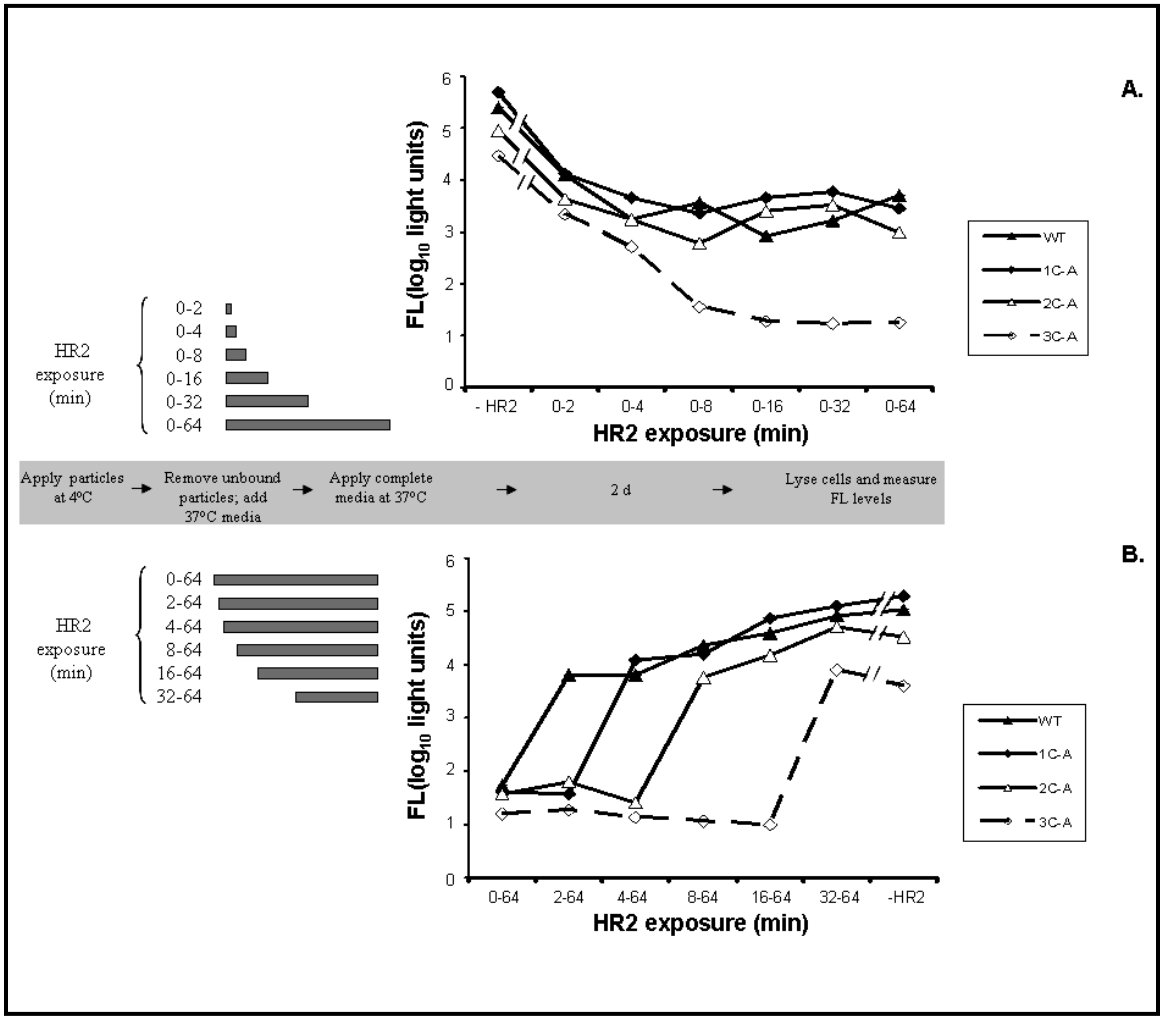

Fig. 17. Time Course of Entrance Into and Exit from HR2-sensitive Folding States. HIV particles normalized to p24 content were pre-bound to HeLa-CEACAM cells at 4°C for 1 hour. Unbound particles were then aspirated and 37°C serum free DMEM with or without HR2 peptide (25μM) were added to the cells. The HR2 peptides were subsequently removed at 0, 2, 4, 8, 16, and 32 min time intervals (**A**) or added at 0, 2, 4, 8, 16, and 32 min time intervals after the temperature shift (**B**). At the 64 min time point, all cells were rinsed, replenished with DMEM supplemented with 10% FBS, and luciferase accumulations were assayed 2 days post-transduction.

In my experiments, I used the HR2 peptide as a tool to monitor the exposure of HR1 (reflecting S unfolding) and subsequent disappearance of HR1 (reflecting S

refolding into post-fusion 6-HBs) during virus entry into cells. In this experimental design, I applied HIV-S pseudoparticles to CEACAM-bearing HeLa cells at 4°C and incubated to equilibrium. Unbound particles were aspirated and replaced with pre-warmed 37°C media, as the 37°C temperature is required for fusion and for S protein conformational changes (Krueger et al., 2001; Zelus et al., 2003). Then, the HR2 peptide (25 μM) was added at the 37°C temperature shift and subsequently removed at 0, 2, 4, 8, 16, 32, 64 min time intervals (Fig. 17A) or added at early 0, 2, 4, 8, 16, 32, 64 min time intervals post the temperature shift (Fig. 17B). At the 64 min time point, all cells were rinsed, replenished with complete media, and then assayed 40 h later for accumulated luciferase, which served as the readout for S-mediated pseudovirus entry.

When HR2 peptide was present from 0-64 min after the 37°C temperature shift, WT S-mediated infection was blocked by more than 1,000-fold (Fig. 17B). However, when HR2 peptide was present from 2-64 min, blockade was only about 20-fold, suggesting that ~ 5% of the entry-related WT S protein refolding events took place within the first 2 min after 37°C temperature shift. When HR2 was added after 16 min at 37°C, blockade was only 2 to 3-fold, again suggesting that ~ 30-50% of entry was completed within 16 min. Quite strikingly, and in sharp contrast to the rapid refolding of the wild type S proteins, the single (1C-A), double (2C-A) and triple (3C-A) endodomain mutant pseudoviruses were more sensitive to inhibition by HR2 peptides added late after 37°C temperature shift, with the extent of this sensitivity to HR2 inhibition correlating directly with the degree of C-A substitution. Entry mediated by the triple mutant S proteins was completely inhibited by HR2 peptides added as late as 16 min after the 37°C shift,

suggesting that the HR1 tri-helix either exposed itself in delayed fashion and / or remained exposed for remarkably prolonged periods in relation to the wild type protein. A reasonable speculation is that this slower fusion kinetics accounted for the general inefficiencies of the endodomain-mutant S proteins in mediating virus entry (Fig. 16B). This same degree of slower fusion kinetics is not revealed by the much longer 4 h cell-cell fusion assay (Fig. 15).

The kinetics of S protein refolding was further examined using a biochemical approach. A distinct experimental advantage of the coronaviruses is that their S proteins can be triggered to refold into 6-HBs in reductionist *in vitro* assays, by relatively simple exposure to soluble receptors at 37^{o}C temperature (Matsuyama and Taguchi, 2002; Zelus et al., 2003). The resulting 6-HBs, being extraordinarily stable (Yan, Tripet, and Hodges, 2006) can be visualized in Western blots as ~58 kDa protease resistant bands (Matsuyama and Taguchi, 2002). I incubated wild-type and double cysteine mutant (2C-A) virions with soluble receptor (N-CEACAM-Fc) at 4^{o}C, and once at equilibrium, shifted to 37^{o}C for various time periods. Increased levels of 6-HBs were observed with 37^{o}C incubation time (Fig. 18A). Far more striking was the finding that the endodomain mutant 2C-A S proteins were less prone to advancing into 6-HB configurations (Fig. 18A). Similar experiments performed with HIV-S pseudoviruses generated corroborating findings of diminished 6-HBs in 2C-A and 3C-A S proteins (Fig. 18B). The distal carboxy-terminal cysteines, and/or their palmitate adducts, increase the facility of S-mediated refolding into post-fusion forms.

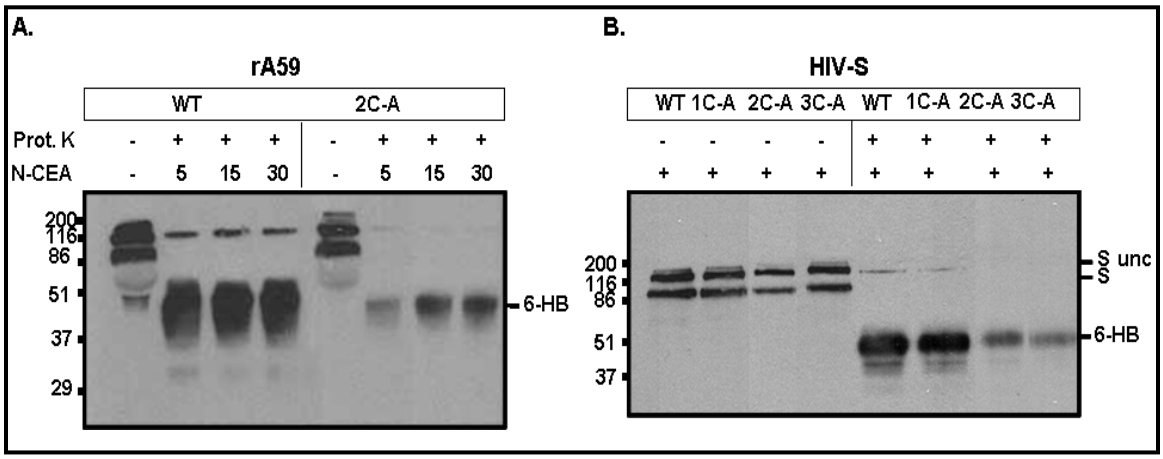

Fig. 18. Effect of Endodomain Cysteine Mutations on the Formation of Post-fusion 6-HB Hairpin Conformations. A. Wild-type and double cysteine mutant (2C-A) rA59 viruses in DMEM supplemented with 5% FBS were incubated with 2μM soluble receptor (N-CEACAM-Fc) at 37°C for 5, 15, 30 minutes. Subsequently, proteinase K (Prot. K) was added to the indicated samples (final concentration 10 μg/ml) and all reactions were incubated for 15 min at 4°C. The protease digestion was halted by addition of electrophoresis sample buffer and samples were immediately subjected to Western immunoblotting. S unc, uncleaved S; 6-HB, protease resistant 6-HB. Molecular weights are shown in kilodaltons. **B.** Concentrated HIV particles in HNB buffer were incubated with 2 μM soluble receptor for 5 minutes at 37°C. Proteinase K digestion, quenching and immunoblotting were performed as described above.

Proteolytic Activation of Coronavirus Entry by Type II Transmembrane Proteases

The membrane fusion process requires an S protein conformational flexibility that is facilitated by proteolytic cleavages. The MHV-S proteins, which were discussed in the previous section, undergo cleavage activation in producer cells during virus assembly (Sturman, Ricard, and Holmes, 1985). On the contrary, the SARS S proteins do not get cleaved in virus producer cells and rely on target cell proteases for their activation

(Simmons et al., 2005). Here we describe the type II transmembrane serine proteases (TTSPs) and more specifically TMPRSS2 as a novel SARS-CoV activating protease.

Effect of TTSPs on Pseudovirus Transductions

Three of the 17 known human TTSPs, TMPRSS2, TMPRSS11a and TMPRSS11d (also known as Human Airway Trypsin or HAT) were selected for study because they are expressed in human lungs and are known to activate cell entry of selected influenza virus strains (Bottcher et al., 2006; Chaipan et al., 2009). On transfection of the three FLAG-tagged TTSP cDNAs into 293T cells, all synthesized FLAG-tagged proteins of the expected molecular weights (Fig. 19). TTSPs are synthesized as inactive single-chain proenzymes (zymogens) and undergo self cleavage into active forms during or after transport to cell surfaces (Afar et al., 2001; Miyake et al., 2009). Cell-associated C-terminal cleavage fragments were observed for TMPRSS11a and 2, but not for 11d, perhaps because the 11d member sheds its peripheral enzymatic domain into extracellular media (Yasuoka et al., 1997). To confirm that the cleaved forms of one TTSP, TMPRSS2, were indeed generated by autocatalytic activity, I generated an inactive mutant harboring a serine to alanine substitution at position 441 (S441A) (Afar et al., 2001). As expected, the $TMPRSS2_{S441A}$ mutant was only present as a full-length ~ 70 kDa zymogen form (Fig. 19).

To reveal the effect of TTSPs on HCoV entry, I co-transfected 293T cells with constant amounts of $ACE2_{C9}$ plasmid along with varying doses of the different $TTSP_{FLAG}$ plasmid DNAs. After two days, these cells were transduced by HIV-SARS S pseudoviruses, as measured by the accumulation of a luciferase reporter gene product that

is encoded in the HIV transducing vector. We selected 293T cells as targets because they support early HIV infection events and because they do not express endogenous TMPRSS2 or 4 (Afar et al., 2001; Bertram et al., 2010; Chaipan et al., 2009).

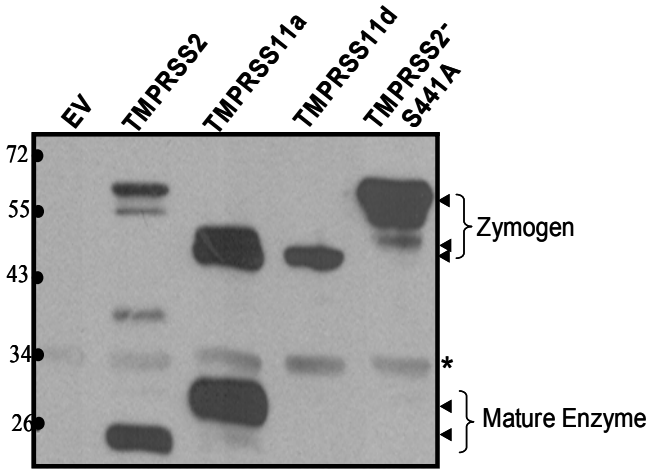

Fig. 19. TTSP Expression into 293T Cells. Cells transfected with pCAGGS plasmids encoding the indicated FLAG-tagged TTSP constructs were lysed at 2 d post-transfection and proteins were evaluated by western immunobloting with anti-FLAG antibodies. Triangles mark the full-length zymogen and mature enzyme forms. The asterisk is next to a non-specific 34 kDa band.

All three TTSPs enhanced SARS S-mediated pseudovirus entry. The augmenting effects varied, with TMPRSS2 > TMPRSS11d > TMPRSS11a (Fig. 20A). Peak effects of TMPRSS2 and TMPRSS11d were observed after 0.2 μg DNA transfection and then declined at the higher 1 μg DNA dose; this was presumably due to toxicities generated by TTSP overexpression. HIV transductions mediated by Vesicular Stomatitis Virus Glycoprotein (VSV G) and Ebola Zaire Glycoprotein (Ebo GP) spikes were not affected

by the presence of TMPRSS2 (Fig. 20B), indicating that this particular TTSP exhibits restricted, S– specific enhancing effects.

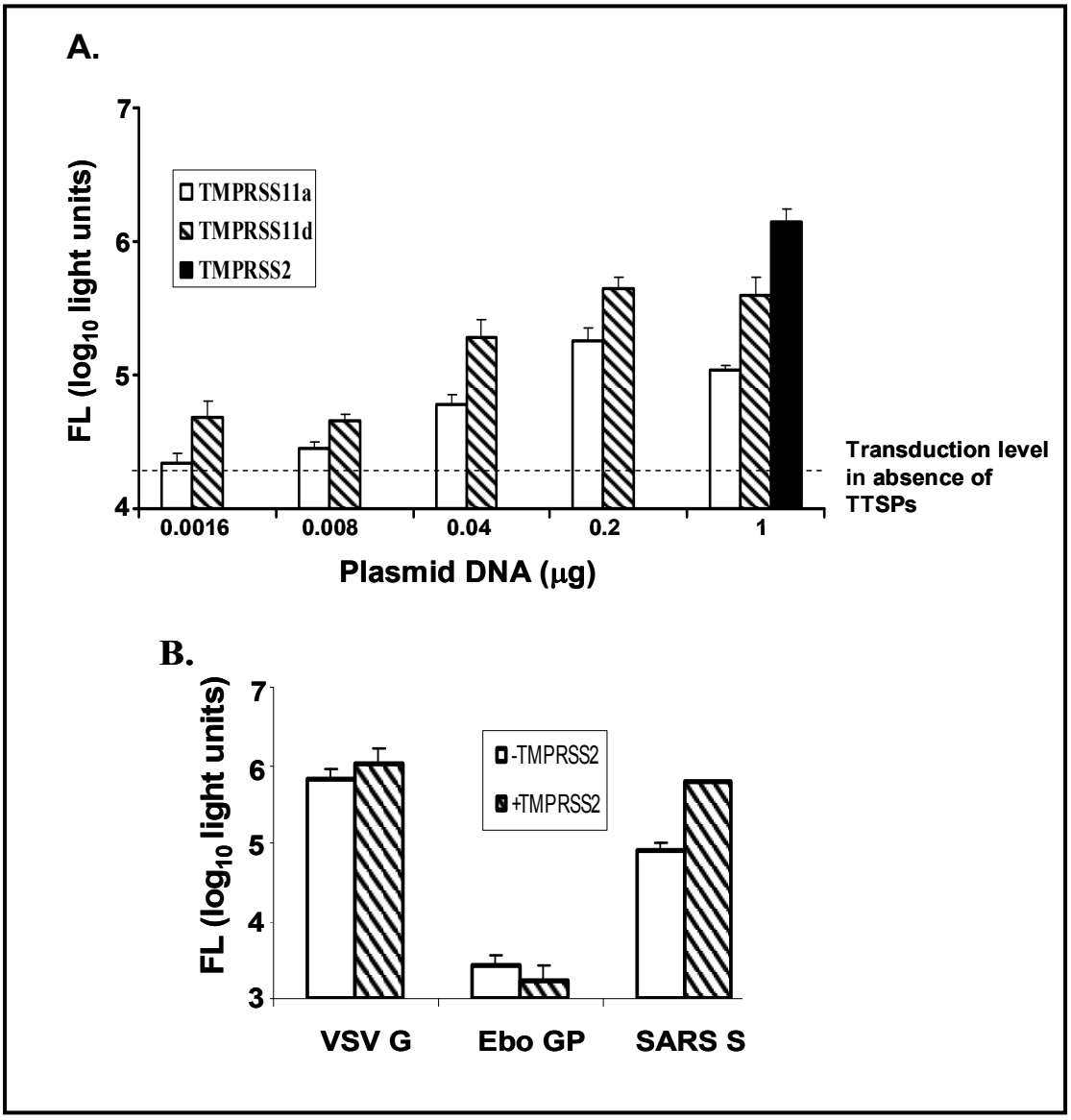

Fig. 20. Effect of TTSPs on HIV-SARS S Entry. A. 293T cells (10^6) were transfected with ACE2 (1 μg) along with indicated amounts of the TTSP plasmids. At 2 d post-transfection, cells were inoculated with HIV-SARS S and luciferase accumulations were evaluated 27 h later. The dotted line represents the transduction level in target cells transfected with ACE2 and empty vector. **B.** 293T cells co-transfected with equal

amounts of either ACE2 + empty vector (white bars) or ACE2 + TMPRSS2 (hatched bars) were inoculated with HIV-VSVG, -Ebo GP, or –SARS S pseudoviruses at 2 d post-transfection. Luciferase accumulations were evaluated 27 h later. Error bars represent standard deviations (n=3). Experiments were repeated three times with similar results.

TMPRSS2 Functions at the Cell Surface

I focused on the most potent TTSP, TMPRSS2, and determined whether this protease activates SARS S for plasma membrane – localized fusion using a cell-cell fusion assay. Briefly, effector 293T cells were co-transfected with plasmids encoding SARS S and T7 RNA polymerase, while target 293T cells were co-transfected with plasmids encoding ACE2, TMPRSS2, and a luciferase reporter under control of a T7 RNA polymerase promoter (Fig. 21A). After a 3 hour co-culture of effector and target cells, cell-cell fusions clearly discernable as microscopic ~ 10 to 20-cell syncytia, were corroborated by luciferase assays, which indicated a ~10 fold increase in membrane fusion (Fig. 21B). HCoV-NL63 S protein-mediated membrane fusion was also enhanced by TMPRSS2, albeit less potently than SARS-CoV S (Fig. 21B). These data confirmed that the TMPRSS2 protease can exert its fusion-promoting effects on two somewhat distantly related HCoV S proteins, and that these effects can take place at cell surfaces.

Endosomal cathepsin L is a known S-activating protease (Bosch, Bartelink, and Rottier, 2008; Simmons et al., 2005). Many cysteine proteases in the endosomal/lysosomal compartment, including cathepsin L, become activated and function optimally at acidic pH (Honey and Rudensky, 2003). To determine whether TMPRSS2 at the target cell surface might nullify any requirements for this and related

acid pH-dependent proteases during SARS S-mediated virus entry, the endosomal H+ / ATPase inhibitor bafilomycin A1 (Yoshimori et al., 1991) or the endosomotropic weak base NH_4Cl (Gordon, Hart, and Young, 1980) was applied to target cells immediately before and during HIV-SARS S inoculation.

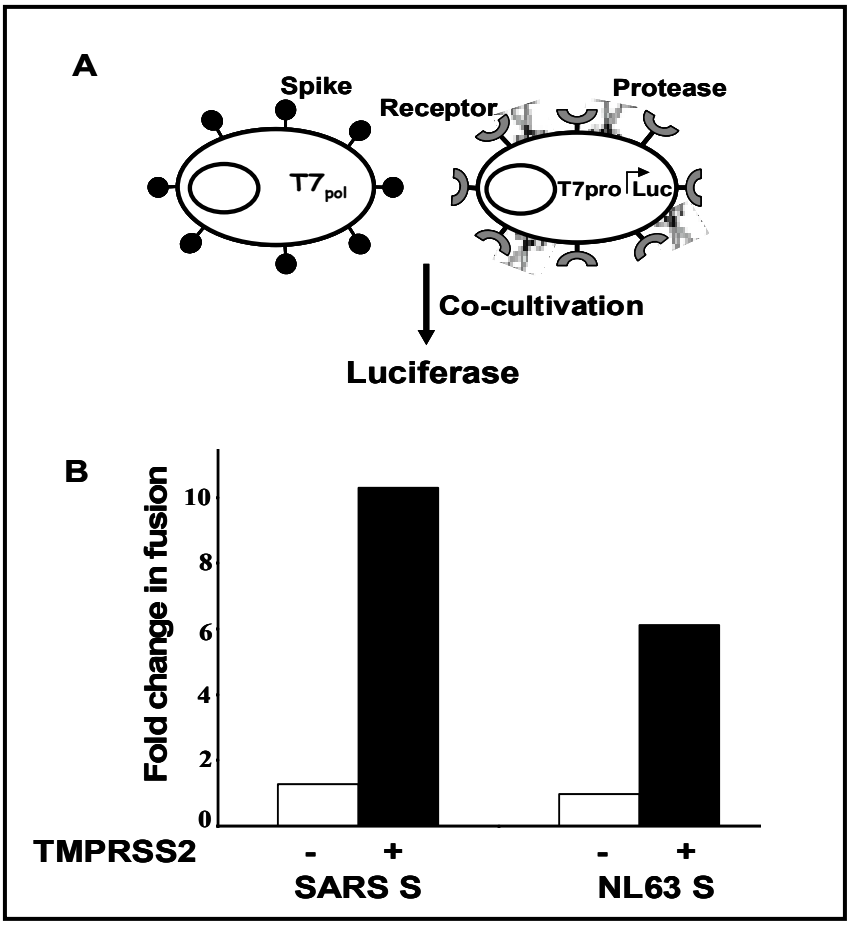

Fig. 21. TMPRSS2 Effect on SARS S-Mediated Membrane Fusion. A. Schematic diagram of cell-cell fusion. Effector 293T cells were generated by co-transfection of plasmids encoding the indicated spike constructs along pCAG-T7pol (1 μg DNA per 10^6 cells). Target 293T cells were generated by co-transfection of pcDNA3.1-ACE2 + pCAGGS-empty vector (-) or pcDNA3.1-ACE2 + pCAGGS-TMPRSS2 (+) together with pEMC-T7pro-luc. **B.** Luciferase readings 3 h after co-cultivation of effector and target cells (1:1 ratio) were plotted as fold change in fusion over negative controls without S proteins.

These inhibitors of endosomal acidification potently suppressed S-mediated transductions (Fig. 22), with 2 and 3 - $\log_{10}$ reductions by NH_4Cl and bafilomycin A1, respectively. Suppressions were eliminated by TMPRSS2 (Fig. 3-13), indicating that TMPRSS2 fully activates SARS S-mediated entry (~ 1,000-fold) when acid pH-dependent protease(s) are absent. The findings in Fig. 22 thus reveal the indiscriminate nature of SARS S entry functions, with either the cell-surface neutral pH TMPR serine protease or the endosomal acid pH-requiring (likely cathepsin) cysteine proteases operating as entry catalysts.

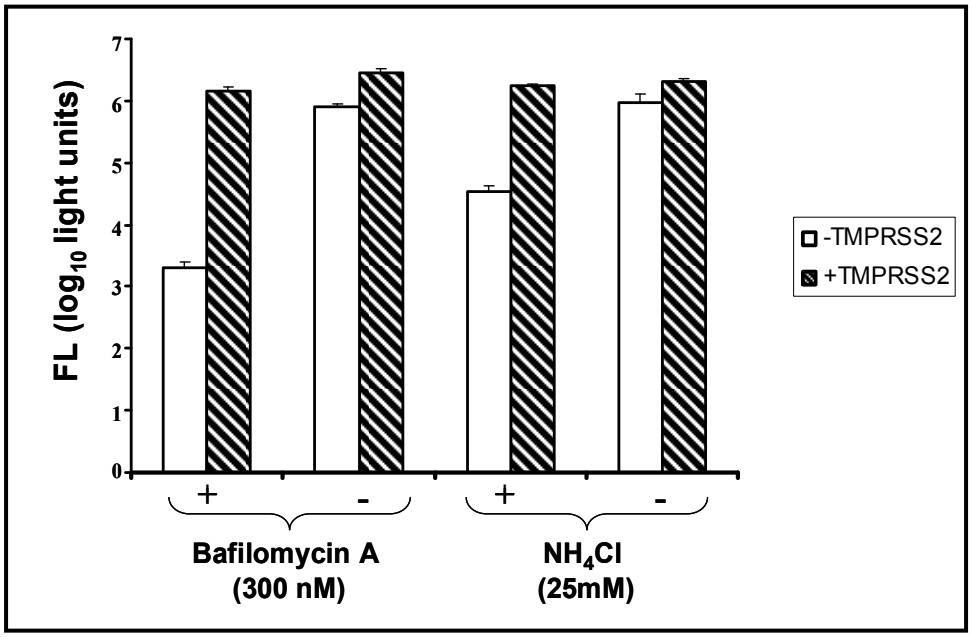

Fig. 22. TMPRSS2 Effect on HIV-SARS S Entry into Drug-Treated Cells. 293T cells were co-transfected (1 μg per 10^6 cells) with ACE2 + empty vector (white bars) or with ACE2 + TMPRSS2 (hatched bars). One day later, and 1 h prior to transduction with HIV-SARS S pseudoviruses, cells were incubated with Bafilomycin A1 (300nM) or NH_4Cl (25mM). Vehicle controls were DMSO and water for Bafilomycin A1 and NH_4Cl, respectively. HIV-SARS S particles were then concentrated onto cells by a 2 h

spinoculation. Bafilomycin and NH_4Cl remained on cells during and after spinoculation, until 6 h post-transduction, at which time cells were rinsed and replenished with fresh media. Luciferase accumulations were determined at 28 h post-transduction. Error bars represent standard deviations (n=3). The experiment was repeated three times with similar results.

SARS S Protein Cleavage by TMPRSS2

I assumed that the S proteins would be the relevant TTSP substrates for enhancing virus entry. Proteolyses at two positions, designated S1-S2 and S2', are necessary to enhance S-mediated membrane fusions (Belouzard, Chu, and Whittaker, 2009) and there are arginines at both of these cleavage sites that could comprise TTSP substrates (Antalis et al., 2010; Kam et al., 2009). To determine whether incoming S proteins on pseudoviruses might be cleaved specifically by TMPRSS2, I generated target hACE2-293 cells with or without $TMPRSS2_{FLAG}$ and adsorbed HIV-SARS S particles by spinoculation. After rinsing steps, cells and bound viruses were incubated for 1h at 37^{o}C, lysed, and S proteins visualized by immunoblotting. There was slight but convincing evidence of TMPRSS2-specific SARS S cleavage, as indicated by the presence of C-terminal ~ 120 and ~ 85 kDa S fragments (Fig. 23). The extent of proteolysis was admittedly low; however it is certainly conceivable that this very small proportion of S proteins undergoing cleavage represents the activated S proteins operating in pseudovirus entry.

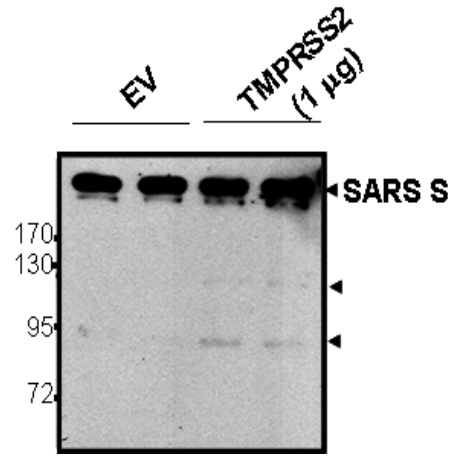

Fig. 23. Cleavage of SARS S Proteins during Virus Entry. HIV-SARS S pseudoviruses were spinoculated onto target hACE2-293 cells transfected 2 days earlier with pCAGGS empty vector or pCAGGS-TMPRSS2 (1 μg per 10^6 cells, in duplicate). After spinoculation, cells were incubated at 37°C for 1 h to allow for cleavage of S proteins by cell-surface TMPRSS2. After removing unbound pseudovirions and washing, cells were lysed and evaluated by immunoblotting for S proteins using anti-C9 tag antibody. Molecular weights are shown in kilodaltons.

I also evaluated the cleavage of S proteins during assembly in virus producer cells expressing TMPRSS2. Interestingly, HIV pseudoviruses harboring SARS-CoV spikes that were pre-cleaved by TMPRSS2 displayed reduced transduction potentials (Fig. 24). This was in sharp contrast to the augmentation of SARS S-mediated entry when TMPRSS2 was expressed in target cells (Fig. 20) and also in contrast to published reports on activation of influenza HA by TMPRSS2 during virus production (Bottcher et al., 2009; Bottcher et al., 2006). HIV-Ebola GP pseudoviruses produced in cells expressing TMPRSS2 were slightly augmented in their entry, while HIV-VSV G pseudoviruses transduction potential was not affected by the presence of TMPRSS2 (Fig. 24). These

results suggest that premature cleavage of SARS S leads to inactivation rather than activation of its fusogenic potential. In order to get fusion activation, SARS S has to be cleaved at the right time and place, i.e. after ACE2 receptor engagement on target cell surfaces.

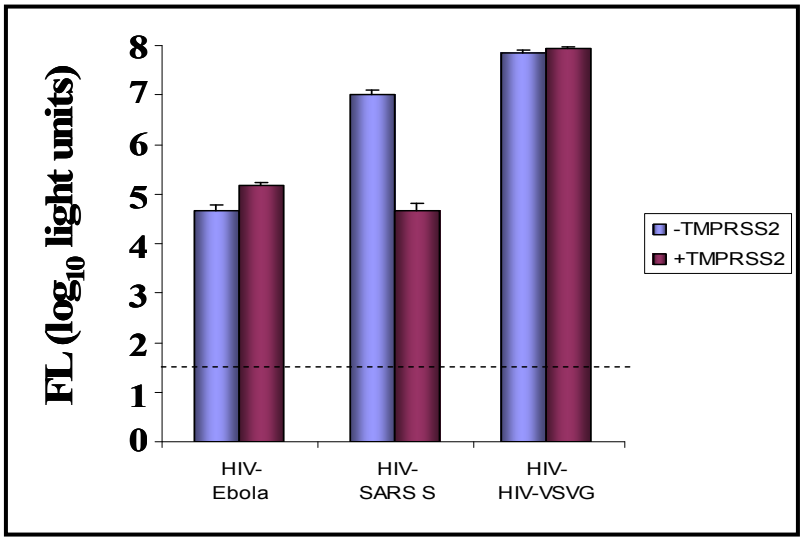

Fig. 24. TMPRSS2 in Producer Cells Decreases SARS S Transduction Potential. HIV-particles produced in +/- TMPRSS2 293T cells were used to transduce target hACE2-293 cells. Luciferase accumulated in the cells was assayed 2 days post-transduction. The dotted line represents the limit of detection for the assay.

ACE2 Protein Cleavage by TMPRSS2

The discovery that S proteins were targeted by TMPRSS2 led me to consider whether the integral-membrane ACE2 proteins might also be substrates. Thus I

introduced graded doses of the TTSP plasmids along with constant amounts of pcDNA3.1-ACE2$_{C9}$ into 293T cells, and evaluated expressed proteins 2 days later.

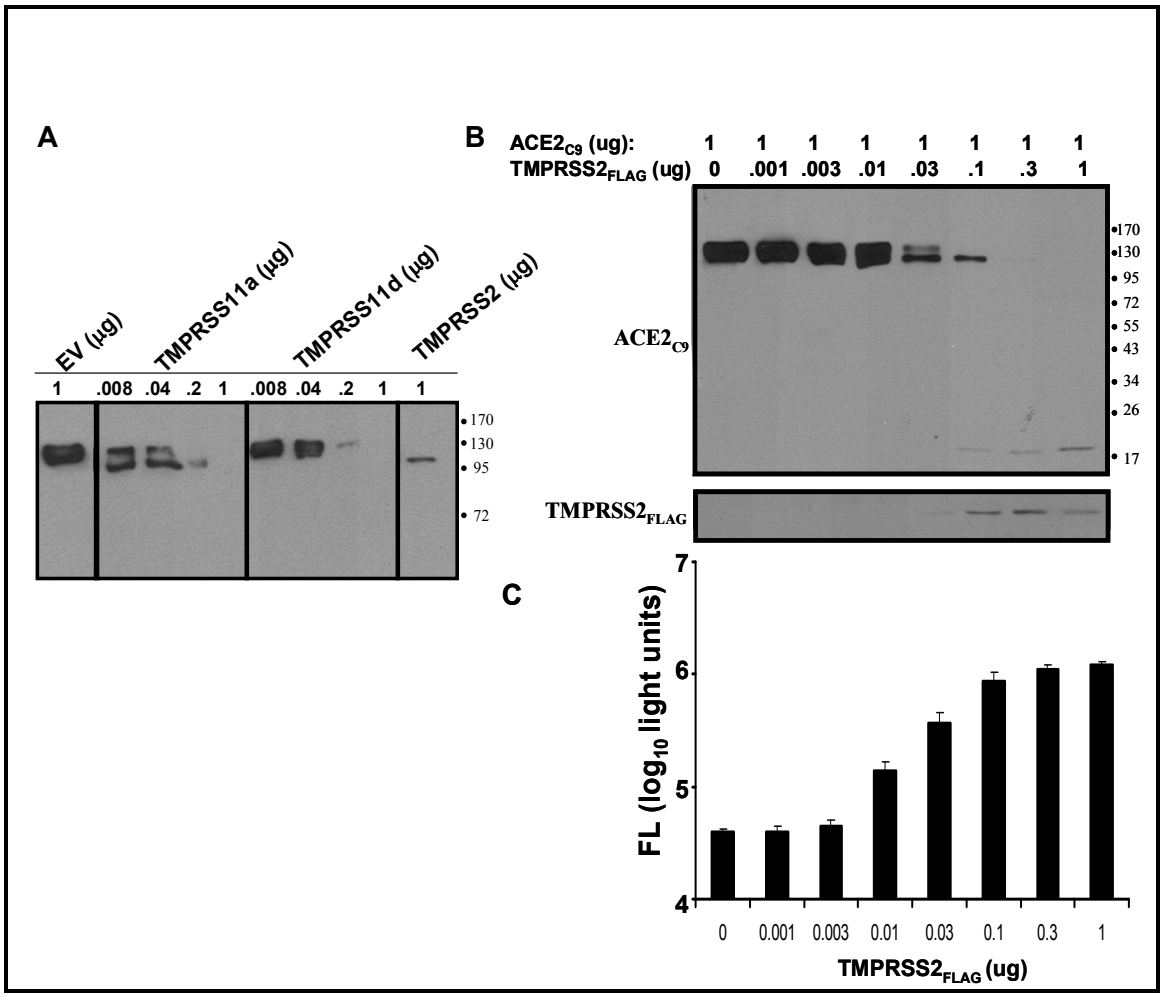

Fig. 25. Effect of TTSP Expression on ACE2 and HIV-SARS S Transductions. A. Cells (10^6) transfected with constant 1 μg amounts of ACE2 and increasing doses of the indicated TTSPs or pCAGGS empty vector (EV) were analyzed at 2 d post-transfection by immunoblotting for the C9 epitope appended to the ACE2 C-terminus. **B.** Cells transfected with 1 μg amounts of ACE2$_{C9}$ and the indicated amounts of TMPRSS2 were analyzed at 2 d post-transfection with anti-C9 and anti-FLAG tag antibodies respectively. **C.** Parallel unlysed cell cultures were transduced with HIV-SARS S pseudoviruses and luciferase accumulations were measured at 40 h post-transduction.

A striking finding was that all three TTSPs targeted ACE2 for distinctive proteolysis (Fig. 25A). In a separate experiment, 293T cultures with gradually increasing levels of TMPRSS2 revealed doses ultimately eliminating the full-length ACE2, leaving a slightly smaller ~ 115 kDa (perhaps underglycosylated) form and a ~ 20 kDa C-terminal ACE2 fragment (Fig. 25B). Remarkably, these cultures with undetectable complete ACE2 were ~30 fold more susceptible to HIV-S transduction than controls (Fig. 25C), suggesting that few receptors can mediate efficient entry provided that the relevant protease is nearby to activate incoming virions. These findings raised additional questions about the levels and distributions of ACE2 and TMPRSS2 on susceptible cell surfaces.

ACE2 Associations with TMPRSS2

We hypothesized that ACE2 and TMPRSS2 interact both in cellular exocytic pathways and cell surfaces, and that cleavage of ACE2 was a result of these interactions. This was first evaluated by Taylor Heald-Sargent using immunofluorescence assays (IFAs). Briefly, she co-synthesized $ACE2_{C9}$ and $TMPRSS2_{FLAG}$ in 293T cells, fixed cells without permeabilization, and then used a human IgG1 Fc –tagged form of the SARS S receptor-binding domain (RBD) to detect ACE2 and a mouse anti-FLAG antibody to detect TMPRSS2. The confocal images (Fig. 26A) indicated that cells expressing surface TMPRSS2 typically did not have ACE2. Thus it was likely that TMPRSS2 cleaved ACE2 before it reached the cell surface or shortly afterwards. On slides transfected with low amounts of TMPRSS2 (1:0.1 and 1:0.01 ACE2:TMPRSS2 plasmid ratios), rare cells were identified with both ACE2 and TMPRSS2 (Fig. 26B). In these cells, the receptor and protease colocalized on the plasma membrane, although the levels of each were

decreased compared to cells expressing either protein alone. Therefore, the majority of cells expressing TMPRSS2 had undetectable ACE2, but when TMPRSS2 was scarce, ACE2 localized to TMPRSS2 containing regions.

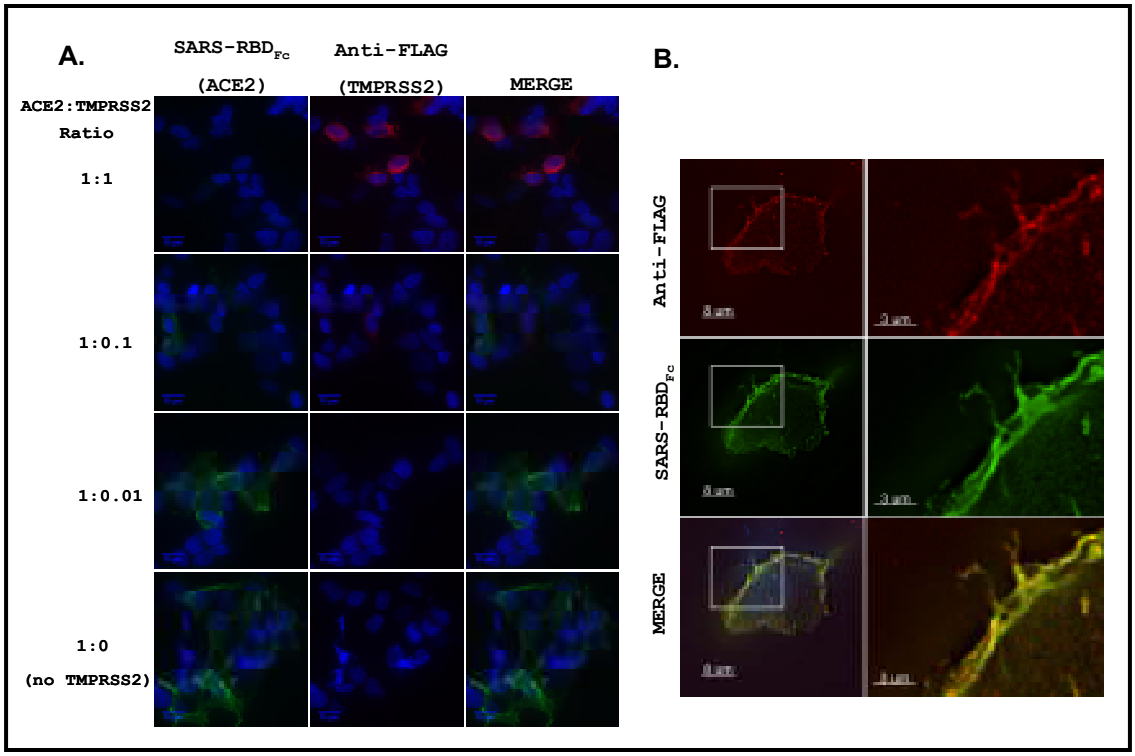

Fig. 26. Cellular Localization of TMPRSS2 and ACE2. A. Cells were co-transfected with ACE2 and TMPRSS2 at various ACE2:TMPRSS2 ratios. 24 h post-transfection cells were fixed without permeabilization and incubated with anti-FLAG and SARS-RBD_{Fc}. Secondary antibodies, anti-human IgG (green) and anti-mouse IgG (red), were used to detect bound SARS-RBD_{Fc} and anti-FLAG antibodies, respectively. All images were obtained using identical acquisition times and display levels. **B.** A representative ACE2+ TMPRSS2+ cell from the 1:0.1 ACE2:TMPRSS2 DNA ratio.

To further evaluate ACE2 – TMPRSS2 interactions, I used an immunoprecipitation-immunoblot (IP-IB) assay. Transfected 293T cells were dissolved

in a buffer containing Nonidet P-40 and sodium deoxycholate; this detergent formulation is known to completely lyse cells while preserving selected membrane protein interactions (Opstelten et al., 1995).

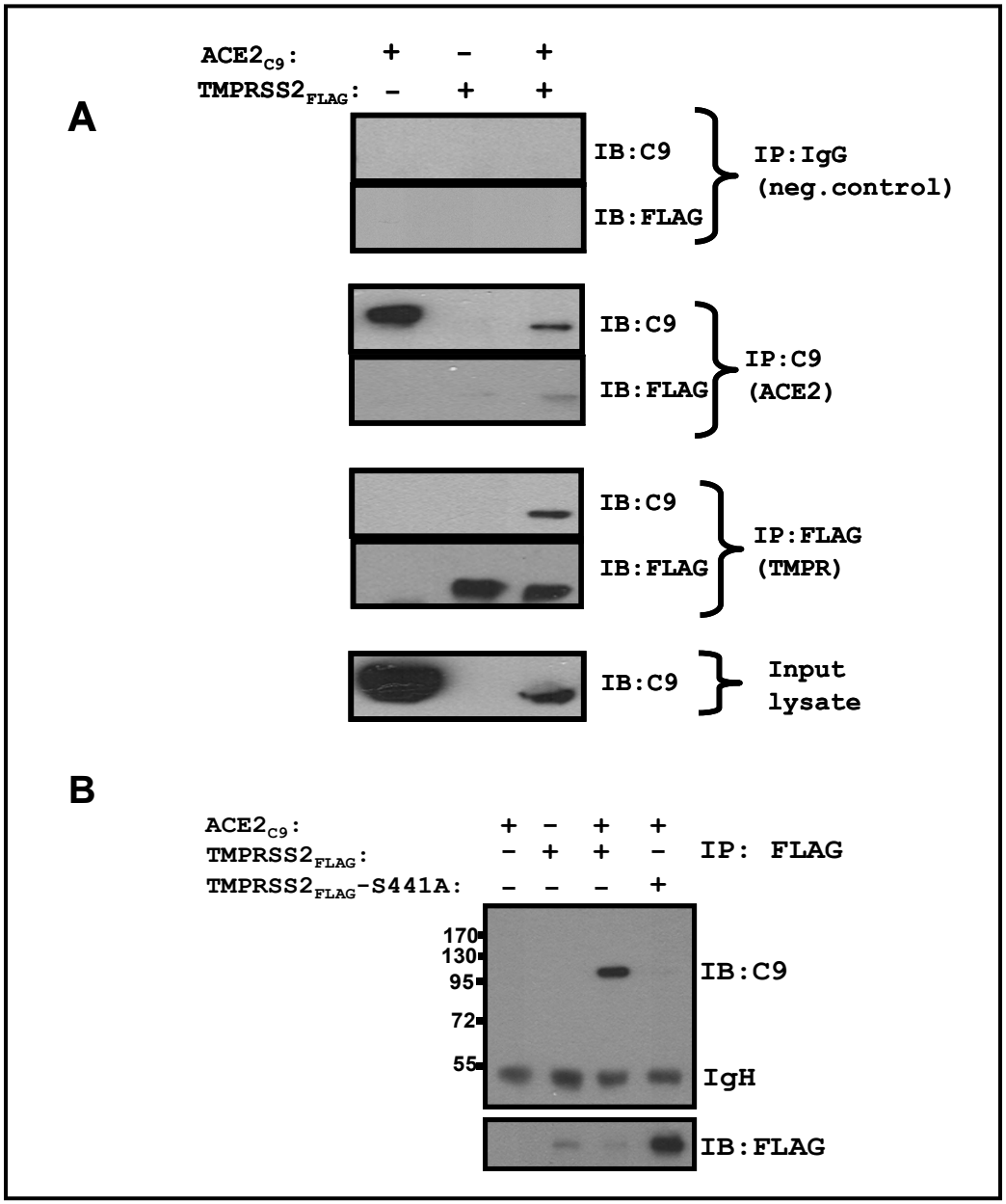

Fig. 27. Interaction between TMPRSS2 and ACE2. A. 293T cells transfected with pCAGGS-TMPRSS2$_{FLAG}$ (0.5 μg per 10^6 cells) and pcDNA3.1-ACE2$_{C9}$ (1 μg per 10^6 cells), individually or in combination, were lysed and subsequently incubated with rabbit anti-FLAG, mouse anti-C9, or mouse IgG antibody on protein G magnetic beads. Eluted proteins were analyzed by immunoblotting using the indicated antibodies. **B**. Lysates from 293T cells transfected with pCAGGS-TMPRSS2$_{FLAG}$ (0.5 μg per 10^6 cells) or pCAGGS-TMPRSS2(S441A)$_{FLAG}$ (0.5 μg per 10^6 cells), individually or in combination with pcDNA3.1-ACE2$_{C9}$ (1 μg per 10^6 cells), were subjected to immunoprecipitations using rabbit anti-FLAG antibody. Eluted proteins were analyzed by immunoblotting using mouse anti-C9 antibody.

From these lysates, ACE2$_{C9}$ and TMPRSS2$_{FLAG}$ were captured onto magnetic protein G beads using mouse anti-C9 and rabbit anti-FLAG antibodies, respectively, and then detected proteins by immunoblotting using the same epitope-specific antibodies.

The results (Fig. 27) revealed specific co-IP of both TMPRSS2 and ACE2 by either the C9 or FLAG antibodies. As there was digestion of the ~ 130 kDa ACE2 form in these cultures (see Fig. 25), the predominant IP form of ACE2 was ~ 115 kDa. I attempted to determine whether the complete ~ 130 kDa ACE2 might co-IP with the catalytically inactive TMPRSS2-S441A. While the anti-FLAG IPs efficiently adhered both the wild type and the inactive mutant TMPRSS2(S441A)$_{FLAG}$, the co-IP of ACE2 was only observed with the wild type form (Fig. 27B). These data indicated that enzymatic activity was required for TMPRSS2 association with ACE2.

ACE2:TMPRSS2 Associations in Cis and in Trans

Some TTSPs, notably HAT, will cleave cellular substrates both in cis and in trans, i.e., when presented from neighboring cells (Beaufort et al., 2007). This is because some

TTSPs shed their catalytic C-terminal domains into media (Szabo and Bugge, 2008; Yasuoka et al., 1997), thereby creating paracrine proteolytic activities.

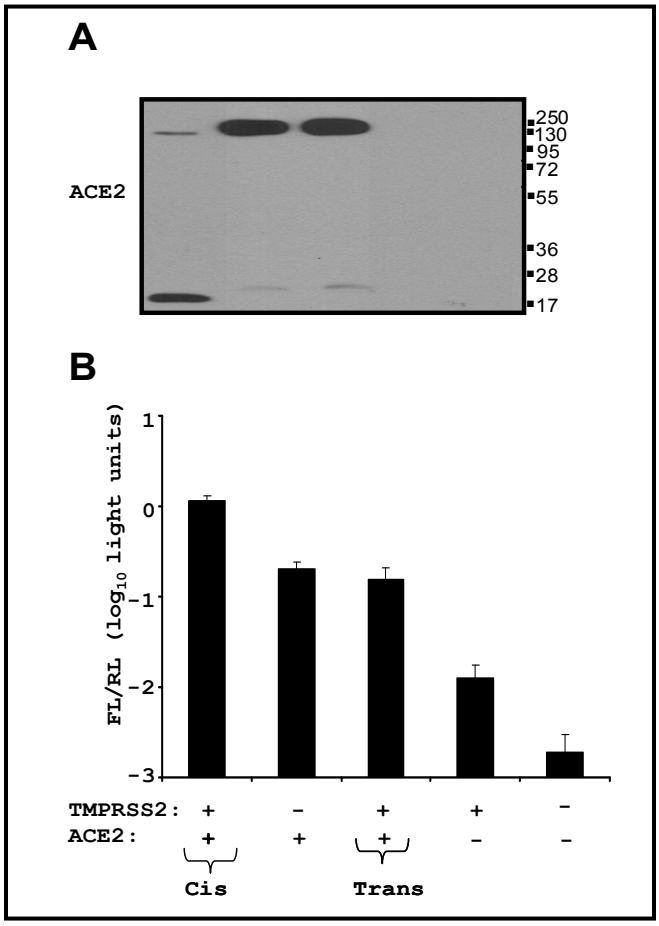

Fig. 28. ACE2:TMPRSS2 Associations in Cis and in Trans. Four 293T cell populations were transfected with renilla luciferase (RL) control plasmid along with empty vector (EV), TMPRSS2 and ACE2 plasmids, either alone or together, as indicated. One day later, cell populations were cocultivated as indicated by the "+" signs. **A.** After a 20 h co-cultivation period, cells were lysed and evaluated for ACE2 cleavage by immunoblotting using anti-C9 tag antibody. **B.** After a 20 h co-cultivation period, cells were transduced with HIV-SARS S. Firefly luciferase relative to renilla luciferase (FL/RL) was measured 27 hptd. Error bars represent standard deviations (n=3). The experiment was repeated three times with similar results.

I sought to determine whether the TMPRSS2 that fosters SARS S entry and cleaves ACE2 in cis would do the same in trans. To this end, a mixed population of target cells was generated, with half being ACE2+ and the other half TMPRSS2+. These cells were both challenged with SARS S pseudotype viruses and evaluated for ACE2 cleavage. If TMPRSS2 extended its effect broadly, then the mixed populations would be highly susceptible to S-mediated entry and would also have cleaved ACE2. Unlike the condition in which ACE2 and TMPRSS2 were expressed in the same cells, the expression of these two proteins on separate cells did not foster virus entry above that observed when only ACE2 was expressed (Fig. 28A). In addition, the ACE2 proteins were not proteolyzed when TMPRSS2 was on separate cells, even though the TMPRSS2+ and ACE2+ cells were contacting each other in the monolayers (Fig. 28B). This was in striking contrast to the ACE2 digestion during cis presentation of TMPRSS2. These data suggest that the relevant in vivo targets are those in which both ACE2 and TMPRSS2 entry factors are simultaneously present in the same cells, and that extracellularly shed or adjacent TMPRSS2 has no effect on infection.

Effect of TTSPs on SARS-CoV Infections

To determine whether the TMPRSS2 also increased cell susceptibility to authentic SARS-CoV infections, Jincun Zhao at the University of Iowa challenged the transfected 293T cells with authentic SARS-CoV (Urbani strain). He evaluated SARS N RNA levels at 6 h post-infection by qRT-PCR (Fig. 29A) and I evaluated SARS S and N protein levels at 24 h post-infection by immunoblotting (Fig. 29B). There was 9-fold more SARS N RNA in cells expressing TMPRSS2 compared to cells expressing the

enzymatically-inactive TMPRSS2 (S441A) [$p < 0.0005$]. These viral RNAs were translated to generate significantly more N proteins in the TMPRSS2+ cells (Fig. 29B). Additionally there was significantly more S protein in the TMPRSS2+ cells. These findings, notably the comparisons of proteolytically active and inactive TMPRSS2s, allowed us to assign natural infection-enhancing activity to proteolysis.

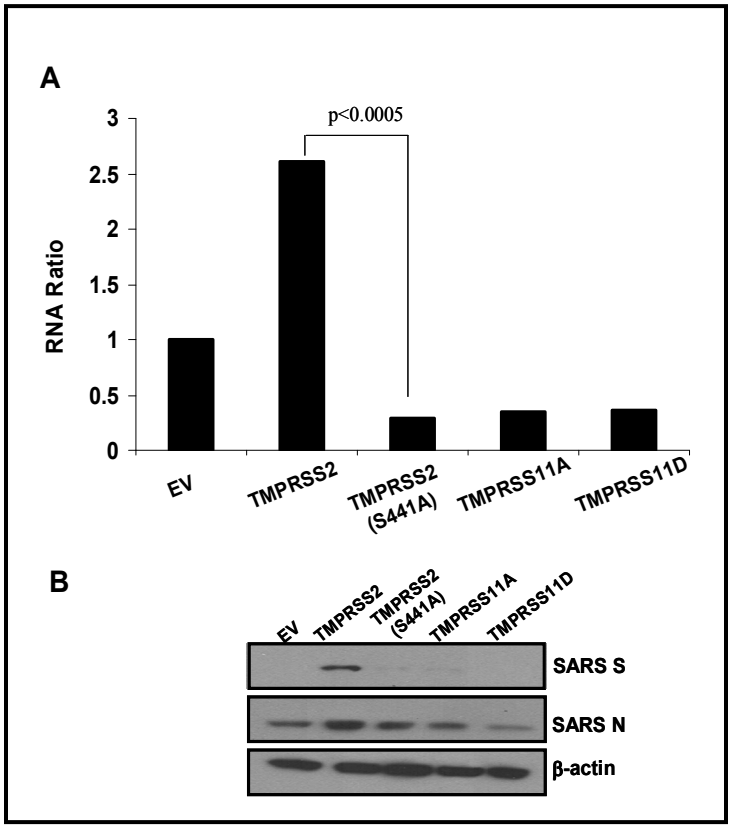

Fig. 29. **Effect of TTSPs on SARS-CoV Infections**. Cells transfected with ACE2 and each TTSP were challenged with SARS–CoV at MOI = 0.1. **A.** SARS-CoV N and human GAPDH-gene specific RNAs were quantified by real-time PCR and levels of SARS N gene amplicons were normalized to that of GAPDH amplicons. Data is plotted as ratio of each RNA to the empty vector RNA. Statistics was performed using Student's

t-test for unpaired samples on ΔCT values (n = 3). The experiment was performed twice. **B.** SARS S, N and β actin protein levels were evaluated at 24 hpi by immunoblotting using anti-SARS S, anti-SARS N and anti-β actin antibodies.

Relationship between SARS S: ACE2 Affinity and TMPRSS2 Activation

We hypothesized that TTSPs may especially support coronaviruses having low affinities for their receptors; for example, zoonotic coronaviruses entering new host organisms bearing orthologous receptors (Li et al., 2005c). These viruses might benefit from the TMPRSS2-mediated rapid activation at the cell surface before eluting away. By contrast, endosome – localized activations are delayed until after subcellular virus transport (Matsuyama et al., 2005) and demand that viruses remain attached to ACE2 receptors for much longer times. I began to test this hypothesis by determining whether HIV-SARS S pseudoviruses that bound ACE2 with low affinity were greatly enhanced in their entry by TMPRSS2. To this end, I used site-directed mutagenesis to generate S proteins with mutations in the ACE2 receptor binding domain (RBD) known to affect the affinity of S for ACE2. Residues N479 and T487 in the RBD of SARS-CoV S protein appear to be critical for high affinity association with the ACE2 receptor (Li et al., 2005c). Thus, changing the aspargine at position 479 to a lysine reduces the binding affinity of SARS-CoV RBD to ACE2 by ~ 30 fold, while changing the threonine at position 487 to a serine reduces the affinity by ~ 22 fold (Li et al., 2005c). Of note, changes in these residues were suggested to contribute to adaptation of SARS-CoV from palm civets to humans (Li et al., 2005c).

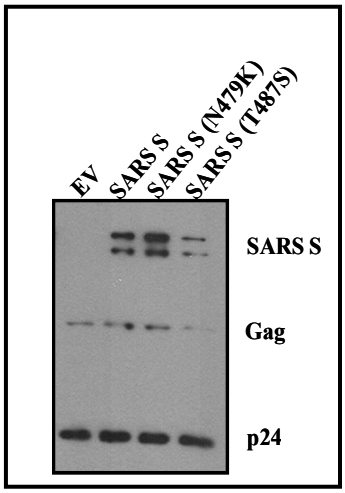

Fig. 30. Incorporation of SARS S RBD Variants into HIV Particles. Pseudotyped HIV particles were produced in 293T cells by co-transfection of plasmid DNAs encoding the indicated spikes together with the HIV vector (pNL4.3-Luc R-E-). Released particles were harvested from culture media and concentrated by pelleting through 30% sucrose. Proteins present in cell lysates and in virion particles were detected by immunoblotting using C9 tag (SARS S) and p24-specific MAbs.

SARS S proteins harboring the RBD mutations, N479K and T487S, were efficiently incorporated into HIV particles relative to Gag and p24 proteins (Fig.30). These same HIV particles harboring SARS S (wt) or SARS S with the indicated RBD mutations were used to transduce target cells expressing ACE2 +/- TMPRSS2, with the expectation that TMPRSS2 would be more effective in augmenting the entry of SARS S proteins with RBD mutations. The data (Fig. 31) revealed that SARS S N479K proteins were less efficient than the wild-type counterparts in mediating entry into ACE2 positive

cells, consistent with the fact that the mutation lowered the spike-receptor affinity by ~ 30 fold (Li et al., 2005c).

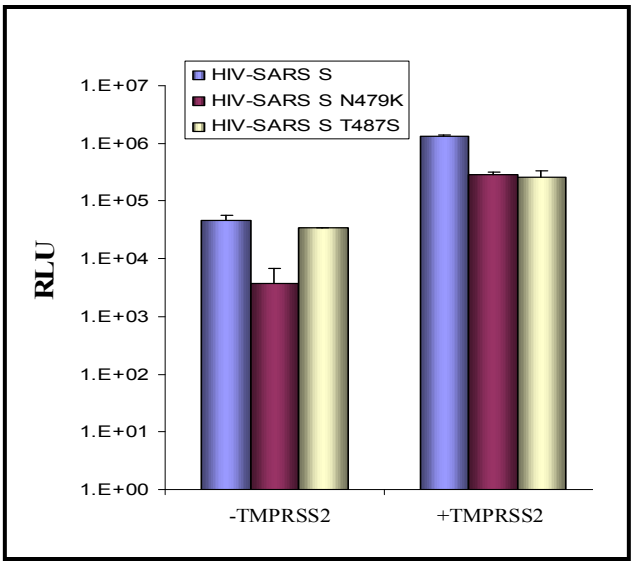

Fig. 31. Effect of RBD Mutations on SARS S-mediated Entry into 293T Cells Expressing TMPRSS2. 293T cells (10^6) were transfected with pCDNA3.1-$ACE2_{C9}$ (1 μg) along with 0.05 μg of pCAGGS-$TMPRSS2_{FLAG}$ or pCAGGS empty vector. At 2 d post-transfection, cells were inoculated with the indicated HIV-SARS S pseudoviruses and luciferase accumulations were evaluated 27 h later.

TMPRSS2 augmented SARS S (wt)-mediated entry ~28 fold and SARS S N479K-mediated entry ~75 fold (Fig. 31). Even though the TMPRSS2 augmentation of the low affinity SARS S protein seemed to be more than the wild-type one, the data were not strong enough to conclude that cell surface TMPRSS2 offered an advantage to low binding viruses.

Localization of Receptors and Proteases in Lipid Rafts: Roles for Lipid Rafts as Virus Entry Factors

I used a biochemical fractionation approach to evaluate localization of ACE2 receptor and TMPRSS2 protease in lipid rafts or detergent resistant membranes (DRMs). The tight packing organization of lipid rafts confers their resistance to some detergents, such as Triton X-100 (TX-100) at cold temperature, and allows their purification from low density fractions after floatation in a sucrose gradient (Chazal and Gerlier, 2003). In my experiments, I used 0.2 % TX-100, a detergent concentration often used to prepare DRMs from several cell lines (Giurisato et al., 2003). Evaluation of proteins in each fraction by silver staining indicated that most proteins were solubilized by TX-100 and present in fractions 8 and 9 (Fig. 32). However, a very small subset of proteins was enriched in fraction 3, which should contain low density DRMs.

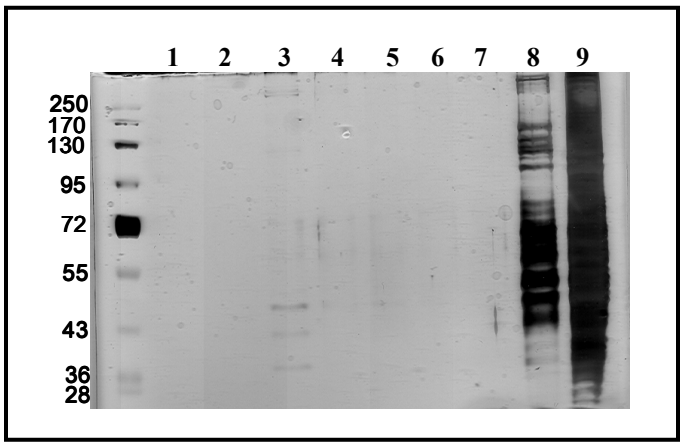

Fig. 32. Protein Profile in Each Gradient Fraction Evaluated by Silver Staining. 25 µl from each fraction was loaded in a 10% SDS gel. Following electrophoresis, the gel was fixed and silver stained. As expected, the majority of proteins are in fractions 8 and

9, while only a few proteins are present in fraction 3, which is where the low density membranes (lipid rafts) should float. Molecular weights are shown in kilodaltons.

To confirm that fraction 3 contained DRMs, I incubated 293T cells with cholera toxin subunit B peroxidase conjugate (CTB-HRP) prior to lysis in cold detergent and subsequent fractionation. CTB-HRP binds to ganglioside GM1, which is enriched in DRMs (Brown, 2006). A small portion of each fraction was spotted into nitrocellulose and the results revealed that GM1 was concentrated in fraction 3 (Fig. 33).

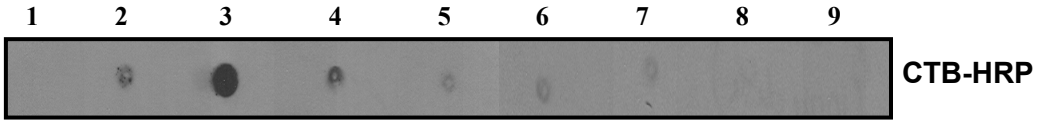

Fig. 33. Cholera Toxin B-HRP as a Marker of Lipid Rafts. 3 μl from each fraction (1-9) containing cholera toxin B-HRP was spotted onto nitrocellulose membrane and subsequently visualized on film using chemiluminescence reagents.

To determine whether cell surface ACE2 and TMPRSS2 were localized in lipid raft fractions, I biotinylated cell surface proteins prior to lysis in cold TX-100. The biotin reagent that was used, Sulfo-NHS-LC-Biotin, is a membrane impermeable reagent that reacts efficiently with primary amine-containing molecules. Following fractionation of the gradients, the biotinylated proteins present in fractions 3, 4, 8 and 9 were pulled down with streptavidin beads and eluted proteins were analyzed by western blotting. The data (Fig. 34A) revealed that ACE2 was present exclusively in lipid raft containing fraction 3,

consistent with an earlier report that suggested ACE2 was a lipid raft-associated protein (Lu, Liu, and Tam, 2008). On the contrary, the majority of cell-surface TMPRSS2 proteins were associated with non-raft fractions 8 and 9 and only a small subset were associated with raft-containing fraction 3 (Fig. 34B).

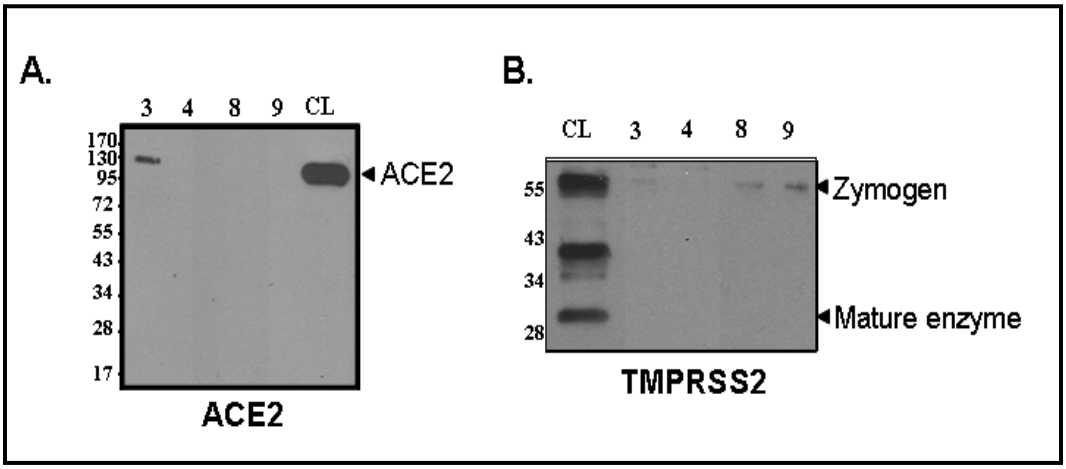

Fig. 34. ACE2 and TMPRSS2 Association with Detergent Resistant Membranes (DRMs). Surface proteins of 293T cells transfected with ACE2 (**A**.) or TMPRSS2 (**B.**) were biotinylated and subsequently subjected to lysis in cold-detergent. Following precipitation with streptavidin beads, the biotinylated proteins present in fractions 3, 4, 8 and 9 were separated by gel electrophoresis and detected with anti-C9 tag antibody (ACE2) and anti-FLAG tag antibody (TMPRSS2). A portion (2/1000) of each cell lysate (CL), which was not subjected to streptavidin pull-down, was electrophoresed alongside the other samples. Molecular weights are shown in kilodaltons.

The previous experiments were informative in terms of ACE2 and TMPRSS2 localization in plasma membrane lipid microdomains; however, these experiments were not performed in the context of virus binding and internalization. To this end, I incubated

293T cells with HIV-bald and HIV-SARS S pseudoparticles prior to biotinylation and subsequent lysis in cold TX-100. The data (Fig. 35) indicated that a large proportion of TMPRSS2 was localized to lipid raft-containing fraction 3 following virus binding and internalization.

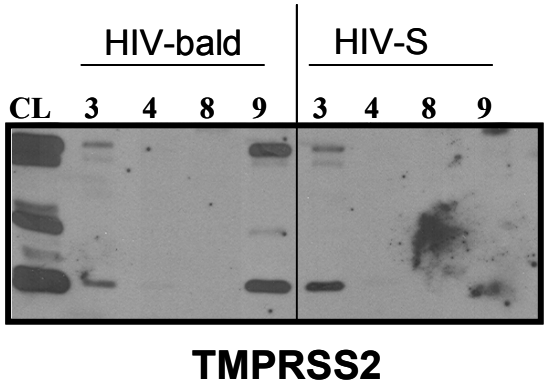

Fig. 35. TMPRSS2 association with lipid rafts during virus entry. 293T cells co-transfected with ACE2 and TMPRSS2 were incubated with the indicated HIV particles for 1 hour at 37°C and subsequently surface biotinylated and lysed in cold detergent as described above. The biotinylated proteins were captured using streptavidin beads and further subjected to SDS-PAGE and immunoblotting using anti-FLAG antibody. A portion (2/1000) of each cell lysate (CL), which was not subjected to streptavidin pull-down, was electrophoresed alongside the other samples. Molecular weights are shown in kilodaltons.

β1 Integrin: A Putative Coreceptor For HCOV-NL63 S-Mediated Entry

Integrins are cell surface heterodimers composed of α and β glycoprotein subunits. Besides operating in cell adhesion, migration and differentiation (Hynes, 2002), they are also used by a variety of viruses for cell entry (Stewart and Nemerow,

2007). Integrins may directly bind to viruses and they may also direct viruses to the endosomal proteases needed for viral protein cleavage and activation of cell entry potentials, as was recently demonstrated for Ebola virus (Schornberg et al., 2009). Of note, HCoV-NL63 contains the well-defined integrin binding motif Asn-Gly-Arg (NGR) (Koivunen, Gay, and Ruoslahti, 1993) in its S sequence. Furthermore, NL63 S proteins are not cleaved in virus producer cells and rely on target cell proteases, perhaps endosomal cathepsins for activation. These facts led us to hypothesize that integrins might be involved in HCoV-NL63 S-mediated entry.

We used the HIV based-pseudotype system to determine whether β1 integrins are involved in coronavirus entry. In essence, HIV cores can be decorated with different glycoproteins and past literature has shown that these pseudotypes are good mimics of authentic viral entry (Moore et al., 2004). Relative extents of pseudovirus transduction are measured by the accumulation of a luciferase reporter gene product that is encoded in the HIV transducing vector (He et al., 1995).

Pseudovirus transduction into HEK293 cells stably expressing the ACE2 receptor (hACE2-293) was performed in the presence or absence of a monoclonal anti-β1 integrin antibody (MAb1965, Millipore) at the indicated dilutions (Fig. 36). The results revealed significant blockade ($p < 0.05$) of NL63 S, but not SARS S or VSV G-mediated entry, indicating that β1 integrins did not interfere with HIV replication events. The effect of antibody blockade on NL63 S-mediated transduction was dose-dependent, with the greatest effect of ~ 40 fold decrease in transduction at the highest antibody concentration. Interestingly, Ebola GP-mediated transduction was only slightly inhibited by the addition

of integrin β1 blocking antibody. I expected a much bigger inhibitory effect of the integrin β1 blocking antibody on Ebola virus entry, which would be consistent with previously published findings (Schornberg et al., 2009).

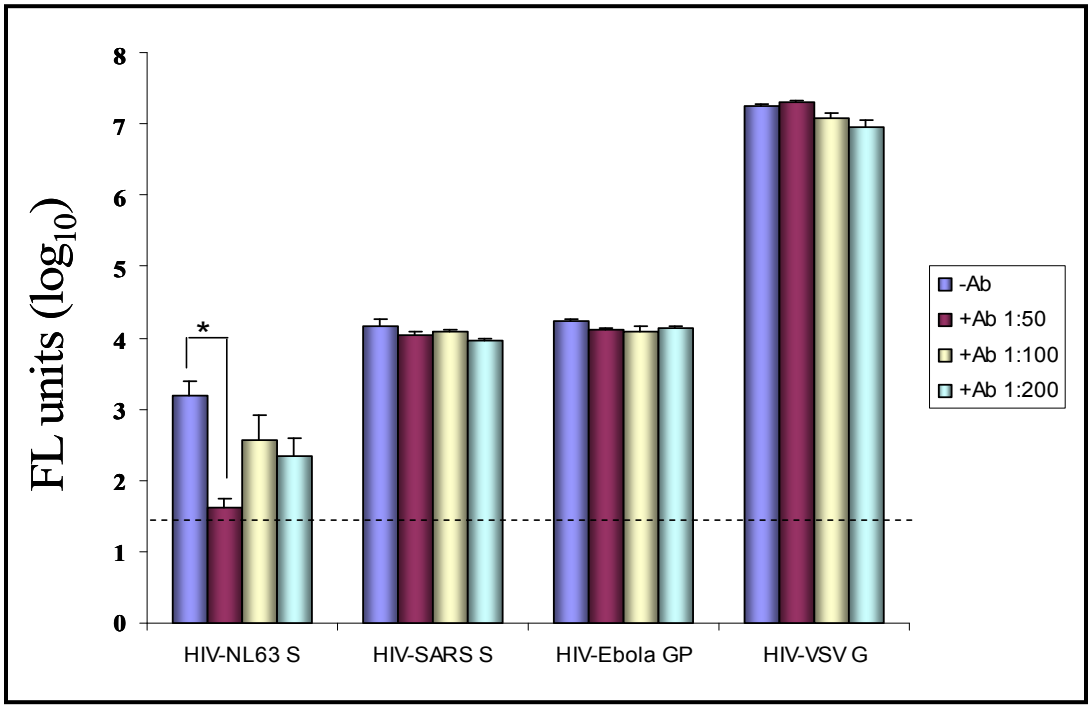

Fig. 36. Inhibition of NL63 S-mediated virus entry by β1 integrin antibody. 293T-ACE2 cells were incubated with or without anti-β1 integrin antibody (MAb 1965, Millipore) at the indicated dilutions in serum free media for 30 min at 37°C. The indicated HIV transducing particles were then spinoculated onto cells. Cell lysates were evaluated for firefly luciferase (FL) reporter product accumulations at 24 hours post-transduction. The dashed bar indicates the assay lower limit of detection. Note the log10 FL scale; similar results were obtained in three independent experiments. * $p<0.05$ Student's t-test for unpaired samples.

To determine whether β1 integrins were specifically involved in HCoV-NL63 S-mediated entry, I used a siRNA approach to knock-down the β1 integrin levels in hACE2-293 cells. As shown in Fig. 37A, transfection of the integrin β1 (ITGB1) specific siRNA, but not the negative control non-target siRNA, resulted in diminution of integrin β1 levels in hACE2-293 cells. Notably, reducing the levels of β1 integrins in hACE2-293 cells significantly ($p<0.05$) lowered the susceptibility to NL63 S-mediated transduction by ~ 5 fold, while susceptibility to SARS S-mediated transduction actually increased by ~ 3 fold, as compared to transductions in cells transfected with the non-target control siRNA (Fig. 37B).

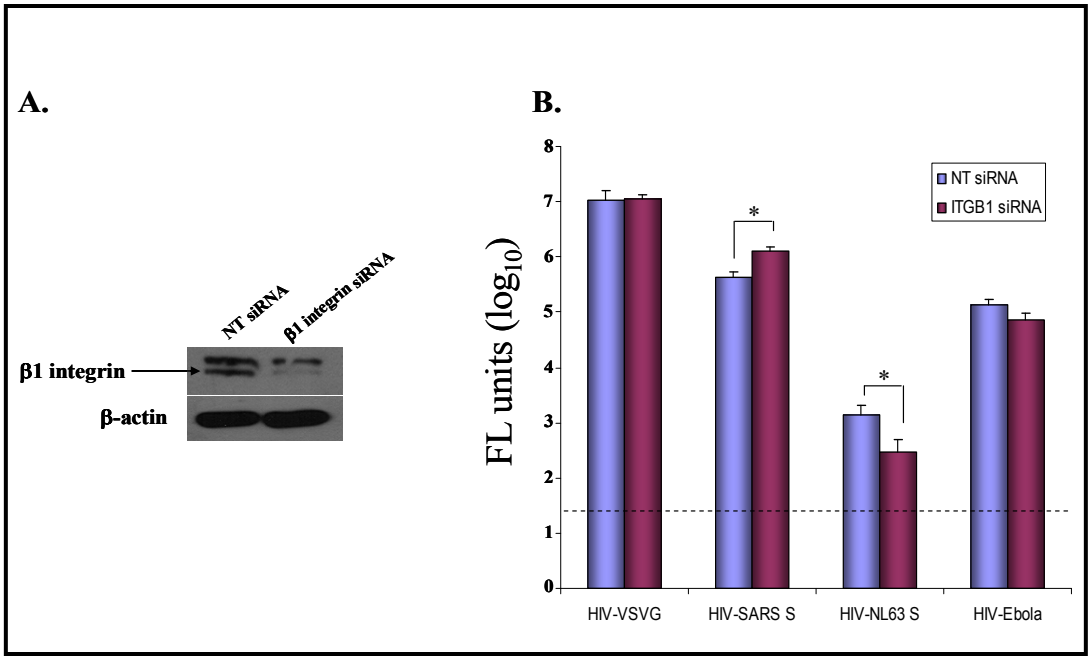

Fig. 37. Relative resistance to NL63 S-mediated transduction after β1-integrin knockdown. **A.** 293T-ACE2 cells were transfected with non-target negative control (NT) or β1-integrin specific (ITGB1) siRNAs. 2 days later, cells were transduced with

the indicated pseudoviruses and FL reporter accumulations were measured after 40 h. The dashed bar indicates the lower limit of assay detection. **B.** 293T-ACE2 cells were lysed 48h after introducing the indicated siRNAs, and β1-integrin levels (arrow) were compared to β-actin control levels by immunoblotting. * $p<0.05$ Student's t-test for unpaired samples.

To determine whether the effect of β1 integrins on NL63 S-mediated entry was related to the requirement for proteolytic cleavage of NL63 S proteins, I generated a NL63 S protein that contained multibasic furin enzyme recognition sites at two positions (Fig. 38), in analogy to the cleavage sites in SARS S proteins (Belouzard, Chu, and Whittaker, 2009). I hypothesized that this form of NL63 S would be cleaved by furin proteases in virus producer cells; such that it would not require endosomal protease cleavage and/or β1 integrins in virus target cells.

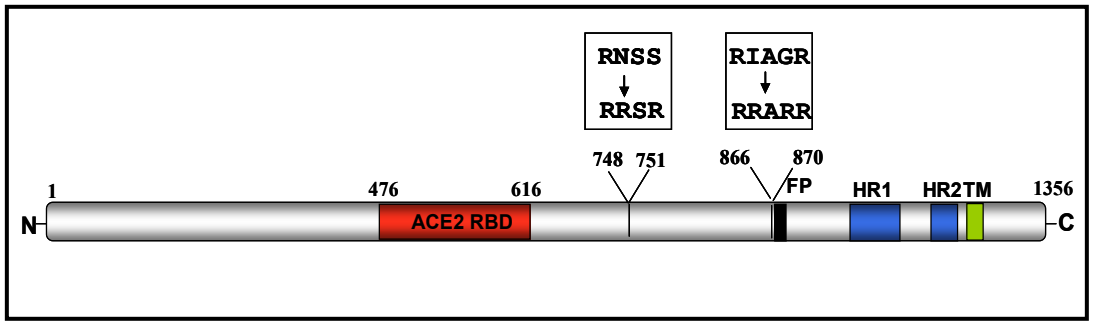

Fig. 38. Engineering furin cleavage sites in HCoV-NL63 S. The NL63 S protein is depicted in linear fashion. The ACE2 receptor binding domain (RBD) is shown in red, fusion peptide (FP) is shown in black, heptad repeats (HR) 1 and 2 are shown in blue and the transmembrane (TM) region is shown in green. The first furin cleavage site was engineered at position 748-751 by changing the wild-type sequence from RNSS to RRSR. The second furin cleavage site was engineered at position 866-870 by changing the wild-type sequence from RIAGR to RRARR.

The cleaved (cl) forms of NL63 S proteins were efficiently incorporated into budding HIV pseudoparticles (Fig. 39A). The NL63 S (cl) contains an expected ~65 kDa C-terminal fragment, generated by proteolysis at the engineered site positioned immediately N-terminal to the fusion peptide.

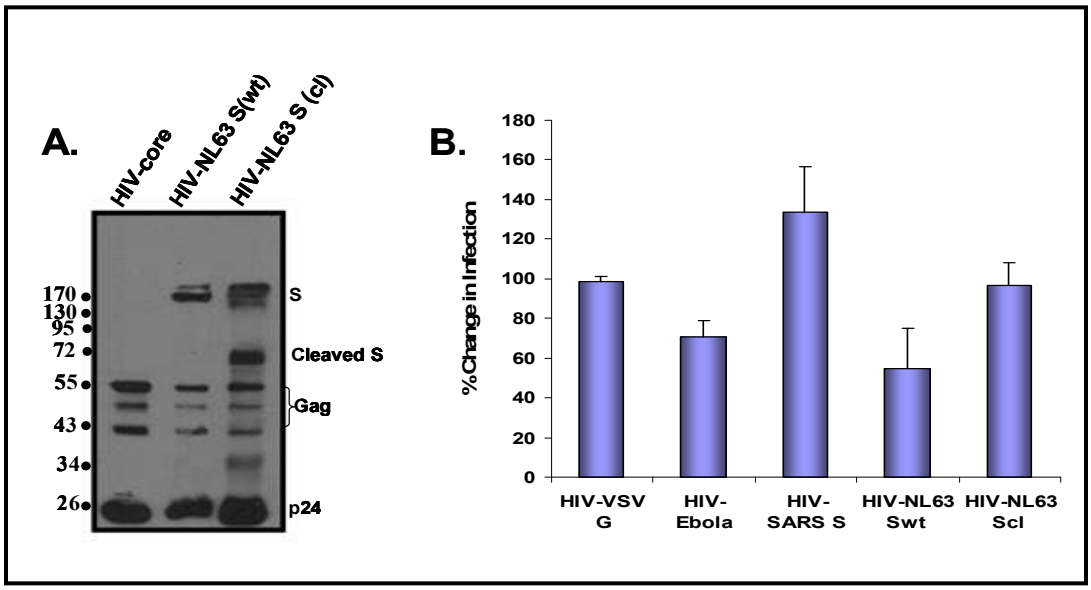

Fig. 39. β1-integrin independent entry by cleaved NL63 S proteins. A. Pseudotyped HIV particles were produced in 293T cells by co-transfection of plasmid DNAs encoding the indicated spikes together with the HIV vector (pNL4.3-Luc R-E-). Released particles were harvested from culture media and concentrated by pelleting through 30% sucrose. Proteins present in pseudovirus particles were detected by immunoblotting using S- and HIV Gag p24-specific MAbs. **B.** 293T-ACE2 cells were transfected with non-target negative control (NT) or β1-integrin specific (ITGB1) siRNAs. 50 h later, the cells were transduced with the indicated HIV-particles and luciferase accumulated in cells was evaluated after 40 h. The data are depicted as % change in infection of ITGB1 siRNA treated cells compared to NT siRNA treated cells which were set at 100%.

The HIV particles bearing NL63 S (wt) or NL63 S (cl) (Fig. 39A) as well as HIV particles bearing VSV G, Ebola GP and SARS S, were used to transduce hACE2-293 cells that were pre-transfected with β1 integrin or non-target siRNAs (Fig. 39B). Unlike the wild-type NL63 S, the transductions mediated by NL63 S (cl) were not affected by the β1-integrin knockdown. This finding that pre-cleaved NL63 S proteins had no need for β1-integrins reinforced the hypothesis that integrins might not be used as coreceptors per se, but rather as conduits to the appropriate protease-rich endosomal compartments (Caswell, Vadrevu, and Norman, 2009; Schornberg et al., 2009).

The NL63 S protein sequence contains an NGR motif at positions 197-199 that could interact with β1 integrins. The NGR sequence is found in the extracellular matrix protein fibronectin and is important to the interaction of fibronectin with the α5β1 integrin receptor (Koivunen, Gay, and Ruoslahti, 1993; Koivunen, Wang, and Ruoslahti, 1994). To reveal the potential role of this NGR motif in NL63-S mediated entry, I used site-directed mutagenesis to mutate the arginine at position 199 to a lysine (R199K). The mutant NL63 S proteins displaying NGK rather than NGR motifs were less efficient (~ 16 fold) than wild-type proteins in mediating entry into hACE2-293 cells (Fig. 40). The decrease in NL63 S (R199K) –mediated entry was not due to inefficient incorporation of the mutant proteins into HIV particles, since both NL63 S (wt) and NL63 S (R199K) were equally incorporated into HIV particles (data not shown). We do not rule out that the R199K mutation in NL63 S might affect protein folding and intrinsic activity. More importantly, we are not certain whether the NL63 S NGR motif is displayed on a surface and available for interaction with β1 integrins, since structural data are not available yet

for any coronavirus spike ectodomain. It would be interesting to determine whether NL63 spike interacts with soluble β1 integrin heterodimers via the NGR motif.

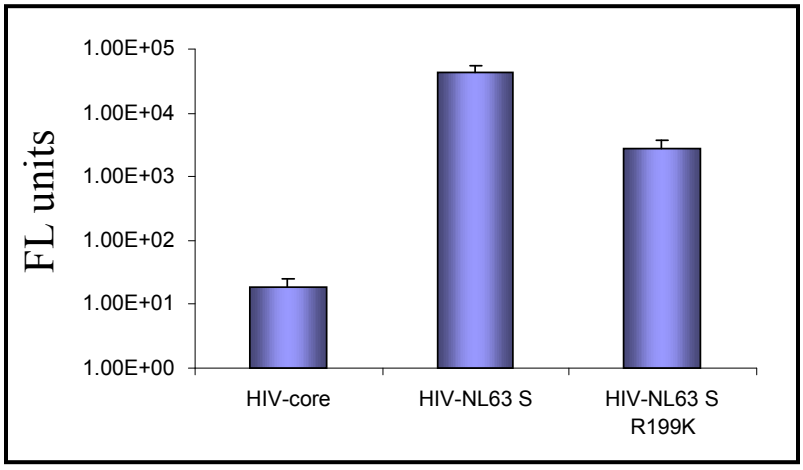

Fig. 40. Transduction Potentials of NL63 S proteins. HIV particles harboring no glycoproteins (core), NL63 S (wt), or NL63 S (R199K) were used to transduce target hACE2-293 cells. Luciferase accumulated in these cells was evaluated 40 h post-transduction and the raw values are plotted.

CHAPTER IV

DISCUSSION

Spike Protein Palmitoylations as Virus Entry and Assembly Factors

Viral fusion proteins have distinctive, sequence-specific TM and ENDO domains. Deleting or replacing these regions with similar hydrophobic sequences can eliminate fusion function (Bissonnette et al., 2009; Broer et al., 2006; Helseth et al., 1990; Melikyan et al., 1999; Shang, Yue, and Hunter, 2008). This sequence specificity indicates that the TM and ENDO domains have functions beyond mere anchoring of their respective ECTO domains. In addition to amino acid sequence specificities, the transmembrane spans of viral fusion proteins appear to have unusual length requirements as well. While a 20-residue alpha helix can vertically span a lipid bilayer, viral fusion proteins have hydrophobic, putative TM spans ranging from ~25 to ~50 residues. There are several proposed operating mechanisms for these lengthy hydrophobic helices. One view is that the long hydrophobic stretches, if positioned during pre-fusion states at oblique angles relative to the viral membrane plane, might create local membrane deformations or "dimples" pointing toward the target membrane. Such membrane deformations help bring the two membranes into close contact (Chernomordik and Kozlov, 2003; Cohen and Melikyan, 2004). Another viewpoint is that long hydrophobic

anchoring helices are required so that they can be accommodated at various orientations within the curved membrane architectures arising during bilayer fusions (Langosch, Hofmann, and Ungermann, 2007) (see Fig. 1).

Coronavirus S proteins have distinctive TM-ENDO domain features that might further reveal fusion operating mechanisms. The portion of the coronavirus S transmembrane-cytoplasmic region that is highly hydrophobic and likely alpha helical includes ~ 42 amino acids, from K1263 to D1305 in MHV A59 (see Fig. 4). The C-terminal part of this region comprises the cysteine-rich motif, and if all cysteines are palmitoylated as is strongly suggested by ^{3}H palmitate labeling (Bos et al., 1995; Petit et al., 2007), then this region would be extraordinarily lipophilic. Indeed, each S trimer would add twenty seven 16-carbon chain lipids to the inner virion membrane leaflet. Several reports evaluating truncated coronavirus S proteins missing part or all of these acylated tails have provided valuable data on the minimal tail lengths required to preserve biological function (Bos et al., 1995; Bosch et al., 2005; Petit et al., 2007; Ye, Montalto-Morrison, and Masters, 2004). We used a more subtle approach to evaluate tail activities by substituting one or more of the nine cysteines in the palmitoylation motif with alanines. We expected that the reduced palmitoylation in the C-A mutants would have deleterious effects on membrane fusion, in accordance with earlier reports (Bos et al., 1995), but would not entirely eliminate fusion activities in the way that the truncation mutants do, making it so that we could get some insights into the specific points in the fusion reaction where the palmitates might be operating.

One of our findings was that the distal cysteine-to-alanine substitutions in the endodomain reduced spike protein incorporation into virions. Hydrophobic palmitates may determine assembly of spike into virus particles by helping position the ENDO domain along the cytoplasmic face of lipid bilayers, thereby facilitating interaction with the assembly-orchestrating M protein. It has already been established that the S-M interaction is generally dependent on S protein palmitoylation, since addition of a pharmacologic inhibitor of palmitoylation (2-bromopalmitate) inhibits efficient S-M complex formation (Thorp et al., 2006). In fact, palmitoylation is known to regulate protein-protein interactions (Shmueli et al., 2010). Our data indicate that the most distal carboxy-terminal cysteines / palmitates are crucial elements for S incorporation. Notably, for other class I fusion proteins such as HIV-1 Env and influenza HA, palmitoylation of ENDO domain cysteines is also required for assembly (Chen, Takeda, and Lamb, 2005; Rousso, 2000), although these requirements vary with influenza virus strains. For HIV and influenza, assembly and budding take place at or near the plasma membrane in lipid raft microdomains (Ono and Freed, 2001; Takeda et al., 2003; Zhang, Pekosz, and Lamb, 2000), and the requirements for glycoprotein incorporation into virions might be explained by the biophysical partitioning of palmitoylated proteins into lipid rafts (Melkonian et al., 1999). Coronaviruses bud into the endoplasmic reticulum Golgi intermediate complex (ERGIC) (Krijnse-Locker et al., 1994; Tooze, Tooze, and Warren, 1984), where raft-defining lipids are relatively rare (van Meer, Voelker, and Feigenson, 2008). Thus, the palmitate requirements for S assembly are less clear, but it is

possible that the extraordinary degree of S palmitoylation might organize adjacent ER lipids into rigid arrays that are similar to plasma membrane raft-like environments.

The efficiency of the S-M interaction in MHV appears to be more sensitive to changes in palmitoylation than in SARS-CoV. A recent report showed that a palmitoylation-null SARS S protein, in which all 9 ENDO domain cysteines were mutated to alanines, was fully capable of interacting with SARS M protein (McBride and Machamer, 2010). In contrast to MHV S protein, SARS spike contains an ER retrieval signal in its cytoplasmic tails that helps it localize to the virus assembly site (McBride, Li, and Machamer, 2007). Thus, SARS spikes might not rely on palmitoylation for interacting with the assembly orchestrator M proteins, as much as MHV spikes do.

In our experiments, there were direct relationships between S assembly and S-mediated membrane fusion competence. For example, relative to wild-type S, the 2C-A mutant was poorly incorporated into virions (Fig. 12B) and was compromised in its membrane fusing potential (Figs. 16B and 17). These relationships argue for a sorting process at the budding sites, with inclusion of S proteins into virions according to palmitoylation status. This sorting process may insure that only the most palmitoylated and most fast-fusing S proteins are integrated into secreted virions. S proteins with less palmitoylation sort to cell surfaces as free proteins and perform related cell-cell fusions. This cell-cell fusion activity appears to be far less dependent on quick fusion reactions, as the wild type and nC-A mutants were indistinguishable in our assays of syncytial formation (Fig. 15).

On cell surfaces, the wild type and nC-A mutant S proteins likely occupy similar raft-like environments because all S forms were equally incorporated into the HIV-based pseudoviruses that are known to bud from lipid raft microdomains (Nguyen and Hildreth, 2000) (Fig. 16A). Using these HIV-S pseudoviruses, we found that the stepwise substitution of one, two and then three C-terminal cysteines caused progressively declining transduction. This result could not be explained by any obvious defects in S protein structure or density on pseudoviruses, as uncleaved and cleaved S forms were equally abundant in all viruses (Fig. 16A). Therefore we sought out more subtle effects of the endodomain mutations on the virus entry process by using HR2 peptides, potent inhibitors of virus entry, as probes for the intermediate folded S protein conformations (Fig. 17). By adding HR2 peptides into media at various times before and after initiating the S refolding reaction, we could assess the time required for S proteins to enter into and out of the intermediate prehairpin state (see Fig. 1). These experiments yielded enlightening results, allowing us to conclude that the endodomain mutants remained HR2-sensitive for prolonged periods, in essence slowing the kinetics of refolding relative to wild type S proteins.

Endodomain mutant S proteins transition from native- to unfolded prehairpin states at the same rate as wild type spikes, because HR2 peptides added 0-2 min after initiating S refolding resulted in a ~10-fold reduction for all S-mediated transductions (Fig. 17A). Similarly, equivalent inhibitions were observed when HR2 peptides were added 0-4 min after initiation. In contrast, when HR2s were introduced at various times after initiating S refoldings, the nC-A mutants were preferentially blocked (Fig. 17B).

These data support a view in which the duration of the prehairpin state is regulated by the palmitoylated endodomains. The timely completion of hairpin closure appears to correlate with virus infectivity.

As we expected, the kinetics of S protein refolding was also reflected by the relative abundances of proteinase K-resistant 6-HB hairpin forms in the various virus preparations. Our experiments here were modeled after Taguchi et al., who found that coronavirus S proteins can be triggered to refold into 6-HBs by exposure to soluble receptors (Matsuyama and Taguchi, 2002). Indeed, soluble receptors created increasing 6-HB levels with increasing incubation time (Fig. 18A) and the endodomain mutations impeded this 6-HB formation in accordance with the number of endodomain mutations (Fig. 18B). All of these findings solicit speculations on the way in which the ENDO domains, specifically the cysteines and / or their palmitate adducts, change the rate-limiting step of the membrane fusion reaction. Given that the ENDO domain nC-A mutations progressively extend the HR2-sensitive stage, we suggest that the absence of these cysteines-palmitates raises an activation energy barrier between the HR2-sensitive and 6-HB stage. It is known that the SARS-CoV HR2 regions exist in monomer-trimer equilibrium (McReynolds et al., 2008). The idea is that the equilibrium has to be shifted toward monomers, so that separated HR2 helices can each invert relative to HR1 and attach in antiparallel fashion onto the HR1 trimers (see Fig. 1). Given that the HR2 regions in isolation can stick together into trimers (McReynolds et al., 2008), the role of the endodomain cysteines-palmitates could be to anchor the transmembrane spans such that a separation of HR2 monomers is maintained in the native S structure. This

prevention of HR2 trimerization in the native structure would then allow membrane fusion to occur in a timely fashion. We take our cues here from the cryo-EM reconstructions of HIV that reveal a tripod-like arrangement for virus spikes coming out of the virion membrane (Zhou et al., 2007; Zhu et al., 2006). Class I protein – mediated membrane fusion may depend on pre-fusion spikes with separated HR2 domains. Palmitoylation of juxtamembranous cysteines may induce the transmembrane domain to tilt relative to the lipid bilayer plane, as suggested by Abrami *et al.* (Abrami et al., 2008), who found that unusually long transmembrane spans could be accommodated within membrane interiors if palmitoylated endodomain cysteines were nearby to presumably keep the spans from adopting a perpendicular orientation relative to the membrane. If this concept applies to the S proteins, then extracellular extension from the membrane bilayer might be progressively more oblique with increasing endodomain palmitoylation, and in turn, the degree to which HR2 regions remain separated and poised for the membrane fusion reaction would relate to the extent of endodomain palmitoylation.

One final and obvious point about our study is that the workings of viral fusion proteins can only be partially understood by analyzing the structure and function of soluble protein ECTO domains. The way that viral fusion proteins are embedded into virion and infected-cell membranes is crucial to our understanding. For the coronaviruses, extensive palmitoylation of fusion protein endodomains may set up a metastable membrane embedment that is both preferentially selected for assembly into virions and is set up for rapid membrane fusion – related refolding.

Proteolytic Activation of Coronavirus Entry by Type II Transmembrane Proteases

Surface glycoproteins facilitating virus-cell membrane fusions are synthesized and maintained in precursor intermediate folding states, and proteolysis permits refolding and energy release required to create stable virus-cell linkages and membrane coalescence. In my dissertation research, I evaluated the proteolytic priming of SARS-CoV S proteins and identified TMPRSS2 as a novel activating protease. This finding was relevant to the field, as revealed by the publication of two other reports with similar findings (Glowacka et al., 2011; Matsuyama et al., 2010), which were put forward after our manuscript was submitted for review (Shulla et al., 2011).

We began by evaluating several TTSPs for activation of S protein entry functions and found that TMPRSS2, a member of the Hepsin/TMPRSS subfamily (Bugge, Antalis, and Wu, 2009), was potent in enhancing S-mediated entry, more so than TMPR11a or 11d (HAT). The TMPRSS2 levels providing ~10 fold augmentation of SARS S-mediated entry in 293T human embryonic kidney cells were similar to those found endogenously in Calu3 human airway epithelial cells (Taylor Heald-Sargent's unpublished data). Notably, TMPRSS2 is expressed in epithelial cells lining the nose, trachea and distal airways, including alveoli and type II pneumocytes as determined by *in situ* hybridization studies (Donaldson et al., 2002). As such, TMPRSS2 may be a relevant protease for lower-airway SARS-CoV infections.

TMPRSS2 expressed in virus target 293T cells was potent in augmenting SARS S-mediated entry. This augmentation of cell entry was specific to SARS S, since VSV G-and Ebola GP-mediated entry was not affected by TMPRSS2 (Fig. 20B). Furthermore,

the augmentation was most likely due to activating cleavage of SARS S, as evidenced by the presence of SARS S cleavage fragments in 293T target cells expressing TMPRSS2 (Fig. 23). At present we do not know the exact SARS S sequence motifs that are recognized and cleaved by TMPRSS2. A recent report by Kam *et al*. (Kam et al., 2009) indicated that the related TMPRSS11a cleaved a purified recombinant form of SARS S protein at two sites: R667 and R797, which correspond to the activating cleavage sites determined by Belouzard *et al.* (Belouzard, Chu, and Whittaker, 2009). TMPRSS2 could potentially cleave SARS S at positions R667 (SLLR/STSQ) and R797 (PTKR/SFIE), since both of these sites are similar to the plasminogen activated receptor 2 (PAR2) motif (SKGR/SLIG), which is a known substrate for TMPRSS2 (Wilson et al., 2005).

TMPRSS2-mediated cleavage of SARS S at position R797 is particularly interesting. This scission occurs immediately N-terminal to the putative fusion peptide (Madu et al., 2009) and as such it could liberate the fusion peptide from intervening sequences and allow for the membrane fusion event to occur. We view this activating TMPRSS2-mediated proteolysis occurring after SARS spikes have unfolded into the prehairpin intermediates and fusion peptide have inserted into the target membrane, which is analogous to the proteolytic activation of MHV2 proposed by Matsuyama *et al*. (Matsuyama and Taguchi, 2009) (Fig. 41). The concept of activating proteolysis occurring at a very specific stage during the viral fusion protein unfolding is novel among class I fusion proteins and certainly requires further mechanistic understanding.

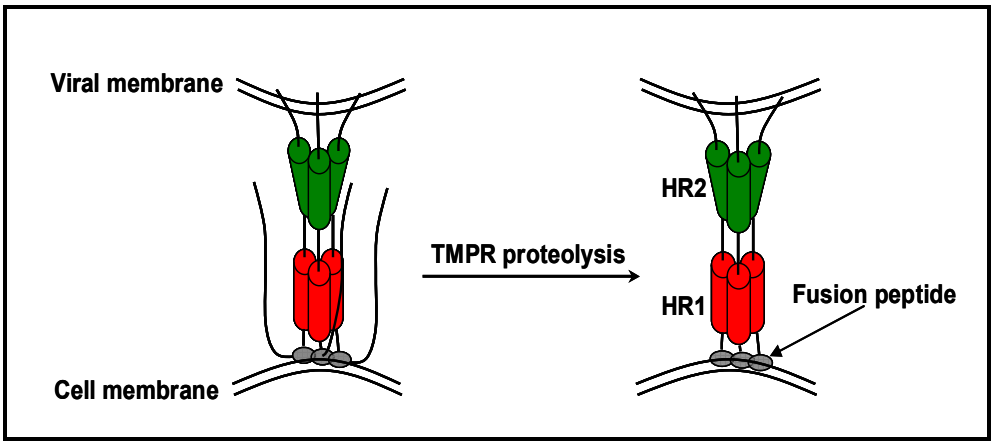

Fig. 41. Model for TMPRSS2-Mediated Proteolysis of SARS S. A SARS S protein trimer is depicted in its prehairpin conformation which is thought to be generated upon ACE2 receptor engagement. TMPRSS2-mediated cleavage N-terminal to the fusion peptide might remove sterically interfering sequences, thus allowing for membrane fusion to occur.

In contrast to the activating effect when expressed in virus target cells, TMPRSS2 expression in virus producer cells led to premature proteolysis and inactivation of SARS S proteins (Fig. 24). This is in sharp contrast to the TMPRSS2-mediated cleavage activation of influenza HA0 proteins during their transport in exocytic pathways (Bottcher et al., 2006) and to numerous furin-cleaved viral glycoproteins (Klenk and Garten, 1994). It is possible that *in vivo* expression of TMPRSS2 may cause SARS-CoV reduced infectivities, in analogy to the pseudovirus context. Interestingly, patients in late stage human SARS disease had very low levels of infectious virus but severe immunopathologies (Peiris et al., 2003), and there is evidence that non-infectious SARS

virus particles are pro-inflammatory and could elicit responses characteristic of late stage SARS immunopathologies (Tseng et al., 2005a).

SARS-CoV appears to have remarkable resourcefulness, as either endosomal acidophilic proteases or cell-surface TMPRSS2 could provide equivalent ~ 1,000-fold enhanced entry. In contrast, only serine proteases target influenza HA (Chaipan et al., 2009) and only cysteine proteases target Ebola GP (Chandran et al., 2005) during entry. Are these two divergent protease activities completely redundant or are there contexts in which TTSPs are specifically required? Our hypothesis is that certain *in vivo* infections require the cell surface activities of TTSPs. Indeed, very recent data by Huang *et al.* (Huang et al., 2011) showed that SARS-CoV, harboring spikes that were pre-cleaved with soluble trypsin protease, could bypass the inhibitory effects of interferon-inducible transmembrane (IFITM) proteins, which are present in endosomal compartments. Thus, TMPRSS2 and other TTSPs providing cell surface proteolytic activation and possible immune evasion could determine SARS-CoV cell and tissue tropism. The importance of TMPRSS2 during *in vivo* infections can be addressed pharmacologically by infecting human airway epithelial cultures (Sims et al., 2005) in the presence of type-specific protease inhibitors (Otlewski et al., 2005), or genetically by infecting mice lacking selected transmembrane proteases (Kim et al., 2006). Taylor Heald-Sargent in the Gallagher lab is currently using short hairpin RNAs (shRNAs) to knock-down TMPRSS2 levels in Calu-3 human airway epithelial cells and evaluate SARS S-mediated entry.

The TMPRSS2 – mediated enhancement of SARS virus entry was accompanied by remarkable changes in ACE2. At low doses, TMPRSS2 converted ACE2 from ~ 130

kDa to ~ 115 kDa forms, a change we believe comes either from ACE2 deglycosylation or from a failure to initially glycosylate the six predicted N-glycan sites in the ACE2 ectodomain (Tipnis et al., 2000). TMPRSS2 and the related hepsin protease are known to interfere with protein N-glycosylation by an unknown mechanism (Bertram et al., 2010), and so it is possible that under- or non-glycosylated membrane proteins are common to cells expressing various TTSPs. Increasing amounts of TMPRSS2 converted the detectable portion of ACE2 to a ~ 20 kDa C-terminal fragment. We did not identify the sister ectodomain fragment in culture media, but did readily detect soluble ACE2 liberated from cells by TNF-alpha converting enzyme (TACE), an unrelated protease known to cleave ACE2 (Jia et al., 2009; Lambert et al., 2005). It is possible that TTSPs cleave at multiple arginines and lysines throughout ACE2, leaving only short peptides (Hooper et al., 2001). At any rate, this ACE2 diminution amounts to "shedding", a well-known phenomenon thus far attributed only to tumor necrosis factor-α converting enzyme (TACE). On the basis of the ~20kDa fragment mobility in Fig. 25B, the TMPRSS2 cleaves more N-terminal than TACE (Iwata, Silva Enciso, and Greenberg, 2009; Jia et al., 2009), and indeed we have found that a TACE-resistant ACE2 (Jia et al., 2009) is subject to TMPRSS2 shedding (data not shown), indicating distinct protease targets. That ACE2 shedding is achieved by at least two divergent proteases suggests multiple post-translational regulations of this enzyme, testifying to the importance of ACE2 regulation in SARS pathogenesis (Kuba et al., 2005) and lung homeostasis in general (Imai et al., 2005).

ACE2 diminution in response to TMPRSS2 was readily apparent by immunofluorescence microscopy as well. Indeed, the inverse relationships between TMPRSS2 and ACE2 levels on cell surfaces (Fig. 26A) again suggested that TMPRSS2 associates with ACE2 during or after exocytic transport, and that TMPRSS2 occludes, degrades, and / or sheds the vast majority of the ACE2 that is capable of binding to viral S proteins. The findings also highlight the miniscule, virtually undetectable ACE2 levels that will support SARS virus entry as long as the TMPRSS2 protease is available. In concert with this view, 293T cells, which are thought to have little if any ACE2 (Moore et al., 2004), were made susceptible to SARS S entry by TMPRSS2 alone (Fig. 28B). The readily detectable host susceptibility determinant here is the protease, not the primary virus receptor.

The results of co-immunoprecipitation analyses supported the view that ACE2 and TMPRSS2 associate together. While catalytically-inactive TMPRSS2 (S441A) did not co-precipitate ACE2, the wild type TMPRSS2 did, and this ACE2:TMPRSS2 connection was striking given that the overall ACE2 levels were low in the presence of the active TMPRSS2 protease. These findings indicated an unusually stable tethering of the active enzyme, but not the inactive zymogen, with one of its substrates. It is possible that most of the ACE2-TMPRSS2 interaction that was observed by immunoprecipitating whole cell lysates is a reflection of intracellular rather than cell surface association. A future direction would be to restrict the analysis only to ACE2 and TMPRSS2 present at the cell surface. Furthermore, it would be important to determine the interacting regions in ACE2 and TMPRSS2 proteins so that association of these two entry factors can be

correlated with efficiency of virus entry. One possibility is that these two proteins interact by disulfide linkages, as recent experiments in the Gallagher lab do suggest.

TTSPs are known to shed their enzyme-active domains into extracellular environments (Antalis et al., 2010). For example, soluble TMPRSS2 is enriched in the seminal fluid of the prostate (Afar et al., 2001; Lucas et al., 2008)and soluble HAT is commonly found in the sputum of patients with chronic respiratory disease (Yasuoka et al., 1997). This is interesting because soluble proteases, such as trypsin and elastase, are known to activate SARS S proteins that were already bound to ACE2 receptors (Matsuyama et al., 2005). Thus we asked whether TMPRSS2 might operate in "trans" to activate SARS S-mediated entry into adjacent ACE2+ cells. We found no evidence for this; adjacent TMPRSS2 did not influence SARS S-mediated entry. Corroborating this finding, we further demonstrated that TMPRSS2 did not digest ACE2 when the two membrane proteins were expressed in adjacent cells. Therefore we suggest that the cells most susceptible to SARS-CoV infection are those in which ACE2 and TTSPs are simultaneously present, and that at least the TMPRSS2 on ACE2-negative cells has limited paracrine activities on ACE2 or SARS-CoV infections.

Following publication of our findings, Glowacka *et al*. (Glowacka et al., 2011) showed once again that TMPRSS2 activates SARS-CoV S protein to mediate fusion. Furthermore, they showed that ACE2 and TMPRSS2 were co-expressed in type II pneumocytes, which are SARS-CoV target cells *in vivo*. The latter finding implicates the relevance of TMPRSS2 in activating SARS-CoV S in the lungs of infected individuals.

Localization of Receptors and Proteases in Lipid Rafts: Roles for Lipid Rafts as Virus Entry Factors

Cell surface lipid rafts serve as platforms for entry of several viruses, including coronaviruses (Chazal and Gerlier, 2003). The importance of membrane rafts and cholesterol for coronavirus cell entry has been extensively documented (Choi, Aizaki, and Lai, 2005; Glende et al., 2008; Lu, Liu, and Tam, 2008; Nomura et al., 2004; Thorp and Gallagher, 2004). However, the evidence for localization of ACE2 receptor in lipid rafts was somewhat controversial, since it was shown that ACE2 associates with lipid raft containing fractions in African green monkey kidney (Vero) cells (Lu, Liu, and Tam, 2008), but not Chinese hamster ovary (CHO) cells (Warner et al., 2005). In our experiments we focused only at the relevant cell surface localized ACE2 and determined that ACE2 was entirely associated with lipid raft containing fractions in human embryonic kidney (293T) cells. The discrepancy in the literature with respect to ACE2 raft localization is most likely due to the methodologies used rather than the difference in cell types. Indeed, in our own experiments we observed that evaluating total (intracellular + cell surface) ACE2 protein levels resulted in complete ACE2 association with non-raft fractions (data not shown). Only when the analysis was restricted to the small amount of ACE2 protein present on the cell surface and not the pool of protein accumulated intracellularly, we were able to detect complete association of ACE2 with TX-100 resistant membrane fractions (Fig. 34A).

We expected TMPRSS2 to partition into lipid microdomains together with ACE2, since our data argued that infecting viruses depended simultaneously on these two

proteins. The fact that TMPRSS2 degraded ACE2 made it challenging to microscopically identify cells in which both these proteins were present. However, when rare ACE2+-TMPRSS2+ cells were found, clear co-localizations were immediately evident (Fig. 26). Notably, TMPRSS2 is set apart from other TTSPs by its longer, potentially palmitoylated 84-residue cytoplasmic tail (Bugge, Antalis, and Wu, 2009), which may confer positioning into lipid rafts. Our data indicated that only ~30% of cell surface TMPRSS2 proteins were associated with TX-100 resistant membranes, while the rest were present in non-raft fractions. However, the ratio of TMPRSS2 present in raft vs. non-raft fractions changed upon binding and entry of SARS-S bearing HIV pseudoparticles. We view that the SARS-CoV susceptible cell may be defined by tendencies for the ACE2 and TMPRSS2 to congregate together in lipid raft microdomains.

We do not know the exact role of lipid rafts in SARS-CoV entry yet. It is possible that membrane rafts act as a lipid planar milieu favoring interactions between ACE2 and TMPRSS2 that have some intrinsic affinity for each other. Also membrane rafts may dictate a particular route of entry into cells, such as the one involving lipid raft resident caveolin proteins. It has been suggested that the human coronavirus 229E uses lipid rafts and caveolae to enter cells (Nomura et al., 2004). Further studies are necessary to identify the route of SARS-CoV entry and to determine whether caveolae are involved in the process.

β1 Integrin: A Putative Coreceptor for HCoV-NL63 S-Mediated Entry

The hypothesis that integrins were involved in human NL63-coronavirus entry was supported by the fact that integrins serve as primary or secondary receptors for both enveloped and nonenveloped viruses (Stewart and Nemerow, 2007). In addition, the primary HCoV-NL63 receptor ACE2 resides in lipid raft microdomains (Lu, Liu, and Tam, 2008), as do integrins (Resh, 2006; van Zanten et al., 2009), and one report documents close association of ACE2 with β1 integrins (Lin et al., 2004).

In our experiments using 293T cells we showed that blocking β1 integrins with specific monoclonal antibodies led to significant reduction in NL63 S-mediated entry, but not SARS S- or VSV G-mediated entry. Furthermore, knock-down of β1 integrin protein levels also led to a reduction in NL63 S-, but not SARS S-mediated entry. We view the effect of β1 integrins on NL63 S-mediated entry linked to the activity of cellular proteases that may be required for cleaving and activating NL63-S proteins. Indeed, HIV particles harboring pre-cleaved NL63 S (cl) proteins were not dependent on β1 integrins for entry as much as HIV particles harboring NL63 S (wt) proteins. We do not know the identity of cellular proteases that might be cleaving NL63 S proteins; however we view endosomal cathepsins as likely candidates, in analogy to SARS S- and Ebola GP-mediated entry (Chandran et al., 2005; Simmons et al., 2005).

Reoviruses, which are nonenveloped viruses, also depend on endosomal cathepsins B and L cleavage for productive entry into cells (Ebert et al., 2002). In addition, reoviruses require β1-integrins for efficient infection (Maginnis et al., 2006). Interestingly, pre-treating reoviruses with exogenous chymotrypsin protease relieves the

need for β1 integrins (Maginnis et al., 2006), similar to our findings with NL63 S (cl).

Beta-1 integrins might be important for shuttling virions into appropriate protease-rich endocytic compartments. The endocytosis of integrin heterodimers occurs by both clathrin-dependent and clathrin-independent endocytic mechanisms (Caswell, Vadrevu, and Norman, 2009). The cytoplasmic tails of β1 integrins contain NPXY (X is any aminoacid) motifs, which are known to interact with endocytic adaptor proteins and be recruited in clathrin coated pits (Pellinen et al., 2008). Notably, β1 integrins containing mutations in the NPXY motifs did not support productive reovirus entry into cells due to the trafficking of viruses into lysosome-like organelles (Maginnis et al., 2008). It would be interesting to determine whether the same β1 integrin cytoplasmic motifs are involved in HCoV-NL63 S-mediated entry into the endocytic organelles that provide the milieu for productive infection.

We don't know yet which β1 integrin heterodimer is involved in HCoV-NL63 entry. As shown in Fig. 42, β1 integrins can pair with at least 10 different α- subunits, thus forming the largest integrin subfamily. It is known that HEK293 cells, which we have used in our studies of virus entry, express αv and α5 integrins (Li et al., 2001) that could pair with β1 integrins. We view α5β1 integrin heterodimer as a likely candidate, mainly because NL63 S proteins contain the well-known α5β1 integrin binding motif NGR in their sequences (Koivunen, Gay, and Ruoslahti, 1993). Mutation of this motif in NL63 S (R199K) resulted in reduction of virus entry, suggesting that there might be a possible interaction between NL63 S and α5β1 integrin via the NGR motif.

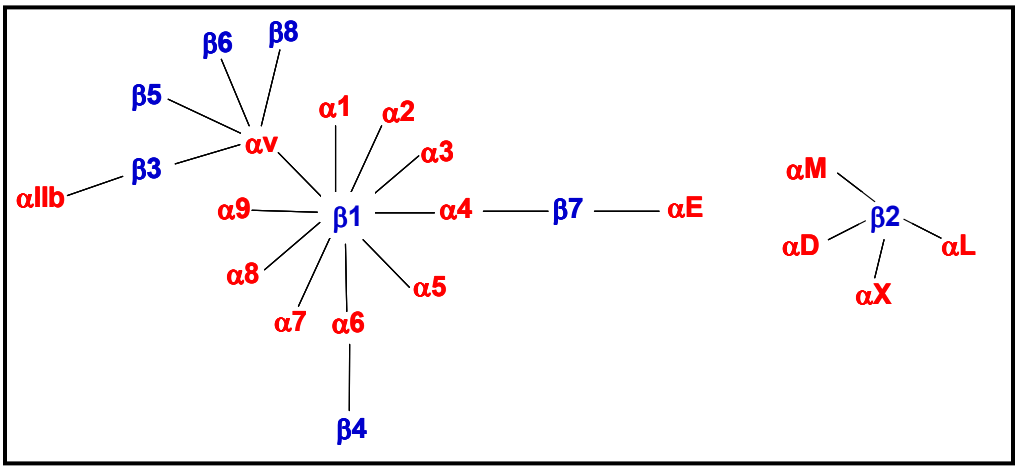

Fig. 42. Major Integrin Pairings. β integrins are shown in blue and alpha integrins in red. 8 β-subunits and 16 α-subunits are depicted. Lines connecting α and β integrins indicate the known pairings of the two subunits.

The entry of several human coronaviruses in differentiated airway epithelial cell cultures has been evaluated and infection appears ta take place preferentially from the apical rather than the basolateral surface of these cells (Jia et al., 2005; Tseng et al., 2005b). Almost all integrins expressed in airway epithelia are concentrated in the basement membranes; however they can be rapidly induced around the lateral and apical surfaces upon injury (Sheppard, 2003). Other viruses, such as adenoviruses access basoletaral integrins for their entry by disrupting tight junctions (Walters et al., 2002). It is not known whether HCoV-NL63 uses similar aggressive methods for entry, or instead relies on coinfections with other viral pathogens. Of note, respiratory infections do cause epithelial lung injury, and very often HCoV-229E and HCoV-NL63 are accompanied by

a second respiratory virus infection (van der Hoek et al., 2005).

REFERENCES

Abrahamyan, L. G., Mkrtchyan, S. R., Binley, J., Lu, M., Melikyan, G. B., and Cohen, F. S. (2005). The cytoplasmic tail slows the folding of human immunodeficiency virus type 1 Env from a late prebundle configuration into the six-helix bundle. *J Virol* **79**(1)**,** 106-15.

Abrami, L., Kunz, B., Iacovache, I., and van der Goot, F. G. (2008). Palmitoylation and ubiquitination regulate exit of the Wnt signaling protein LRP6 from the endoplasmic reticulum. *Proc Natl Acad Sci U S A* **105**(14)**,** 5384-9.

Afar, D. E., Vivanco, I., Hubert, R. S., Kuo, J., Chen, E., Saffran, D. C., Raitano, A. B., and Jakobovits, A. (2001). Catalytic cleavage of the androgen-regulated TMPRSS2 protease results in its secretion by prostate and prostate cancer epithelia. *Cancer Res* **61**(4)**,** 1686-92.

Akula, S. M., Pramod, N. P., Wang, F. Z., and Chandran, B. (2002). Integrin alpha3beta1 (CD 49c/29) is a cellular receptor for Kaposi's sarcoma-associated herpesvirus (KSHV/HHV-8) entry into the target cells. *Cell* **108**(3)**,** 407-19.

Ali, A., Avalos, R. T., Ponimaskin, E., and Nayak, D. P. (2000). Influenza virus assembly: effect of influenza virus glycoproteins on the membrane association of M1 protein. *J Virol* **74**(18)**,** 8709-19.

Anderson, J. L., and Hope, T. J. (2005). Intracellular trafficking of retroviral vectors: obstacles and advances. *Gene Ther* **12**(23)**,** 1667-78.

Antalis, T. M., Buzza, M. S., Hodge, K. M., Hooper, J. D., and Netzel-Arnett, S. (2010). The cutting edge: membrane-anchored serine protease activities in the pericellular microenvironment. *Biochem J* **428**(3)**,** 325-46.

Aoki, Y., Aizaki, H., Shimoike, T., Tani, H., Ishii, K., Saito, I., Matsuura, Y., and Miyamura, T. (1998). A human liver cell line exhibits efficient translation of HCV RNAs produced by a recombinant adenovirus expressing T7 RNA polymerase. *Virology* **250**(1)**,** 140-50.

Backovic, M., and Jardetzky, T. S. (2009). Class III viral membrane fusion proteins. *Curr Opin Struct Biol* **19**(2)**,** 189-96.

Baltimore, D. (1970). RNA-dependent DNA polymerase in virions of RNA tumour viruses. *Nature* **226**(5252)**,** 1209-11.

Barbouche, R., Miquelis, R., Jones, I. M., and Fenouillet, E. (2003). Protein-disulfide isomerase-mediated reduction of two disulfide bonds of HIV envelope glycoprotein 120 occurs post-CXCR4 binding and is required for fusion. *J Biol Chem* **278**(5)**,** 3131-6.

Barcena, M., Oostergetel, G. T., Bartelink, W., Faas, F. G., Verkleij, A., Rottier, P. J., Koster, A. J., and Bosch, B. J. (2009). Cryo-electron tomography of mouse hepatitis virus: Insights into the structure of the coronavirion. *Proc Natl Acad Sci U S A* **106**(2)**,** 582-7.

Bart, K. J., Orenstein, W. A., and Hinman, A. R. (1986). The virtual elimination of rubella and mumps from the United States and the use of combined measles, mumps and rubella vaccines (MMR) to eliminate measles. *Dev Biol Stand* **65,** 45-52.

Barton, E. S., Forrest, J. C., Connolly, J. L., Chappell, J. D., Liu, Y., Schnell, F. J., Nusrat, A., Parkos, C. A., and Dermody, T. S. (2001). Junction adhesion molecule is a receptor for reovirus. *Cell* **104**(3)**,** 441-51.

Beaufort, N., Leduc, D., Eguchi, H., Mengele, K., Hellmann, D., Masegi, T., Kamimura, T., Yasuoka, S., Fend, F., Chignard, M., and Pidard, D. (2007). The human airway trypsin-like protease modulates the urokinase receptor (uPAR, CD87) structure and functions. *Am J Physiol Lung Cell Mol Physiol* **292**(5)**,** L1263-72.

Belouzard, S., Chu, V. C., and Whittaker, G. R. (2009). Activation of the SARS coronavirus spike protein via sequential proteolytic cleavage at two distinct sites. *Proc Natl Acad Sci U S A* **106**(14)**,** 5871-6.

Belouzard, S., Madu, I., and Whittaker, G. R. (2010). Elastase-mediated activation of the severe acute respiratory syndrome coronavirus spike protein at discrete sites within the S2 domain. *J Biol Chem* **285**(30)**,** 22758-63.

Benbacer, L., Kut, E., Besnardeau, L., Laude, H., and Delmas, B. (1997). Interspecies aminopeptidase-N chimeras reveal species-specific receptor recognition by canine coronavirus, feline infectious peritonitis virus, and transmissible gastroenteritis virus. *J Virol* **71**(1)**,** 734-7.

Beniac, D. R., Devarennes, S. L., Andonov, A., He, R., and Booth, T. F. (2007). Conformational Reorganization of the SARS Coronavirus Spike Following Receptor Binding: Implications for Membrane Fusion. *PLoS ONE* **2**(10)**,** e1082.

Bentz, J., and Mittal, A. (2000). Deployment of membrane fusion protein domains during fusion. *Cell Biol Int* **24**(11)**,** 819-38.

Bergelson, J. M., Shepley, M. P., Chan, B. M., Hemler, M. E., and Finberg, R. W. (1992). Identification of the integrin VLA-2 as a receptor for echovirus 1. *Science* **255**(5052)**,** 1718-20.

Berget, S. M., Moore, C., and Sharp, P. A. (1977). Spliced segments at the 5' terminus of adenovirus 2 late mRNA. *Proc Natl Acad Sci U S A* **74**(8)**,** 3171-5.

Bertram, S., Glowacka, I., Blazejewska, P., Soilleux, E., Allen, P., Danisch, S., Steffen, I., Choi, S. Y., Park, Y., Schneider, H., Schughart, K., and Pohlmann, S. (2010). TMPRSS2 and TMPRSS4 Facilitate Trypsin-Independent Spread of Influenza Virus in Caco-2 Cells. *J Virol* **84**(19)**,** 10016-25.

Bissonnette, M. L., Donald, J. E., DeGrado, W. F., Jardetzky, T. S., and Lamb, R. A. (2009). Functional analysis of the transmembrane domain in paramyxovirus F protein-mediated membrane fusion. *J Mol Biol* **386**(1)**,** 14-36.

Bonavia, A., Zelus, B. D., Wentworth, D. E., Talbot, P. J., and Holmes, K. V. (2003). Identification of a receptor-binding domain of the spike glycoprotein of human coronavirus HCoV-229E. *J Virol* **77**(4)**,** 2530-8.

Bos, E. C., Heijnen, L., Luytjes, W., and Spaan, W. J. (1995). Mutational analysis of the murine coronavirus spike protein: effect on cell-to-cell fusion. *Virology* **214**(2)**,** 453-63.

Bos, E. C., Luytjes, W., van der Meulen, H. V., Koerten, H. K., and Spaan, W. J. (1996). The production of recombinant infectious DI-particles of a murine coronavirus in the absence of helper virus. *Virology* **218**(1)**,** 52-60.

Boscarino, J. A., Logan, H. L., Lacny, J. J., and Gallagher, T. M. (2008). Envelope protein palmitoylations are crucial for murine coronavirus assembly. *J Virol* **82**(6)**,** 2989-99.

Bosch, B. J., Bartelink, W., and Rottier, P. J. (2008). Cathepsin L functionally cleaves the severe acute respiratory syndrome coronavirus class I fusion protein upstream of rather than adjacent to the fusion peptide. *J Virol* **82**(17)**,** 8887-90.

Bosch, B. J., de Haan, C. A., Smits, S. L., and Rottier, P. J. (2005). Spike protein assembly into the coronavirion: exploring the limits of its sequence requirements. *Virology* **334**(2)**,** 306-18.

Bosch, B. J., Martina, B. E., Van Der Zee, R., Lepault, J., Haijema, B. J., Versluis, C., Heck, A. J., De Groot, R., Osterhaus, A. D., and Rottier, P. J. (2004). Severe acute respiratory syndrome coronavirus (SARS-CoV) infection inhibition using spike protein heptad repeat-derived peptides. *Proc Natl Acad Sci U S A* **101**(22)**,** 8455-60.

Bosch, B. J., van der Zee, R., de Haan, C. A., and Rottier, P. J. (2003). The coronavirus spike protein is a class I virus fusion protein: structural and functional characterization of the fusion core complex. *J Virol* **77**(16)**,** 8801-11.

Bottcher, E., Freuer, C., Steinmetzer, T., Klenk, H. D., and Garten, W. (2009). MDCK cells that express proteases TMPRSS2 and HAT provide a cell system to propagate influenza viruses in the absence of trypsin and to study cleavage of HA and its inhibition. *Vaccine* **27**(45)**,** 6324-9.

Bottcher, E., Matrosovich, T., Beyerle, M., Klenk, H. D., Garten, W., and Matrosovich, M. (2006). Proteolytic activation of influenza viruses by serine proteases TMPRSS2 and HAT from human airway epithelium. *J Virol* **80**(19)**,** 9896-8.

Breslin, J. J., Mork, I., Smith, M. K., Vogel, L. K., Hemmila, E. M., Bonavia, A., Talbot, P. J., Sjostrom, H., Noren, O., and Holmes, K. V. (2003). Human coronavirus 229E: receptor binding domain and neutralization by soluble receptor at 37 degrees C. *J Virol* **77**(7)**,** 4435-8.

Broer, R., Boson, B., Spaan, W., Cosset, F. L., and Corver, J. (2006). Important role for the transmembrane domain of severe acute respiratory syndrome coronavirus spike protein during entry. *J Virol* **80**(3)**,** 1302-10.

Brojatsch, J., Naughton, J., Rolls, M. M., Zingler, K., and Young, J. A. (1996). CAR1, a TNFR-related protein, is a cellular receptor for cytopathic avian leukosis-sarcoma viruses and mediates apoptosis. *Cell* **87**(5)**,** 845-55.

Brown, D. A. (2006). Lipid rafts, detergent-resistant membranes, and raft targeting signals. *Physiology (Bethesda)* **21,** 430-9.

Bugge, T. H., Antalis, T. M., and Wu, Q. (2009). Type II transmembrane serine proteases. *J Biol Chem* **284**(35)**,** 23177-81.

Bullough, P. A., Hughson, F. M., Skehel, J. J., and Wiley, D. C. (1994). Structure of influenza haemagglutinin at the pH of membrane fusion. *Nature* **371**(6492)**,** 37-43.

Burkhard, P., Stetefeld, J., and Strelkov, S. V. (2001). Coiled coils: a highly versatile protein folding motif. *Trends Cell Biol* **11**(2)**,** 82-8.

Butel, J. S. (2000). Viral carcinogenesis: revelation of molecular mechanisms and etiology of human disease. *Carcinogenesis* **21**(3)**,** 405-26.

Cadd, T. L., Skoging, U., and Liljestrom, P. (1997). Budding of enveloped viruses from the plasma membrane. *Bioessays* **19**(11)**,** 993-1000.

Campbell, S. M., Crowe, S. M., and Mak, J. (2001). Lipid rafts and HIV-1: from viral entry to assembly of progeny virions. *J Clin Virol* **22**(3)**,** 217-27.

Carr, C. M., Chaudhry, C., and Kim, P. S. (1997). Influenza hemagglutinin is spring-loaded by a metastable native conformation. *Proc Natl Acad Sci U S A* **94**(26)**,** 14306-13.

Casais, R., Dove, B., Cavanagh, D., and Britton, P. (2003). Recombinant avian infectious bronchitis virus expressing a heterologous spike gene demonstrates that the spike protein is a determinant of cell tropism. *J Virol* **77**(16)**,** 9084-9.

Casey, J. R., Grinstein, S., and Orlowski, J. (2010). Sensors and regulators of intracellular pH. *Nat Rev Mol Cell Biol* **11**(1)**,** 50-61.

Caswell, P. T., Vadrevu, S., and Norman, J. C. (2009). Integrins: masters and slaves of endocytic transport. *Nat Rev Mol Cell Biol* **10**(12)**,** 843-53.

Cathomen, T., Naim, H. Y., and Cattaneo, R. (1998). Measles viruses with altered envelope protein cytoplasmic tails gain cell fusion competence. *J Virol* **72**(2)**,** 1224-34.

Cavanagh, D., Davis, P. J., Pappin, D. J., Binns, M. M., Boursnell, M. E., and Brown, T. D. (1986). Coronavirus IBV: partial amino terminal sequencing of spike polypeptide S2 identifies the sequence Arg-Arg-Phe-Arg-Arg at the cleavage site of the spike precursor propolypeptide of IBV strains Beaudette and M41. *Virus Res* **4**(2)**,** 133-43.

Chaipan, C., Kobasa, D., Bertram, S., Glowacka, I., Steffen, I., Tsegaye, T. S., Takeda, M., Bugge, T. H., Kim, S., Park, Y., Marzi, A., and Pohlmann, S. (2009). Proteolytic activation of the 1918 influenza virus hemagglutinin. *J Virol* **83**(7)**,** 3200-11.

Chambers, P., Pringle, C. R., and Easton, A. J. (1990). Heptad repeat sequences are located adjacent to hydrophobic regions in several types of virus fusion glycoproteins. *J Gen Virol* **71 (Pt 12),** 3075-80.

Chan, D. C., Fass, D., Berger, J. M., and Kim, P. S. (1997). Core structure of gp41 from the HIV envelope glycoprotein. *Cell* **89**(2)**,** 263-73.

Chan, D. C., and Kim, P. S. (1998). HIV entry and its inhibition. *Cell* **93**(5)**,** 681-4.

Chandran, K., and Nibert, M. L. (1998). Protease cleavage of reovirus capsid protein mu1/mu1C is blocked by alkyl sulfate detergents, yielding a new type of infectious subvirion particle. *J Virol* **72**(1)**,** 467-75.

Chandran, K., Sullivan, N. J., Felbor, U., Whelan, S. P., and Cunningham, J. M. (2005). Endosomal proteolysis of the Ebola virus glycoprotein is necessary for infection. *Science* **308**(5728)**,** 1643-5.

Chang, K. W., and Gombold, J. L. (2001). Effects of amino acid insertions in the cysteine-rich domain of the MHV-A59 spike protein on cell fusion. *Adv Exp Med Biol* **494,** 205-11.

Chang, K. W., Sheng, Y., and Gombold, J. L. (2000). Coronavirus-induced membrane fusion requires the cysteine-rich domain in the spike protein. *Virology* **269**(1)**,** 212-24.

Chazal, N., and Gerlier, D. (2003). Virus entry, assembly, budding, and membrane rafts. *Microbiol Mol Biol Rev* **67**(2)**,** 226-37.

Chen, B. J., Takeda, M., and Lamb, R. A. (2005). Influenza virus hemagglutinin (H3 subtype) requires palmitoylation of its cytoplasmic tail for assembly: M1 proteins of two subtypes differ in their ability to support assembly. *J Virol* **79**(21)**,** 13673-84.

Chernomordik, L. V., and Kozlov, M. M. (2003). Protein-lipid interplay in fusion and fission of biological membranes. *Annu Rev Biochem* **72,** 175-207.

Chernomordik, L. V., and Kozlov, M. M. (2008). Mechanics of membrane fusion. *Nat Struct Mol Biol* **15**(7)**,** 675-83.

Cherry, J. D. (2004). The chronology of the 2002-2003 SARS mini pandemic. *Paediatr Respir Rev* **5**(4)**,** 262-9.

Choi, K. S., Aizaki, H., and Lai, M. M. (2005). Murine coronavirus requires lipid rafts for virus entry and cell-cell fusion but not for virus release. *J Virol* **79**(15)**,** 9862-71.

Choi, S. Y., Bertram, S., Glowacka, I., Park, Y. W., and Pohlmann, S. (2009). Type II transmembrane serine proteases in cancer and viral infections. *Trends Mol Med* **15**(7)**,** 303-12.

Chow, L. T., Gelinas, R. E., Broker, T. R., and Roberts, R. J. (1977). An amazing sequence arrangement at the 5' ends of adenovirus 2 messenger RNA. *Cell* **12**(1)**,** 1-8.

Cohen, F. S., and Melikyan, G. B. (2004). The energetics of membrane fusion from binding, through hemifusion, pore formation, and pore enlargement. *J Membr Biol* **199**(1)**,** 1-14.

Colman, P. M., and Lawrence, M. C. (2003). The structural biology of type I viral membrane fusion. *Nat Rev Mol Cell Biol* **4**(4)**,** 309-19.

Corse, E., and Machamer, C. E. (2002). The cytoplasmic tail of infectious bronchitis virus E protein directs Golgi targeting. *J Virol* **76**(3)**,** 1273-84.

Cseke, G., Maginnis, M. S., Cox, R. G., Tollefson, S. J., Podsiad, A. B., Wright, D. W., Dermody, T. S., and Williams, J. V. (2009). Integrin alphavbeta1 promotes infection by human metapneumovirus. *Proc Natl Acad Sci U S A* **106**(5)**,** 1566-71.

Davies, H. A., and Macnaughton, M. R. (1979). Comparison of the morphology of three coronaviruses. *Arch Virol* **59**(1-2)**,** 25-33.

de Groot, R. J., Luytjes, W., Horzinek, M. C., van der Zeijst, B. A., Spaan, W. J., and Lenstra, J. A. (1987). Evidence for a coiled-coil structure in the spike proteins of coronaviruses. *J Mol Biol* **196**(4)**,** 963-6.

de Haan, C. A., Kuo, L., Masters, P. S., Vennema, H., and Rottier, P. J. (1998). Coronavirus particle assembly: primary structure requirements of the membrane protein. *J Virol* **72**(8)**,** 6838-50.

de Haan, C. A., Masters, P. S., Shen, X., Weiss, S., and Rottier, P. J. (2002). The group-specific murine coronavirus genes are not essential, but their deletion, by reverse genetics, is attenuating in the natural host. *Virology* **296**(1)**,** 177-89.

de Haan, C. A., and Rottier, P. J. (2005). Molecular interactions in the assembly of coronaviruses. *Adv Virus Res* **64,** 165-230.

de Haan, C. A., Smeets, M., Vernooij, F., Vennema, H., and Rottier, P. J. (1999). Mapping of the coronavirus membrane protein domains involved in interaction with the spike protein. *J Virol* **73**(9)**,** 7441-52.

de Haan, C. A., Stadler, K., Godeke, G. J., Bosch, B. J., and Rottier, P. J. (2004). Cleavage inhibition of the murine coronavirus spike protein by a furin-like enzyme affects cell-cell but not virus-cell fusion. *J Virol* **78**(11)**,** 6048-54.

de Haan, C. A., van Genne, L., Stoop, J. N., Volders, H., and Rottier, P. J. (2003). Coronaviruses as vectors: position dependence of foreign gene expression. *J Virol* **77**(21)**,** 11312-23.

de Haan, C. A., Vennema, H., and Rottier, P. J. (2000). Assembly of the coronavirus envelope: homotypic interactions between the M proteins. *J Virol* **74**(11)**,** 4967-78.

Delmas, B., Gelfi, J., L'Haridon, R., Vogel, L. K., Sjostrom, H., Noren, O., and Laude, H. (1992). Aminopeptidase N is a major receptor for the entero-pathogenic coronavirus TGEV. *Nature* **357**(6377)**,** 417-20.

Delmas, B., and Laude, H. (1990). Assembly of coronavirus spike protein into trimers and its role in epitope expression. *J Virol* **64**(11)**,** 5367-75.

Dimitrov, D. S. (2004). Virus entry: molecular mechanisms and biomedical applications. *Nat Rev Microbiol* **2**(2)**,** 109-22.

Donaldson, S. H., Hirsh, A., Li, D. C., Holloway, G., Chao, J., Boucher, R. C., and Gabriel, S. E. (2002). Regulation of the epithelial sodium channel by serine proteases in human airways. *J Biol Chem* **277**(10)**,** 8338-45.

Drosten, C., Gunther, S., Preiser, W., van der Werf, S., Brodt, H. R., Becker, S., Rabenau, H., Panning, M., Kolesnikova, L., Fouchier, R. A., Berger, A., Burguiere, A. M., Cinatl, J., Eickmann, M., Escriou, N., Grywna, K., Kramme, S., Manuguerra, J. C., Muller, S., Rickerts, V., Sturmer, M., Vieth, S., Klenk, H. D., Osterhaus, A. D., Schmitz, H., and Doerr, H. W. (2003). Identification of a novel coronavirus in patients with severe acute respiratory syndrome. *N Engl J Med* **348**(20)**,** 1967-76.

Du, L., Kao, R. Y., Zhou, Y., He, Y., Zhao, G., Wong, C., Jiang, S., Yuen, K. Y., Jin, D. Y., and Zheng, B. J. (2007). Cleavage of spike protein of SARS coronavirus by protease factor Xa is associated with viral infectivity. *Biochem Biophys Res Commun* **359**(1)**,** 174-9.

Duncan, R. (1996). The Low pH-Dependent Entry of Avian Reovirus Is Accompanied by Two Specific Cleavages of the Major Outer Capsid Protein μ2C. *Virology* **219**(1)**,** 179-89.

Dveksler, G. S., Pensiero, M. N., Cardellichio, C. B., Williams, R. K., Jiang, G. S., Holmes, K. V., and Dieffenbach, C. W. (1991). Cloning of the mouse hepatitis virus (MHV) receptor: expression in human and hamster cell lines confers susceptibility to MHV. *J Virol* **65**(12)**,** 6881-91.

Ebert, D. H., Deussing, J., Peters, C., and Dermody, T. S. (2002). Cathepsin L and cathepsin B mediate reovirus disassembly in murine fibroblast cells. *J Biol Chem* **277**(27)**,** 24609-17.

Eblen, S. T., Slack, J. K., Weber, M. J., and Catling, A. D. (2002). Rac-PAK signaling stimulates extracellular signal-regulated kinase (ERK) activation by regulating formation of MEK1-ERK complexes. *Mol Cell Biol* **22**(17)**,** 6023-33.

Eckert, D. M., and P. S. Kim (2001). Design of potent inhibitors of HIV-1 entry from the gp41 N-peptide region. *Proc Natl Acad Sci U S A* **98,** 11187-11192.

Elion, G. B. (1993). Acyclovir: discovery, mechanism of action, and selectivity. *J Med Virol* **Suppl 1,** 2-6.

Esper, F., Weibel, C., Ferguson, D., Landry, M. L., and Kahn, J. S. (2005). Evidence of a novel human coronavirus that is associated with respiratory tract disease in infants and young children. *J Infect Dis* **191**(4)**,** 492-8.

Feire, A. L., Koss, H., and Compton, T. (2004). Cellular integrins function as entry receptors for human cytomegalovirus via a highly conserved disintegrin-like domain. *Proc Natl Acad Sci U S A* **101**(43)**,** 15470-5.

Feng, Y., Broder, C. C., Kennedy, P. E., and Berger, E. A. (1996). HIV-1 entry cofactor: functional cDNA cloning of a seven-transmembrane, G protein-coupled receptor. *Science* **272**(5263)**,** 872-7.

Fleming, J. O., Stohlman, S. A., Harmon, R. C., Lai, M. M., Frelinger, J. A., and Weiner, L. P. (1983). Antigenic relationships of murine coronaviruses: analysis using monoclonal antibodies to JHM (MHV-4) virus. *Virology* **131**(2)**,** 296-307.

Follis, K. E., York, J., and Nunberg, J. H. (2006). Furin cleavage of the SARS coronavirus spike glycoprotein enhances cell-cell fusion but does not affect virion entry. *Virology* **350**(2)**,** 358-69.

Fouchier, R. A., Kuiken, T., Schutten, M., van Amerongen, G., van Doornum, G. J., van den Hoogen, B. G., Peiris, M., Lim, W., Stohr, K., and Osterhaus, A. D. (2003). Aetiology: Koch's postulates fulfilled for SARS virus. *Nature* **423**(6937)**,** 240.

Fraile, A., and Garcia-Arenal, F. (2010). The coevolution of plants and viruses: resistance and pathogenicity. *Adv Virus Res* **76,** 1-32.

Furuta, R. A., Wild, C. T., Weng, Y., and Weiss, C. D. (1998). Capture of an early fusion-active conformation of HIV-1 gp41. *Nat Struct Biol* **5**(4)**,** 276-9.

Gallagher, T. M. (1997). A role for naturally occurring variation of the murine coronavirus spike protein in stabilizing association with the cellular receptor. *J Virol* **71**(4)**,** 3129-37.

Gallagher, T. M., Parker, S. E., and Buchmeier, M. J. (1990). Neutralization-resistant variants of a neurotropic coronavirus are generated by deletions within the amino-terminal half of the spike glycoprotein. *J Virol* **64**(2)**,** 731-41.

Gern, J. E. (2010). The ABCs of rhinoviruses, wheezing, and asthma. *J Virol* **84**(15)**,** 7418-26.

Giancotti, F. G. (2000). Complexity and specificity of integrin signalling. *Nat Cell Biol* **2**(1)**,** E13-4.

Giurisato, E., McIntosh, D. P., Tassi, M., Gamberucci, A., and Benedetti, A. (2003). T cell receptor can be recruited to a subset of plasma membrane rafts, independently of cell signaling and attendantly to raft clustering. *J Biol Chem* **278**(9)**,** 6771-8.

Glende, J., Schwegmann-Wessels, C., Al-Falah, M., Pfefferle, S., Qu, X., Deng, H., Drosten, C., Naim, H. Y., and Herrler, G. (2008). Importance of cholesterol-rich membrane microdomains in the interaction of the S protein of SARS-coronavirus with the cellular receptor angiotensin-converting enzyme 2. *Virology* **381**(2), 215-21.

Glowacka, I., Bertram, S., Muller, M. A., Allen, P., Soilleux, E., Pfefferle, S., Steffen, I., Tsegaye, T. S., He, Y., Gnirss, K., Niemeyer, D., Schneider, H., Drosten, C., and Pohlmann, S. (2011). Evidence that TMPRSS2 activates the SARS-coronavirus spike-protein for membrane fusion and reduces viral control by the humoral immune response. *J Virol* 85(9), 4122-34.

Godeke, G. J., de Haan, C. A., Rossen, J. W., Vennema, H., and Rottier, P. J. (2000). Assembly of spikes into coronavirus particles is mediated by the carboxy-terminal domain of the spike protein. *J Virol* **74**(3)**,** 1566-71.

Gombold, J. L., Hingley, S. T., and Weiss, S. R. (1993). Fusion-defective mutants of mouse hepatitis virus A59 contain a mutation in the spike protein cleavage signal. *J Virol* **67**(8)**,** 4504-12.

Gonzalez, J. M., Gomez-Puertas, P., Cavanagh, D., Gorbalenya, A. E., and Enjuanes, L. (2003). A comparative sequence analysis to revise the current taxonomy of the family Coronaviridae. *Arch Virol* **148**(11)**,** 2207-35.

Gordon, A. H., Hart, P. D., and Young, M. R. (1980). Ammonia inhibits phagosome-lysosome fusion in macrophages. *Nature* **286**(5768)**,** 79-80.

Graham, F. L., and van der Eb, A. J. (1973). A new technique for the assay of infectivity of human adenovirus 5 DNA. *Virology* **52**(2)**,** 456-67.

Graham, K. L., Halasz, P., Tan, Y., Hewish, M. J., Takada, Y., Mackow, E. R., Robinson, M. K., and Coulson, B. S. (2003). Integrin-using rotaviruses bind alpha2beta1 integrin alpha2 I domain via VP4 DGE sequence and recognize alphaXbeta2 and alphaVbeta3 by using VP7 during cell entry. *J Virol* **77**(18)**,** 9969-78.

Grau, A. J., Urbanek, C., and Palm, F. (2010). Common infections and the risk of stroke. *Nat Rev Neurol* **6**(12)**,** 681-94.

Greber, U. F. (2002). Signalling in viral entry. *Cell Mol Life Sci* **59**(4)**,** 608-26.

Greber, U. F., Webster, P., Weber, J., and Helenius, A. (1996). The role of the adenovirus protease on virus entry into cells. *Embo J* **15**(8)**,** 1766-77.

Green, N., Shinnick, T. M., Witte, O., Ponticelli, A., Sutcliffe, J. G., and Lerner, R. A. (1981). Sequence-specific antibodies show that maturation of Moloney leukemia virus envelope polyprotein involves removal of a COOH-terminal peptide. *Proc Natl Acad Sci U S A* **78**(10)**,** 6023-7.

Grosse, B., and Siddell, S. G. (1994). Single amino acid changes in the S2 subunit of the MHV surface glycoprotein confer resistance to neutralization by S1 subunit-specific monoclonal antibody. *Virology* **202**(2)**,** 814-24.

Guan, Y., Zheng, B. J., He, Y. Q., Liu, X. L., Zhuang, Z. X., Cheung, C. L., Luo, S. W., Li, P. H., Zhang, L. J., Guan, Y. J., Butt, K. M., Wong, K. L., Chan, K. W., Lim, W., Shortridge, K. F., Yuen, K. Y., Peiris, J. S., and Poon, L. L. (2003). Isolation and characterization of viruses related to the SARS coronavirus from animals in southern China. *Science* **302**(5643)**,** 276-8.

Haijema, B. J., Volders, H., and Rottier, P. J. (2003). Switching species tropism: an effective way to manipulate the feline coronavirus genome. *J Virol* **77**(8)**,** 4528-38.

Hallenberger, S., Bosch, V., Angliker, H., Shaw, E., Klenk, H. D., and Garten, W. (1992). Inhibition of furin-mediated cleavage activation of HIV-1 glycoprotein gp160. *Nature* **360**(6402)**,** 358-61.

Hamming, I., Cooper, M. E., Haagmans, B. L., Hooper, N. M., Korstanje, R., Osterhaus, A. D., Timens, W., Turner, A. J., Navis, G., and van Goor, H. (2007). The emerging role of ACE2 in physiology and disease. *J Pathol* **212**(1)**,** 1-11.

Hamre, D., and Procknow, J. J. (1966). A new virus isolated from the human respiratory tract. *Proc Soc Exp Biol Med* **121**(1)**,** 190-3.

Hanssen, I. M., Lapidot, M., and Thomma, B. P. (2010). Emerging viral diseases of tomato crops. *Mol Plant Microbe Interact* **23**(5)**,** 539-48.

Harrison, S. C. (2008). Viral membrane fusion. *Nat Struct Mol Biol* **15**(7)**,** 690-8.

Harrison, S. C., Olson, A. J., Schutt, C. E., Winkler, F. K., and Bricogne, G. (1978). Tomato bushy stunt virus at 2.9 A resolution. *Nature* **276**(5686)**,** 368-73.

He, J., Choe, S., Walker, R., Di Marzio, P., Morgan, D. O., and Landau, N. R. (1995). Human immunodeficiency virus type 1 viral protein R (Vpr) arrests cells in the G2 phase of the cell cycle by inhibiting p34cdc2 activity. *J Virol* **69**(11)**,** 6705-11.

He, Y., Bowman, V. D., Mueller, S., Bator, C. M., Bella, J., Peng, X., Baker, T. S., Wimmer, E., Kuhn, R. J., and Rossmann, M. G. (2000). Interaction of the poliovirus receptor with poliovirus. *Proc Natl Acad Sci U S A* **97**(1)**,** 79-84.

Heldwein, E. E., Lou, H., Bender, F. C., Cohen, G. H., Eisenberg, R. J., and Harrison, S. C. (2006). Crystal structure of glycoprotein B from herpes simplex virus 1. *Science* **313**(5784)**,** 217-20.

Helseth, E., Olshevsky, U., Gabuzda, D., Ardman, B., Haseltine, W., and Sodroski, J. (1990). Changes in the transmembrane region of the human immunodeficiency virus type 1 gp41 envelope glycoprotein affect membrane fusion. *J Virol* **64**(12)**,** 6314-8.

Hofer, F., Gruenberger, M., Kowalski, H., Machat, H., Huettinger, M., Kuechler, E., and Blaas, D. (1994). Members of the low density lipoprotein receptor family mediate

cell entry of a minor-group common cold virus. *Proc Natl Acad Sci U S A* **91**(5)**,** 1839-42.

Hofmann, H., Pyrc, K., van der Hoek, L., Geier, M., Berkhout, B., and Pohlmann, S. (2005). Human coronavirus NL63 employs the severe acute respiratory syndrome coronavirus receptor for cellular entry. *Proc Natl Acad Sci U S A* **102**(22)**,** 7988-93.

Holmes, K. V., Doller, E. W., and Sturman, L. S. (1981). Tunicamycin resistant glycosylation of coronavirus glycoprotein: demonstration of a novel type of viral glycoprotein. *Virology* **115**(2)**,** 334-44.

Honey, K., and Rudensky, A. Y. (2003). Lysosomal cysteine proteases regulate antigen presentation. *Nat Rev Immunol* **3**(6)**,** 472-82.

Hooper, J. D., Clements, J. A., Quigley, J. P., and Antalis, T. M. (2001). Type II transmembrane serine proteases. Insights into an emerging class of cell surface proteolytic enzymes. *J Biol Chem* **276**(2)**,** 857-60.

Howard, M. W., Travanty, E. A., Jeffers, S. A., Smith, M. K., Wennier, S. T., Thackray, L. B., and Holmes, K. V. (2008). Aromatic amino acids in the juxtamembrane domain of severe acute respiratory syndrome coronavirus spike glycoprotein are important for receptor-dependent virus entry and cell-cell fusion. *J Virol* **82**(6)**,** 2883-94.

Huang, I. C., Bailey, C. C., Weyer, J. L., Radoshitzky, S. R., Becker, M. M., Chiang, J. J., Brass, A. L., Ahmed, A. A., Chi, X., Dong, L., Longobardi, L. E., Boltz, D., Kuhn, J. H., Elledge, S. J., Bavari, S., Denison, M. R., Choe, H., and Farzan, M. (2011). Distinct patterns of IFITM-mediated restriction of filoviruses, SARS coronavirus, and influenza A virus. *PLoS Pathog* **7**(1)**,** e1001258.

Huang, I. C., Bosch, B. J., Li, F., Li, W., Lee, K. H., Ghiran, S., Vasilieva, N., Dermody, T. S., Harrison, S. C., Dormitzer, P. R., Farzan, M., Rottier, P. J., and Choe, H. (2006). SARS coronavirus, but not human coronavirus NL63, utilizes cathepsin L to infect ACE2-expressing cells. *J Biol Chem* **281**(6)**,** 3198-203.

Hynes, R. O. (2002). Integrins: bidirectional, allosteric signaling machines. *Cell* **110**(6)**,** 673-87.

Imai, Y., Kuba, K., Rao, S., Huan, Y., Guo, F., Guan, B., Yang, P., Sarao, R., Wada, T., Leong-Poi, H., Crackower, M. A., Fukamizu, A., Hui, C. C., Hein, L., Uhlig, S., Slutsky, A. S., Jiang, C., and Penninger, J. M. (2005). Angiotensin-converting enzyme 2 protects from severe acute lung failure. *Nature* **436**(7047)**,** 112-6.

Isaacs, A., and Lindenmann, J. (1957). Virus interference. I. The interferon. *Proc R Soc Lond B Biol Sci* **147**(927)**,** 258-67.

Iwata, M., Silva Enciso, J. E., and Greenberg, B. H. (2009). Selective and specific regulation of ectodomain shedding of angiotensin-converting enzyme 2 by tumor necrosis factor alpha-converting enzyme. *Am J Physiol Cell Physiol* **297**(5)**,** C1318-29.

Jackson, T., Mould, A. P., Sheppard, D., and King, A. M. (2002). Integrin alphavbeta1 is a receptor for foot-and-mouth disease virus. *J Virol* **76**(3)**,** 935-41.

Jackwood, M. W., Hilt, D. A., Callison, S. A., Lee, C. W., Plaza, H., and Wade, E. (2001). Spike glycoprotein cleavage recognition site analysis of infectious bronchitis virus. *Avian Dis* **45**(2)**,** 366-72.

Jacobson, I. M., and Dienstag, J. L. (1985). Viral hepatitis vaccines. *Annu Rev Med* **36,** 241-61.

Jia, H. P., Look, D. C., Shi, L., Hickey, M., Pewe, L., Netland, J., Farzan, M., Wohlford-Lenane, C., Perlman, S., and McCray, P. B., Jr. (2005). ACE2 receptor expression and severe acute respiratory syndrome coronavirus infection depend on differentiation of human airway epithelia. *J Virol* **79**(23)**,** 14614-21.

Jia, H. P., Look, D. C., Tan, P., Shi, L., Hickey, M., Gakhar, L., Chappell, M. C., Wohlford-Lenane, C., and McCray, P. B., Jr. (2009). Ectodomain shedding of angiotensin converting enzyme 2 in human airway epithelia. *Am J Physiol Lung Cell Mol Physiol* **297**(1)**,** L84-96.

Kadlec, J., Loureiro, S., Abrescia, N. G., Stuart, D. I., and Jones, I. M. (2008). The postfusion structure of baculovirus gp64 supports a unified view of viral fusion machines. *Nat Struct Mol Biol* **15**(10)**,** 1024-30.

Kam, Y. W., Okumura, Y., Kido, H., Ng, L. F., Bruzzone, R., and Altmeyer, R. (2009). Cleavage of the SARS coronavirus spike glycoprotein by airway proteases enhances virus entry into human bronchial epithelial cells in vitro. *PLoS One* **4**(11)**,** e7870.

Kan, B., Wang, M., Jing, H., Xu, H., Jiang, X., Yan, M., Liang, W., Zheng, H., Wan, K., Liu, Q., Cui, B., Xu, Y., Zhang, E., Wang, H., Ye, J., Li, G., Li, M., Cui, Z., Qi, X., Chen, K., Du, L., Gao, K., Zhao, Y. T., Zou, X. Z., Feng, Y. J., Gao, Y. F., Hai, R., Yu, D., Guan, Y., and Xu, J. (2005). Molecular evolution analysis and geographic investigation of severe acute respiratory syndrome coronavirus-like virus in palm civets at an animal market and on farms. *J Virol* **79**(18)**,** 11892-900.

Kemble, G. W., Danieli, T., and White, J. M. (1994). Lipid-anchored influenza hemagglutinin promotes hemifusion, not complete fusion. *Cell* **76**(2)**,** 383-91.

Kielian, M., and Rey, F. A. (2006). Virus membrane-fusion proteins: more than one way to make a hairpin. *Nat Rev Microbiol* **4**(1)**,** 67-76.

Kielian, M. C., and Helenius, A. (1984). Role of cholesterol in fusion of Semliki Forest virus with membranes. *J Virol* **52**(1)**,** 281-3.

Kilby, J. M., Hopkins, S., Venetta, T. M., DiMassimo, B., Cloud, G. A., Lee, J. Y., Alldredge, L., Hunter, E., Lambert, D., Bolognesi, D., Matthews, T., Johnson, M. R., Nowak, M. A., Shaw, G. M., and Saag, M. S. (1998). Potent suppression of HIV-1 replication in humans by T-20, a peptide inhibitor of gp41-mediated virus entry. *Nat Med* **4**(11)**,** 1302-7.

Kim, T. S., Heinlein, C., Hackman, R. C., and Nelson, P. S. (2006). Phenotypic analysis of mice lacking the Tmprss2-encoded protease. *Mol Cell Biol* **26**(3)**,** 965-75.

Klenk, H. D., and Garten, W. (1994). Host cell proteases controlling virus pathogenicity. *Trends Microbiol* **2**(2)**,** 39-43.

Koivunen, E., Gay, D. A., and Ruoslahti, E. (1993). Selection of peptides binding to the alpha 5 beta 1 integrin from phage display library. *J Biol Chem* **268**(27)**,** 20205-10.

Koivunen, E., Wang, B., and Ruoslahti, E. (1994). Isolation of a highly specific ligand for the alpha 5 beta 1 integrin from a phage display library. *J Cell Biol* **124**(3)**,** 373-80.

Krijnse-Locker, J., Ericsson, M., Rottier, P. J., and Griffiths, G. (1994). Characterization of the budding compartment of mouse hepatitis virus: evidence that transport from the RER to the Golgi complex requires only one vesicular transport step. *J Cell Biol* **124**(1-2)**,** 55-70.

Krishnan, H. H., Sharma-Walia, N., Streblow, D. N., Naranatt, P. P., and Chandran, B. (2006). Focal adhesion kinase is critical for entry of Kaposi's sarcoma-associated herpesvirus into target cells. *J Virol* **80**(3)**,** 1167-80.

Krokhin, O., Li, Y., Andonov, A., Feldmann, H., Flick, R., Jones, S., Stroeher, U., Bastien, N., Dasuri, K. V., Cheng, K., Simonsen, J. N., Perreault, H., Wilkins, J., Ens, W., Plummer, F., and Standing, K. G. (2003). Mass spectrometric characterization of proteins from the SARS virus: a preliminary report. *Mol Cell Proteomics* **2**(5)**,** 346-56.

Krueger, D. K., Kelly, S. M., Lewicki, D. N., Ruffolo, R., and Gallagher, T. M. (2001). Variations in disparate regions of the murine coronavirus spike protein impact the initiation of membrane fusion. *J Virol* **75**(6)**,** 2792-802.

Kuba, K., Imai, Y., Rao, S., Gao, H., Guo, F., Guan, B., Huan, Y., Yang, P., Zhang, Y., Deng, W., Bao, L., Zhang, B., Liu, G., Wang, Z., Chappell, M., Liu, Y., Zheng, D., Leibbrandt, A., Wada, T., Slutsky, A. S., Liu, D., Qin, C., Jiang, C., and Penninger, J. M. (2005). A crucial role of angiotensin converting enzyme 2 (ACE2) in SARS coronavirus-induced lung injury. *Nat Med* **11**(8)**,** 875-9.

Kubo, H., Yamada, Y. K., and Taguchi, F. (1994). Localization of neutralizing epitopes and the receptor-binding site within the amino-terminal 330 amino acids of the murine coronavirus spike protein. *J Virol* **68**(9)**,** 5403-10.

Kuo, L., Godeke, G. J., Raamsman, M. J., Masters, P. S., and Rottier, P. J. (2000). Retargeting of coronavirus by substitution of the spike glycoprotein ectodomain: crossing the host cell species barrier. *J Virol* **74**(3)**,** 1393-406.

Kuo, L., and Masters, P. S. (2002). Genetic evidence for a structural interaction between the carboxy termini of the membrane and nucleocapsid proteins of mouse hepatitis virus. *J Virol* **76**(10)**,** 4987-99.

Kusumi, A., and Sako, Y. (1996). Cell surface organization by the membrane skeleton. *Curr Opin Cell Biol* **8**(4)**,** 566-74.

Lai, M. M., and Cavanagh, D. (1997). The molecular biology of coronaviruses. *Adv Virus Res* **48,** 1-100.

Lai, M. M., Liao, C. L., Lin, Y. J., and Zhang, X. (1994). Coronavirus: how a large RNA viral genome is replicated and transcribed. *Infect Agents Dis* **3**(2-3)**,** 98-105.

Lambert, D. W., Yarski, M., Warner, F. J., Thornhill, P., Parkin, E. T., Smith, A. I., Hooper, N. M., and Turner, A. J. (2005). Tumor necrosis factor-alpha convertase (ADAM17) mediates regulated ectodomain shedding of the severe-acute respiratory syndrome-coronavirus (SARS-CoV) receptor, angiotensin-converting enzyme-2 (ACE2). *J Biol Chem* **280**(34)**,** 30113-9.

Langosch, D., Hofmann, M., and Ungermann, C. (2007). The role of transmembrane domains in membrane fusion. *Cell Mol Life Sci* **64**(7-8)**,** 850-64.

Lau, S. K., Woo, P. C., Li, K. S., Huang, Y., Tsoi, H. W., Wong, B. H., Wong, S. S., Leung, S. Y., Chan, K. H., and Yuen, K. Y. (2005). Severe acute respiratory

syndrome coronavirus-like virus in Chinese horseshoe bats. *Proc Natl Acad Sci U S A* **102**(39)**,** 14040-5.

Lazarowitz, S. G., and Choppin, P. W. (1975). Enhancement of the infectivity of influenza A and B viruses by proteolytic cleavage of the hemagglutinin polypeptide. *Virology* **68**(2)**,** 440-54.

Lee, H. J., Shieh, C. K., Gorbalenya, A. E., Koonin, E. V., La Monica, N., Tuler, J., Bagdzhadzhyan, A., and Lai, M. M. (1991). The complete sequence (22 kilobases) of murine coronavirus gene 1 encoding the putative proteases and RNA polymerase. *Virology* **180**(2)**,** 567-82.

Lee, N., Hui, D., Wu, A., Chan, P., Cameron, P., Joynt, G. M., Ahuja, A., Yung, M. Y., Leung, C. B., To, K. F., Lui, S. F., Szeto, C. C., Chung, S., and Sung, J. J. (2003). A major outbreak of severe acute respiratory syndrome in Hong Kong. *N Engl J Med* **348**(20)**,** 1986-94.

Lee, W. M., Monroe, S. S., and Rueckert, R. R. (1993). Role of maturation cleavage in infectivity of picornaviruses: activation of an infectosome. *J Virol* **67**(4)**,** 2110-22.

Leparc-Goffart, I., Hingley, S. T., Chua, M. M., Phillips, J., Lavi, E., and Weiss, S. R. (1998). Targeted recombination within the spike gene of murine coronavirus mouse hepatitis virus-A59: Q159 is a determinant of hepatotropism. *J Virol* **72**(12)**,** 9628-36.

Lescar, J., Roussel, A., Wien, M. W., Navaza, J., Fuller, S. D., Wengler, G., and Rey, F. A. (2001). The Fusion glycoprotein shell of Semliki Forest virus: an icosahedral assembly primed for fusogenic activation at endosomal pH. *Cell* **105**(1)**,** 137-48.

Levental, I., Grzybek, M., and Simons, K. (2010). Greasing their way: lipid modifications determine protein association with membrane rafts. *Biochemistry* **49**(30)**,** 6305-16.

Li, E., Brown, S. L., Stupack, D. G., Puente, X. S., Cheresh, D. A., and Nemerow, G. R. (2001). Integrin alpha(v)beta1 is an adenovirus coreceptor. *J Virol* **75**(11)**,** 5405-9.

Li, F., Berardi, M., Li, W., Farzan, M., Dormitzer, P. R., and Harrison, S. C. (2006). Conformational states of the severe acute respiratory syndrome coronavirus spike protein ectodomain. *J Virol* **80**(14)**,** 6794-800.

Li, F., Li, W., Farzan, M., and Harrison, S. C. (2005a). Structure of SARS coronavirus spike receptor-binding domain complexed with receptor. *Science* **309**(5742)**,** 1864-8.

Li, W., Moore, M. J., Vasilieva, N., Sui, J., Wong, S. K., Berne, M. A., Somasundaran, M., Sullivan, J. L., Luzuriaga, K., Greenough, T. C., Choe, H., and Farzan, M. (2003). Angiotensin-converting enzyme 2 is a functional receptor for the SARS coronavirus. *Nature* **426**(6965)**,** 450-4.

Li, W., Shi, Z., Yu, M., Ren, W., Smith, C., Epstein, J. H., Wang, H., Crameri, G., Hu, Z., Zhang, H., Zhang, J., McEachern, J., Field, H., Daszak, P., Eaton, B. T., Zhang, S., and Wang, L. F. (2005b). Bats are natural reservoirs of SARS-like coronaviruses. *Science* **310**(5748)**,** 676-9.

Li, W., Zhang, C., Sui, J., Kuhn, J. H., Moore, M. J., Luo, S., Wong, S. K., Huang, I. C., Xu, K., Vasilieva, N., Murakami, A., He, Y., Marasco, W. A., Guan, Y., Choe, H., and Farzan, M. (2005c). Receptor and viral determinants of SARS-coronavirus adaptation to human ACE2. *Embo J* **24**(8)**,** 1634-43.

Lin, Q., Keller, R. S., Weaver, B., and Zisman, L. S. (2004). Interaction of ACE2 and integrin beta1 in failing human heart. *Biochim Biophys Acta* **1689**(3)**,** 175-8.

Linder, M. E., and Deschenes, R. J. (2007). Palmitoylation: policing protein stability and traffic. *Nat Rev Mol Cell Biol* **8**(1)**,** 74-84.

Lontok, E., Corse, E., and Machamer, C. E. (2004). Intracellular targeting signals contribute to localization of coronavirus spike proteins near the virus assembly site. *J Virol* **78**(11)**,** 5913-22.

Lu, Y., Liu, D. X., and Tam, J. P. (2008). Lipid rafts are involved in SARS-CoV entry into Vero E6 cells. *Biochem Biophys Res Commun* **369**(2)**,** 344-9.

Lucas, J. M., True, L., Hawley, S., Matsumura, M., Morrissey, C., Vessella, R., and Nelson, P. S. (2008). The androgen-regulated type II serine protease TMPRSS2 is differentially expressed and mislocalized in prostate adenocarcinoma. *J Pathol* **215**(2)**,** 118-25.

Luo, Z., Matthews, A. M., and Weiss, S. R. (1999). Amino acid substitutions within the leucine zipper domain of the murine coronavirus spike protein cause defects in oligomerization and the ability to induce cell-to-cell fusion. *J Virol* **73**(10)**,** 8152-9.

Luytjes, W., Sturman, L. S., Bredenbeek, P. J., Charite, J., van der Zeijst, B. A., Horzinek, M. C., and Spaan, W. J. (1987). Primary structure of the glycoprotein E2 of coronavirus MHV-A59 and identification of the trypsin cleavage site. *Virology* **161**(2)**,** 479-87.

Madu, I. G., Chu, V. C., Lee, H., Regan, A. D., Bauman, B. E., and Whittaker, G. R. (2007). Heparan sulfate is a selective attachment factor for the avian coronavirus infectious bronchitis virus Beaudette. *Avian Dis* **51**(1)**,** 45-51.

Madu, I. G., Roth, S. L., Belouzard, S., and Whittaker, G. R. (2009). Characterization of a highly conserved domain within the severe acute respiratory syndrome coronavirus spike protein S2 domain with characteristics of a viral fusion peptide. *J Virol* **83**(15)**,** 7411-21.

Maginnis, M. S., Forrest, J. C., Kopecky-Bromberg, S. A., Dickeson, S. K., Santoro, S. A., Zutter, M. M., Nemerow, G. R., Bergelson, J. M., and Dermody, T. S. (2006). Beta1 integrin mediates internalization of mammalian reovirus. *J Virol* **80**(6)**,** 2760-70.

Maginnis, M. S., Mainou, B. A., Derdowski, A., Johnson, E. M., Zent, R., and Dermody, T. S. (2008). NPXY motifs in the beta1 integrin cytoplasmic tail are required for functional reovirus entry. *J Virol* **82**(7)**,** 3181-91.

Makino, S., Keck, J. G., Stohlman, S. A., and Lai, M. M. (1986). High-frequency RNA recombination of murine coronaviruses. *J Virol* **57**(3)**,** 729-37.

Malashkevich, V. N., Schneider, B. J., McNally, M. L., Milhollen, M. A., Pang, J. X., and Kim, P. S. (1999). Core structure of the envelope glycoprotein GP2 from Ebola virus at 1.9-A resolution. *Proc Natl Acad Sci U S A* **96**(6)**,** 2662-7.

Markosyan, R. M., Cohen, F. S., and Melikyan, G. B. (2003). HIV-1 envelope proteins complete their folding into six-helix bundles immediately after fusion pore formation. *Mol Biol Cell* **14**(3)**,** 926-38.

Marra, M. A., Jones, S. J., Astell, C. R., Holt, R. A., Brooks-Wilson, A., Butterfield, Y. S., Khattra, J., Asano, J. K., Barber, S. A., Chan, S. Y., Cloutier, A., Coughlin, S. M., Freeman, D., Girn, N., Griffith, O. L., Leach, S. R., Mayo, M., McDonald, H., Montgomery, S. B., Pandoh, P. K., Petrescu, A. S., Robertson, A. G., Schein, J. E., Siddiqui, A., Smailus, D. E., Stott, J. M., Yang, G. S., Plummer, F., Andonov, A., Artsob, H., Bastien, N., Bernard, K., Booth, T. F., Bowness, D., Czub, M., Drebot, M., Fernando, L., Flick, R., Garbutt, M., Gray, M., Grolla, A., Jones, S., Feldmann, H., Meyers, A., Kabani, A., Li, Y., Normand, S., Stroher, U., Tipples, G. A., Tyler, S., Vogrig, R., Ward, D., Watson, B., Brunham, R. C., Krajden, M.,

Petric, M., Skowronski, D. M., Upton, C., and Roper, R. L. (2003). The Genome sequence of the SARS-associated coronavirus. *Science* **300**(5624)**,** 1399-404.

Marsh, M., and Bron, R. (1997). SFV infection in CHO cells: cell-type specific restrictions to productive virus entry at the cell surface. *J Cell Sci* **110 (Pt 1),** 95-103.

Marsh, M., and Helenius, A. (1989). Virus entry into animal cells. *Adv Virus Res* **36,** 107-51.

Martin, I., and Ruysschaert, J. M. (2000). Common properties of fusion peptides from diverse systems. *Biosci Rep* **20**(6)**,** 483-500.

Masters, P. S. (2006). The molecular biology of coronaviruses. *Adv Virus Res* **66,** 193-292.

Masters, P. S., Kuo, L., Ye, R., Hurst, K. R., Koetzner, C. A., and Hsue, B. (2006). Genetic and molecular biological analysis of protein-protein interactions in coronavirus assembly. *Adv Exp Med Biol* **581,** 163-73.

Masters, P. S., and Rottier, P. J. (2005). Coronavirus reverse genetics by targeted RNA recombination. *Curr Top Microbiol Immunol* **287,** 133-59.

Matsuyama, S., Nagata, N., Shirato, K., Kawase, M., Takeda, M., and Taguchi, F. (2010). Efficient activation of the severe acute respiratory syndrome coronavirus spike protein by the transmembrane protease TMPRSS2. *J Virol* **84**(24)**,** 12658-64.

Matsuyama, S., and Taguchi, F. (2002). Receptor-induced conformational changes of murine coronavirus spike protein. *J Virol* **76**(23)**,** 11819-26.

Matsuyama, S., and Taguchi, F. (2009). Two-step conformational changes in a coronavirus envelope glycoprotein mediated by receptor binding and proteolysis. *J Virol* **83**(21)**,** 11133-41.

Matsuyama, S., Ujike, M., Morikawa, S., Tashiro, M., and Taguchi, F. (2005). Protease-mediated enhancement of severe acute respiratory syndrome coronavirus infection. *Proc Natl Acad Sci U S A* **102**(35)**,** 12543-7.

Maxfield, F. R., and McGraw, T. E. (2004). Endocytic recycling. *Nat Rev Mol Cell Biol* **5**(2)**,** 121-32.

McBride, C. E., Li, J., and Machamer, C. E. (2007). The cytoplasmic tail of the severe acute respiratory syndrome coronavirus spike protein contains a novel

endoplasmic reticulum retrieval signal that binds COPI and promotes interaction with membrane protein. *J Virol* **81**(5)**,** 2418-28.

McBride, C. E., and Machamer, C. E. (2010). Palmitoylation of SARS-CoV S protein is necessary for partitioning into detergent-resistant membranes and cell-cell fusion but not interaction with M protein. *Virology* **405**(1)**,** 139-48.

McIntosh, K. (2005). Coronaviruses in the limelight. *J Infect Dis* **191**(4)**,** 489-91.

McIntosh, K., Becker, W. B., and Chanock, R. M. (1967). Growth in suckling-mouse brain of "IBV-like" viruses from patients with upper respiratory tract disease. *Proc Natl Acad Sci U S A* **58**(6)**,** 2268-73.

McReynolds, S., Jiang, S., Guo, Y., Celigoy, J., Schar, C., Rong, L., and Caffrey, M. (2008). Characterization of the prefusion and transition states of severe acute respiratory syndrome coronavirus S2-HR2. *Biochemistry* **47**(26)**,** 6802-8.

McShane, M. P., and Longnecker, R. (2005). Analysis of fusion using a virus-free cell fusion assay. *Methods Mol Biol* **292,** 187-96.

Melikyan, G. B., Lin, S., Roth, M. G., and Cohen, F. S. (1999). Amino acid sequence requirements of the transmembrane and cytoplasmic domains of influenza virus hemagglutinin for viable membrane fusion. *Mol Biol Cell* **10**(6)**,** 1821-36.

Melikyan, G. B., Markosyan, R. M., Hemmati, H., Delmedico, M. K., Lambert, D. M., and Cohen, F. S. (2000). Evidence that the transition of HIV-1 gp41 into a six-helix bundle, not the bundle configuration, induces membrane fusion. *J Cell Biol* **151**(2)**,** 413-23.

Melkonian, K. A., Ostermeyer, A. G., Chen, J. Z., Roth, M. G., and Brown, D. A. (1999). Role of lipid modifications in targeting proteins to detergent-resistant membrane rafts. Many raft proteins are acylated, while few are prenylated. *J Biol Chem* **274**(6)**,** 3910-7.

Mercer, J., Schelhaas, M., and Helenius, A. (2010). Virus entry by endocytosis. *Annu Rev Biochem* **79,** 803-33.

Mitsuya, H., and Broder, S. (1987). Strategies for antiviral therapy in AIDS. *Nature* **325**(6107)**,** 773-8.

Miyake, Y., Yasumoto, M., Tsuzuki, S., Fushiki, T., and Inouye, K. (2009). Activation of a membrane-bound serine protease matriptase on the cell surface. *J Biochem* **146**(2)**,** 273-82.

Miyauchi, K., Kim, Y., Latinovic, O., Morozov, V., and Melikyan, G. B. (2009). HIV enters cells via endocytosis and dynamin-dependent fusion with endosomes. *Cell* **137**(3)**,** 433-44.

Moore, J. P., McKeating, J. A., Weiss, R. A., and Sattentau, Q. J. (1990). Dissociation of gp120 from HIV-1 virions induced by soluble CD4. *Science* **250**(4984)**,** 1139-42.

Moore, J. P., Trkola, A., and Dragic, T. (1997). Co-receptors for HIV-1 entry. *Curr Opin Immunol* **9**(4)**,** 551-62.

Moore, M. J., Dorfman, T., Li, W., Wong, S. K., Li, Y., Kuhn, J. H., Coderre, J., Vasilieva, N., Han, Z., Greenough, T. C., Farzan, M., and Choe, H. (2004). Retroviruses pseudotyped with the severe acute respiratory syndrome coronavirus spike protein efficiently infect cells expressing angiotensin-converting enzyme 2. *J Virol* **78**(19)**,** 10628-35.

Mothes, W., Boerger, A. L., Narayan, S., Cunningham, J. M., and Young, J. A. (2000). Retroviral entry mediated by receptor priming and low pH triggering of an envelope glycoprotein. *Cell* **103**(4)**,** 679-89.

Nakano, M. Y., Boucke, K., Suomalainen, M., Stidwill, R. P., and Greber, U. F. (2000). The first step of adenovirus type 2 disassembly occurs at the cell surface, independently of endocytosis and escape to the cytosol. *J Virol* **74**(15)**,** 7085-95.

Narayanan, K., Maeda, A., Maeda, J., and Makino, S. (2000). Characterization of the coronavirus M protein and nucleocapsid interaction in infected cells. *J Virol* **74**(17)**,** 8127-34.

Neuman, B. W., Adair, B. D., Yoshioka, C., Quispe, J. D., Milligan, R. A., Yeager, M., and Buchmeier, M. J. (2006a). Ultrastructure of SARS-CoV, FIPV, and MHV revealed by electron cryomicroscopy. *Adv Exp Med Biol* **581,** 181-5.

Neuman, B. W., Adair, B. D., Yoshioka, C., Quispe, J. D., Orca, G., Kuhn, P., Milligan, R. A., Yeager, M., and Buchmeier, M. J. (2006b). Supramolecular architecture of severe acute respiratory syndrome coronavirus revealed by electron cryomicroscopy. *J Virol* **80**(16)**,** 7918-28.

Nguyen, D. H., and Hildreth, J. E. (2000). Evidence for budding of human immunodeficiency virus type 1 selectively from glycolipid-enriched membrane lipid rafts. *J Virol* **74**(7)**,** 3264-72.

Nicola, A. V., McEvoy, A. M., and Straus, S. E. (2003). Roles for endocytosis and low pH in herpes simplex virus entry into HeLa and Chinese hamster ovary cells. *J Virol* **77**(9)**,** 5324-32.

Niwa, H., Yamamura, K., and Miyazaki, J. (1991). Efficient selection for high-expression transfectants with a novel eukaryotic vector. *Gene* **108**(2)**,** 193-9.

Nomura, R., Kiyota, A., Suzaki, E., Kataoka, K., Ohe, Y., Miyamoto, K., Senda, T., and Fujimoto, T. (2004). Human coronavirus 229E binds to CD13 in rafts and enters the cell through caveolae. *J Virol* **78**(16)**,** 8701-8.

Okuma, K., Nakamura, M., Nakano, S., Niho, Y., and Matsuura, Y. (1999). Host range of human T-cell leukemia virus type I analyzed by a cell fusion-dependent reporter gene activation assay. *Virology* **254**(2)**,** 235-44.

Ono, A., and Freed, E. O. (2001). Plasma membrane rafts play a critical role in HIV-1 assembly and release. *Proc Natl Acad Sci U S A* **98**(24)**,** 13925-30.

Opstelten, D. J., Raamsman, M. J., Wolfs, K., Horzinek, M. C., and Rottier, P. J. (1995). Envelope glycoprotein interactions in coronavirus assembly. *J Cell Biol* **131**(2)**,** 339-49.

Otlewski, J., Jelen, F., Zakrzewska, M., and Oleksy, A. (2005). The many faces of protease-protein inhibitor interaction. *Embo J* **24**(7)**,** 1303-10.

Parrino, J., and Graham, B. S. (2006). Smallpox vaccines: Past, present, and future. *J Allergy Clin Immunol* **118**(6)**,** 1320-6.

Pedersen, N. C., Boyle, J. F., Floyd, K., Fudge, A., and Barker, J. (1981). An enteric coronavirus infection of cats and its relationship to feline infectious peritonitis. *Am J Vet Res* **42**(3)**,** 368-77.

Peiris, J. S., Chu, C. M., Cheng, V. C., Chan, K. S., Hung, I. F., Poon, L. L., Law, K. I., Tang, B. S., Hon, T. Y., Chan, C. S., Chan, K. H., Ng, J. S., Zheng, B. J., Ng, W. L., Lai, R. W., Guan, Y., and Yuen, K. Y. (2003). Clinical progression and viral load in a community outbreak of coronavirus-associated SARS pneumonia: a prospective study. *Lancet* **361**(9371)**,** 1767-72.

Pelletier, J., and Sonenberg, N. (1988). Internal initiation of translation of eukaryotic mRNA directed by a sequence derived from poliovirus RNA. *Nature* **334**(6180)**,** 320-5.

Pellinen, T., Tuomi, S., Arjonen, A., Wolf, M., Edgren, H., Meyer, H., Grosse, R., Kitzing, T., Rantala, J. K., Kallioniemi, O., Fassler, R., Kallio, M., and Ivaska, J. (2008). Integrin trafficking regulated by Rab21 is necessary for cytokinesis. *Dev Cell* **15**(3)**,** 371-85.

Petit, C. M., Chouljenko, V. N., Iyer, A., Colgrove, R., Farzan, M., Knipe, D. M., and Kousoulas, K. G. (2007). Palmitoylation of the cysteine-rich endodomain of the SARS-coronavirus spike glycoprotein is important for spike-mediated cell fusion. *Virology* **360**(2)**,** 264-74.

Plow, E. F., Haas, T. A., Zhang, L., Loftus, J., and Smith, J. W. (2000). Ligand binding to integrins. *J Biol Chem* **275**(29)**,** 21785-8.

Poon, L. L., Chu, D. K., Chan, K. H., Wong, O. K., Ellis, T. M., Leung, Y. H., Lau, S. K., Woo, P. C., Suen, K. Y., Yuen, K. Y., Guan, Y., and Peiris, J. S. (2005). Identification of a novel coronavirus in bats. *J Virol* **79**(4)**,** 2001-9.

Popik, W., Alce, T. M., and Au, W. C. (2002). Human immunodeficiency virus type 1 uses lipid raft-colocalized CD4 and chemokine receptors for productive entry into CD4(+) T cells. *J Virol* **76**(10)**,** 4709-22.

Qiu, Z., Hingley, S. T., Simmons, G., Yu, C., Das Sarma, J., Bates, P., and Weiss, S. R. (2006). Endosomal proteolysis by cathepsins is necessary for murine coronavirus mouse hepatitis virus type 2 spike-mediated entry. *J Virol* **80**(12)**,** 5768-76.

Raamsman, M. J., Locker, J. K., de Hooge, A., de Vries, A. A., Griffiths, G., Vennema, H., and Rottier, P. J. (2000). Characterization of the coronavirus mouse hepatitis virus strain A59 small membrane protein E. *J Virol* **74**(5)**,** 2333-42.

Rao, P. V., and Gallagher, T. M. (1998). Intracellular complexes of viral spike and cellular receptor accumulate during cytopathic murine coronavirus infections. *J Virol* **72**(4)**,** 3278-88.

Rao, T. K. (1991). Human immunodeficiency virus (HIV) associated nephropathy. *Annu Rev Med* **42,** 391-401.

Reiser, J., Adair, B., and Reinheckel, T. (2010). Specialized roles for cysteine cathepsins in health and disease. *J Clin Invest* **120**(10)**,** 3421-31.

Resh, M. D. (2006). Palmitoylation of ligands, receptors, and intracellular signaling molecules. *Sci STKE* **2006**(359)**,** re14.

Risco, C., Anton, I. M., Muntion, M., Gonzalez, J. M., Carrascosa, J. L., and Enjuanes, L. (1998). Structure and intracellular assembly of the transmissible gastroenteritis coronavirus. *Adv Exp Med Biol* **440,** 341-6.

Roche, S., Bressanelli, S., Rey, F. A., and Gaudin, Y. (2006). Crystal structure of the low-pH form of the vesicular stomatitis virus glycoprotein G. *Science* **313**(5784)**,** 187-91.

Roche, S., Rey, F. A., Gaudin, Y., and Bressanelli, S. (2007). Structure of the prefusion form of the vesicular stomatitis virus glycoprotein G. *Science* **315**(5813)**,** 843-8.

Romanowski, B., de Borba, P. C., Naud, P. S., Roteli-Martins, C. M., De Carvalho, N. S., Teixeira, J. C., Aoki, F., Ramjattan, B., Shier, R. M., Somani, R., Barbier, S., Blatter, M. M., Chambers, C., Ferris, D., Gall, S. A., Guerra, F. A., Harper, D. M., Hedrick, J. A., Henry, D. C., Korn, A. P., Kroll, R., Moscicki, A. B., Rosenfeld, W. D., Sullivan, B. J., Thoming, C. S., Tyring, S. K., Wheeler, C. M., Dubin, G., Schuind, A., Zahaf, T., Greenacre, M., and Sgriobhadair, A. (2009). Sustained efficacy and immunogenicity of the human papillomavirus (HPV)-16/18 AS04-adjuvanted vaccine: analysis of a randomised placebo-controlled trial up to 6.4 years. *Lancet* **374**(9706)**,** 1975-85.

Rota, P. A., Oberste, M. S., Monroe, S. S., Nix, W. A., Campagnoli, R., Icenogle, J. P., Penaranda, S., Bankamp, B., Maher, K., Chen, M. H., Tong, S., Tamin, A., Lowe, L., Frace, M., DeRisi, J. L., Chen, Q., Wang, D., Erdman, D. D., Peret, T. C., Burns, C., Ksiazek, T. G., Rollin, P. E., Sanchez, A., Liffick, S., Holloway, B., Limor, J., McCaustland, K., Olsen-Rasmussen, M., Fouchier, R., Gunther, S., Osterhaus, A. D., Drosten, C., Pallansch, M. A., Anderson, L. J., and Bellini, W. J. (2003). Characterization of a novel coronavirus associated with severe acute respiratory syndrome. *Science* **300**(5624)**,** 1394-9.

Rothman, J. E., and Warren, G. (1994). Implications of the SNARE hypothesis for intracellular membrane topology and dynamics. *Curr Biol* **4**(3)**,** 220-33.

Rottier, P. J., Horzinek, M. C., and van der Zeijst, B. A. (1981). Viral protein synthesis in mouse hepatitis virus strain A59-infected cells: effect of tunicamycin. *J Virol* **40**(2)**,** 350-7.

Rousso, I., Mark B. Mixon, Benjamin K. Chen, and Peter S. Kim (2000). Palmitoylation of the HIV-1 envelope glycoprotein is critical for viral infectivity. *Proc Natl Acad Sci U S A* **97**(25)**,** 13523-5.

Russell, C. J., Jardetzky, T. S., and Lamb, R. A. (2001). Membrane fusion machines of paramyxoviruses: capture of intermediates of fusion. *Embo J* **20**(15)**,** 4024-34.

Sakai, T., Ohuchi, R., and Ohuchi, M. (2002). Fatty acids on the A/USSR/77 influenza virus hemagglutinin facilitate the transition from hemifusion to fusion pore formation. *J Virol* **76**(9)**,** 4603-11.

Salinas, S., Schiavo, G., and Kremer, E. J. (2010). A hitchhiker's guide to the nervous system: the complex journey of viruses and toxins. *Nat Rev Microbiol* **8**(9)**,** 645-55.

Salzwedel, K., West, J. T., and Hunter, E. (1999). A conserved tryptophan-rich motif in the membrane-proximal region of the human immunodeficiency virus type 1 gp41 ectodomain is important for Env-mediated fusion and virus infectivity. *J Virol* **73**(3)**,** 2469-80.

Schickli, J. H., Thackray, L. B., Sawicki, S. G., and Holmes, K. V. (2004). The N-terminal region of the murine coronavirus spike glycoprotein is associated with the extended host range of viruses from persistently infected murine cells. *J Virol* **78**(17)**,** 9073-83.

Schlaepfer, D. D., Hanks, S. K., Hunter, T., and van der Geer, P. (1994). Integrin-mediated signal transduction linked to Ras pathway by GRB2 binding to focal adhesion kinase. *Nature* **372**(6508)**,** 786-91.

Schmidt, M. F., and Schlesinger, M. J. (1980). Relation of fatty acid attachment to the translation and maturation of vesicular stomatitis and Sindbis virus membrane glycoproteins. *J Biol Chem* **255**(8)**,** 3334-9.

Schornberg, K. L., Shoemaker, C. J., Dube, D., Abshire, M. Y., Delos, S. E., Bouton, A. H., and White, J. M. (2009). Alpha5beta1-integrin controls ebolavirus entry by regulating endosomal cathepsins. *Proc Natl Acad Sci U S A* **106**(19)**,** 8003-8.

Schutz, G. J., Kada, G., Pastushenko, V. P., and Schindler, H. (2000). Properties of lipid microdomains in a muscle cell membrane visualized by single molecule microscopy. *Embo J* **19**(5)**,** 892-901.

Shang, L., Yue, L., and Hunter, E. (2008). Role of the membrane-spanning domain of human immunodeficiency virus type 1 envelope glycoprotein in cell-cell fusion and virus infection. *J Virol* **82**(11)**,** 5417-28.

Sheahan, T., Rockx, B., Donaldson, E., Corti, D., and Baric, R. (2008). Pathways of cross-species transmission of synthetically reconstructed zoonotic severe acute respiratory syndrome coronavirus. *J Virol* **82**(17)**,** 8721-32.

Sheppard, D. (2003). Functions of pulmonary epithelial integrins: from development to disease. *Physiol Rev* **83**(3)**,** 673-86.

Shirogane, Y., Takeda, M., Iwasaki, M., Ishiguro, N., Takeuchi, H., Nakatsu, Y., Tahara, M., Kikuta, H., and Yanagi, Y. (2008). Efficient multiplication of human metapneumovirus in Vero cells expressing the transmembrane serine protease TMPRSS2. *J Virol* **82**(17)**,** 8942-6.

Shmueli, A., Segal, M., Sapir, T., Tsutsumi, R., Noritake, J., Bar, A., Sapoznik, S., Fukata, Y., Orr, I., Fukata, M., and Reiner, O. (2010). Ndel1 palmitoylation: a new mean to regulate cytoplasmic dynein activity. *Embo J* **29**(1)**,** 107-19.

Shulla, A., and Gallagher, T. (2009). Role of spike protein endodomains in regulating coronavirus entry. *J Biol Chem* **284**(47)**,** 32725-34.

Shulla, A., Heald-Sargent, T., Subramanya, G., Zhao, J., Perlman, S., and Gallagher, T. (2011). A transmembrane serine protease is linked to the severe acute respiratory syndrome coronavirus receptor and activates virus entry. *J Virol* **85**(2)**,** 873-82.

Simmons, G., Gosalia, D. N., Rennekamp, A. J., Reeves, J. D., Diamond, S. L., and Bates, P. (2005). Inhibitors of cathepsin L prevent severe acute respiratory syndrome coronavirus entry. *Proc Natl Acad Sci U S A* **102**(33)**,** 11876-81.

Simmons, G., Reeves, J. D., Rennekamp, A. J., Amberg, S. M., Piefer, A. J., and Bates, P. (2004). Characterization of severe acute respiratory syndrome-associated coronavirus (SARS-CoV) spike glycoprotein-mediated viral entry. *Proc Natl Acad Sci U S A* **101**(12)**,** 4240-5.

Simons, K., and Ikonen, E. (1997). Functional rafts in cell membranes. *Nature* **387**(6633)**,** 569-72.

Sims, A. C., Baric, R. S., Yount, B., Burkett, S. E., Collins, P. L., and Pickles, R. J. (2005). Severe acute respiratory syndrome coronavirus infection of human ciliated airway epithelia: role of ciliated cells in viral spread in the conducting airways of the lungs. *J Virol* **79**(24)**,** 15511-24.

Skehel, J. J., Bayley, P. M., Brown, E. B., Martin, S. R., Waterfield, M. D., White, J. M., Wilson, I. A., and Wiley, D. C. (1982). Changes in the conformation of influenza virus hemagglutinin at the pH optimum of virus-mediated membrane fusion. *Proc Natl Acad Sci U S A* **79**(4)**,** 968-72.

Skehel, J. J., and Wiley, D. C. (1998). Coiled coils in both intracellular vesicle and viral membrane fusion. *Cell* **95**(7)**,** 871-4.

Skehel, J. J., and Wiley, D. C. (2000). Receptor binding and membrane fusion in virus entry: the influenza hemagglutinin. *Annu Rev Biochem* **69,** 531-69.

Smit, J. M., Bittman, R., and Wilschut, J. (1999). Low-pH-dependent fusion of Sindbis virus with receptor-free cholesterol- and sphingolipid-containing liposomes. *J Virol* **73**(10)**,** 8476-84.

Smith, A. E., and Helenius, A. (2004). How viruses enter animal cells. *Science* **304**(5668)**,** 237-42.

Sollner, T. H., and Rothman, J. E. (1996). Molecular machinery mediating vesicle budding, docking and fusion. *Cell Struct Funct* **21**(5)**,** 407-12.

Song, H. C., Seo, M. Y., Stadler, K., Yoo, B. J., Choo, Q. L., Coates, S. R., Uematsu, Y., Harada, T., Greer, C. E., Polo, J. M., Pileri, P., Eickmann, M., Rappuoli, R., Abrignani, S., Houghton, M., and Han, J. H. (2004). Synthesis and characterization of a native, oligomeric form of recombinant severe acute respiratory syndrome coronavirus spike glycoprotein. *J Virol* **78**(19)**,** 10328-35.

Stanley, W. M. (1935). Isolation of a Crystalline Protein Possessing the Properties of Tobacco-Mosaic Virus. *Science* **81**(2113)**,** 644-5.

Stewart, P. L., and Nemerow, G. R. (2007). Cell integrins: commonly used receptors for diverse viral pathogens. *Trends Microbiol* **15**(11)**,** 500-7.

Sturman, L. S., and Holmes, K. V. (1984). Proteolytic cleavage of peplomeric glycoprotein E2 of MHV yields two 90K subunits and activates cell fusion. *Adv Exp Med Biol* **173,** 25-35.

Sturman, L. S., Ricard, C. S., and Holmes, K. V. (1985). Proteolytic cleavage of the E2 glycoprotein of murine coronavirus: activation of cell-fusing activity of virions by trypsin and separation of two different 90K cleavage fragments. *J Virol* **56**(3)**,** 904-11.

Sturman, L. S., Ricard, C. S., and Holmes, K. V. (1990). Conformational change of the coronavirus peplomer glycoprotein at pH 8.0 and 37 degrees C correlates with virus aggregation and virus-induced cell fusion. *J Virol* **64**(6)**,** 3042-50.

Sturman, L. S., and Takemoto, K. K. (1972). Enhanced growth of a murine coronavirus in transformed mouse cells. *Infect Immun* **6**(4)**,** 501-7.

Sui, J., Li, W., Murakami, A., Tamin, A., Matthews, L. J., Wong, S. K., Moore, M. J., Tallarico, A. S., Olurinde, M., Choe, H., Anderson, L. J., Bellini, W. J., Farzan,

M., and Marasco, W. A. (2004). Potent neutralization of severe acute respiratory syndrome (SARS) coronavirus by a human mAb to S1 protein that blocks receptor association. *Proc Natl Acad Sci U S A* **101**(8)**,** 2536-41.

Supekar, V. M., Bruckmann, C., Ingallinella, P., Bianchi, E., Pessi, A., and Carfi, A. (2004). Structure of a proteolytically resistant core from the severe acute respiratory syndrome coronavirus S2 fusion protein. *Proc Natl Acad Sci U S A* **101**(52)**,** 17958-63.

Szabo, R., and Bugge, T. H. (2008). Type II transmembrane serine proteases in development and disease. *Int J Biochem Cell Biol* **40**(6-7)**,** 1297-316.

Takeda, M., Leser, G. P., Russell, C. J., and Lamb, R. A. (2003). Influenza virus hemagglutinin concentrates in lipid raft microdomains for efficient viral fusion. *Proc Natl Acad Sci U S A* **100**(25)**,** 14610-7.

Talbot, S. J., and Crawford, D. H. (2004). Viruses and tumours--an update. *Eur J Cancer* **40**(13)**,** 1998-2005.

Tamm, L. K., and Han, X. (2000). Viral fusion peptides: a tool set to disrupt and connect biological membranes. *Biosci Rep* **20**(6)**,** 501-18.

Temin, H. M., and Mizutani, S. (1970). RNA-dependent DNA polymerase in virions of Rous sarcoma virus. *Nature* **226**(5252)**,** 1211-3.

Thorp, E. B., Boscarino, J. A., Logan, H. L., Goletz, J. T., and Gallagher, T. M. (2006). Palmitoylations on murine coronavirus spike proteins are essential for virion assembly and infectivity. *J Virol* **80**(3)**,** 1280-9.

Thorp, E. B., and Gallagher, T. M. (2004). Requirements for CEACAMs and cholesterol during murine coronavirus cell entry. *J Virol* **78**(6)**,** 2682-92.

Tipnis, S. R., Hooper, N. M., Hyde, R., Karran, E., Christie, G., and Turner, A. J. (2000). A human homolog of angiotensin-converting enzyme. Cloning and functional expression as a captopril-insensitive carboxypeptidase. *J Biol Chem* **275**(43)**,** 33238-43.

Tooze, J., Tooze, S., and Warren, G. (1984). Replication of coronavirus MHV-A59 in sac- cells: determination of the first site of budding of progeny virions. *Eur J Cell Biol* **33**(2)**,** 281-93.

Tresnan, D. B., Levis, R., and Holmes, K. V. (1996). Feline aminopeptidase N serves as a receptor for feline, canine, porcine, and human coronaviruses in serogroup I. *J Virol* **70**(12)**,** 8669-74.

Triantafilou, K., Takada, Y., and Triantafilou, M. (2001). Mechanisms of integrin-mediated virus attachment and internalization process. *Crit Rev Immunol* **21**(4)**,** 311-22.

Tsang, S. K., McDermott, B. M., Racaniello, V. R., and Hogle, J. M. (2001). Kinetic analysis of the effect of poliovirus receptor on viral uncoating: the receptor as a catalyst. *J Virol* **75**(11)**,** 4984-9.

Tseng, C. T., Perrone, L. A., Zhu, H., Makino, S., and Peters, C. J. (2005a). Severe acute respiratory syndrome and the innate immune responses: modulation of effector cell function without productive infection. *J Immunol* **174**(12)**,** 7977-85.

Tseng, C. T., Tseng, J., Perrone, L., Worthy, M., Popov, V., and Peters, C. J. (2005b). Apical entry and release of severe acute respiratory syndrome-associated coronavirus in polarized Calu-3 lung epithelial cells. *J Virol* **79**(15)**,** 9470-9.

Tyrrell, D. A., Cohen, S., and Schlarb, J. E. (1993). Signs and symptoms in common colds. *Epidemiol Infect* **111**(1)**,** 143-56.

Vabret, A., Mourez, T., Gouarin, S., Petitjean, J., and Freymuth, F. (2003). An outbreak of coronavirus OC43 respiratory infection in Normandy, France. *Clin Infect Dis* **36**(8)**,** 985-9.

van der Hoek, L., Pyrc, K., Jebbink, M. F., Vermeulen-Oost, W., Berkhout, R. J., Wolthers, K. C., Wertheim-van Dillen, P. M., Kaandorp, J., Spaargaren, J., and Berkhout, B. (2004). Identification of a new human coronavirus. *Nat Med* **10**(4)**,** 368-73.

van der Hoek, L., Sure, K., Ihorst, G., Stang, A., Pyrc, K., Jebbink, M. F., Petersen, G., Forster, J., Berkhout, B., and Uberla, K. (2005). Croup is associated with the novel coronavirus NL63. *PLoS Med* **2**(8)**,** e240.

van Meer, G., Voelker, D. R., and Feigenson, G. W. (2008). Membrane lipids: where they are and how they behave. *Nat Rev Mol Cell Biol* **9**(2)**,** 112-24.

van Zanten, T. S., Cambi, A., Koopman, M., Joosten, B., Figdor, C. G., and Garcia-Parajo, M. F. (2009). Hotspots of GPI-anchored proteins and integrin nanoclusters function as nucleation sites for cell adhesion. *Proc Natl Acad Sci U S A* **106**(44)**,** 18557-62.

Veit, M., Kretzschmar, E., Kuroda, K., Garten, W., Schmidt, M. F., Klenk, H. D., and Rott, R. (1991). Site-specific mutagenesis identifies three cysteine residues in the cytoplasmic tail as acylation sites of influenza virus hemagglutinin. *J Virol* **65**(5)**,** 2491-500.

Veit, M., and Schmidt, M. F. (1993). Timing of palmitoylation of influenza virus hemagglutinin. *FEBS Lett* **336**(2)**,** 243-7.

Vennema, H., Godeke, G. J., Rossen, J. W., Voorhout, W. F., Horzinek, M. C., Opstelten, D. J., and Rottier, P. J. (1996). Nucleocapsid-independent assembly of coronavirus-like particles by co-expression of viral envelope protein genes. *Embo J* **15**(8)**,** 2020-8.

Wallin, M., Ekstrom, M., and Garoff, H. (2004). Isomerization of the intersubunit disulphide-bond in Env controls retrovirus fusion. *Embo J* **23**(1)**,** 54-65.

Walters, R. W., Freimuth, P., Moninger, T. O., Ganske, I., Zabner, J., and Welsh, M. J. (2002). Adenovirus fiber disrupts CAR-mediated intercellular adhesion allowing virus escape. *Cell* **110**(6)**,** 789-99.

Wang, L., Junker, D., Hock, L., Ebiary, E., and Collisson, E. W. (1994). Evolutionary implications of genetic variations in the S1 gene of infectious bronchitis virus. *Virus Res* **34**(3)**,** 327-38.

Warner, F. J., Lew, R. A., Smith, A. I., Lambert, D. W., Hooper, N. M., and Turner, A. J. (2005). Angiotensin-converting enzyme 2 (ACE2), but not ACE, is preferentially localized to the apical surface of polarized kidney cells. *J Biol Chem* **280**(47)**,** 39353-62.

Watanabe, R., Matsyama, S., Shirato, K., Maejima, M., Fukushi, S., Morikawa, S., and Taguchi, F. (2008). Entry from cell surface of SARS coronavirus with cleaved S protein as revealed by pseudotype virus bearing cleaved S protein. *J Virol*.

Wehrle, P. F. (1980). A reality in our time--certification of the global eradication of smallpox. *J Infect Dis* **142**(4)**,** 636-8.

Weissenhorn, W., Dessen, A., Harrison, S. C., Skehel, J. J., and Wiley, D. C. (1997). Atomic structure of the ectodomain from HIV-1 gp41. *Nature* **387**(6631)**,** 426-30.

White, J., and Helenius, A. (1980). pH-dependent fusion between the Semliki Forest virus membrane and liposomes. *Proc Natl Acad Sci U S A* **77**(6)**,** 3273-7.

White, J. M., Delos, S. E., Brecher, M., and Schornberg, K. (2008). Structures and mechanisms of viral membrane fusion proteins: multiple variations on a common theme. *Crit Rev Biochem Mol Biol* **43**(3)**,** 189-219.

Wickham, T. J., Mathias, P., Cheresh, D. A., and Nemerow, G. R. (1993). Integrins alpha v beta 3 and alpha v beta 5 promote adenovirus internalization but not virus attachment. *Cell* **73**(2)**,** 309-19.

Wigler, M., Pellicer, A., Silverstein, S., and Axel, R. (1978). Biochemical transfer of single-copy eucaryotic genes using total cellular DNA as donor. *Cell* **14**(3)**,** 725-31.

Wild, C., Greenwell, T. and Matthews, T. (1993). A synthetic peptide from HIV-gp41 is a potent inhibitor of virus-mediated cell-cell fusion. *AIDS Res. Hum. Retroviruses* **9,** 1051-1053.

Williams, R. K., Jiang, G. S., and Holmes, K. V. (1991). Receptor for mouse hepatitis virus is a member of the carcinoembryonic antigen family of glycoproteins. *Proc Natl Acad Sci U S A* **88**(13)**,** 5533-6.

Wilson, I. A., Skehel, J. J., and Wiley, D. C. (1981). Structure of the haemagglutinin membrane glycoprotein of influenza virus at 3 A resolution. *Nature* **289**(5796)**,** 366-73.

Wilson, S., Greer, B., Hooper, J., Zijlstra, A., Walker, B., Quigley, J., and Hawthorne, S. (2005). The membrane-anchored serine protease, TMPRSS2, activates PAR-2 in prostate cancer cells. *Biochem J* **388**(Pt 3)**,** 967-72.

Winter, C., Schwegmann-Wessels, C., Cavanagh, D., Neumann, U., and Herrler, G. (2006). Sialic acid is a receptor determinant for infection of cells by avian Infectious bronchitis virus. *J Gen Virol* **87**(Pt 5)**,** 1209-16.

Wong, S. K., Li, W., Moore, M. J., Choe, H., and Farzan, M. (2004). A 193-amino acid fragment of the SARS coronavirus S protein efficiently binds angiotensin-converting enzyme 2. *J Biol Chem* **279**(5)**,** 3197-201.

Woo, P. C., Lau, S. K., Huang, Y., Tsoi, H. W., Chan, K. H., and Yuen, K. Y. (2005). Phylogenetic and recombination analysis of coronavirus HKU1, a novel coronavirus from patients with pneumonia. *Arch Virol* **150**(11)**,** 2299-311.

Wyss, S., Dimitrov, A. S., Baribaud, F., Edwards, T. G., Blumenthal, R., and Hoxie, J. A. (2005). Regulation of human immunodeficiency virus type 1 envelope

glycoprotein fusion by a membrane-interactive domain in the gp41 cytoplasmic tail. *J Virol* **79**(19)**,** 12231-41.

Xiao, X., Chakraborti, S., Dimitrov, A. S., Gramatikoff, K., and Dimitrov, D. S. (2003). The SARS-CoV S glycoprotein: expression and functional characterization. *Biochem Biophys Res Commun* **312**(4)**,** 1159-64.

Xu, R., and Wilson, I. A. (2011). Structural characterization of an early fusion intermediate of influenza virus hemagglutinin. *J Virol* **85**(10), 5172-5182.

Xu, Y., Liu, Y., Lou, Z., Qin, L., Li, X., Bai, Z., Pang, H., Tien, P., Gao, G. F., and Rao, Z. (2004). Structural basis for coronavirus-mediated membrane fusion. Crystal structure of mouse hepatitis virus spike protein fusion core. *J Biol Chem* **279**(29)**,** 30514-22.

Yan, Z., Tripet, B., and Hodges, R. S. (2006). Biophysical characterization of HRC peptide analogs interaction with heptad repeat regions of the SARS-coronavirus Spike fusion protein core. *J Struct Biol* **155**(2)**,** 162-75.

Yang, C., and Compans, R. W. (1996). Analysis of the cell fusion activities of chimeric simian immunodeficiency virus-murine leukemia virus envelope proteins: inhibitory effects of the R peptide. *J Virol* **70**(1)**,** 248-54.

Yang, C., Spies, C. P., and Compans, R. W. (1995). The human and simian immunodeficiency virus envelope glycoprotein transmembrane subunits are palmitoylated. *Proc Natl Acad Sci U S A* **92**(21)**,** 9871-5.

Yao, Y. X., Ren, J., Heinen, P., Zambon, M., and Jones, I. M. (2004). Cleavage and serum reactivity of the severe acute respiratory syndrome coronavirus spike protein. *J Infect Dis* **190**(1)**,** 91-8.

Yasuoka, S., Ohnishi, T., Kawano, S., Tsuchihashi, S., Ogawara, M., Masuda, K., Yamaoka, K., Takahashi, M., and Sano, T. (1997). Purification, characterization, and localization of a novel trypsin-like protease found in the human airway. *Am J Respir Cell Mol Biol* **16**(3)**,** 300-8.

Ye, R., Montalto-Morrison, C., and Masters, P. S. (2004). Genetic analysis of determinants for spike glycoprotein assembly into murine coronavirus virions: distinct roles for charge-rich and cysteine-rich regions of the endodomain. *J Virol* **78**(18)**,** 9904-17.

Yeager, C. L., Ashmun, R. A., Williams, R. K., Cardellichio, C. B., Shapiro, L. H., Look, A. T., and Holmes, K. V. (1992). Human aminopeptidase N is a receptor for human coronavirus 229E. *Nature* **357**(6377)**,** 420-2.

Yin, H. S., Paterson, R. G., Wen, X., Lamb, R. A., and Jardetzky, T. S. (2005). Structure of the uncleaved ectodomain of the paramyxovirus (hPIV3) fusion protein. *Proc Natl Acad Sci U S A* **102**(26)**,** 9288-93.

Yin, H. S., Wen, X., Paterson, R. G., Lamb, R. A., and Jardetzky, T. S. (2006). Structure of the parainfluenza virus 5 F protein in its metastable, prefusion conformation. *Nature* **439**(7072)**,** 38-44.

Yoshimori, T., Yamamoto, A., Moriyama, Y., Futai, M., and Tashiro, Y. (1991). Bafilomycin A1, a specific inhibitor of vacuolar-type H(+)-ATPase, inhibits acidification and protein degradation in lysosomes of cultured cells. *J Biol Chem* **266**(26)**,** 17707-12.

Yount, B., Roberts, R. S., Sims, A. C., Deming, D., Frieman, M. B., Sparks, J., Denison, M. R., Davis, N., and Baric, R. S. (2005). Severe acute respiratory syndrome coronavirus group-specific open reading frames encode nonessential functions for replication in cell cultures and mice. *J Virol* **79**(23)**,** 14909-22.

Zelus, B. D., Schickli, J. H., Blau, D. M., Weiss, S. R., and Holmes, K. V. (2003). Conformational changes in the spike glycoprotein of murine coronavirus are induced at 37 degrees C either by soluble murine CEACAM1 receptors or by pH 8. *J Virol* **77**(2)**,** 830-40.

Zhang, J., Pekosz, A., and Lamb, R. A. (2000). Influenza virus assembly and lipid raft microdomains: a role for the cytoplasmic tails of the spike glycoproteins. *J Virol* **74**(10)**,** 4634-44.

Zhao, X., Singh, M., Malashkevich, V. N., and Kim, P. S. (2000). Structural characterization of the human respiratory syncytial virus fusion protein core. *Proc Natl Acad Sci U S A* **97**(26)**,** 14172-7.

Zhou, T., Xu, L., Dey, B., Hessell, A. J., Van Ryk, D., Xiang, S. H., Yang, X., Zhang, M. Y., Zwick, M. B., Arthos, J., Burton, D. R., Dimitrov, D. S., Sodroski, J., Wyatt, R., Nabel, G. J., and Kwong, P. D. (2007). Structural definition of a conserved neutralization epitope on HIV-1 gp120. *Nature* **445**(7129)**,** 732-7.

Zhu, P., Liu, J., Bess, J., Jr., Chertova, E., Lifson, J. D., Grise, H., Ofek, G. A., Taylor, K. A., and Roux, K. H. (2006). Distribution and three-dimensional structure of AIDS virus envelope spikes. *Nature* **441**(7095)**,** 847-52.

Zinkernagel, R. M., and Doherty, P. C. (1974). Restriction of in vitro T cell-mediated cytotoxicity in lymphocytic choriomeningitis within a syngeneic or semiallogeneic system. *Nature* **248**(450)**,** 701-2.

VITA

The author, Ana Shulla was born in Tirane, Albania on April 18, 1982 to Lefter and Drita Shulla. She received a Bachelor of Science in Biochemistry from North Central College (Naperville, IL) in June of 2004. After graduation, Ana worked for a year as a research assistant in the laboratory of Dr. Alan Wolfe in the Department of Microbiology and Immunology at Loyola University Medical Center, where she studied a bacterial signaling molecule.

In August of 2005, Ana joined the Department of Microbiology and Immunology at Loyola University Medical Center (Maywood, IL). Shortly thereafter, she joined the laboratory of Dr. Thomas M. Gallagher, where she studied coronavirus entry mechanisms, focusing specifically on identifying viral and host cell cofactors required for entry. While at Loyola, Ana received the Arthur J. Schmitt Dissertation Fellowship.

After completing her Ph.D., Ana will begin a post-doctoral position in Dr. Glenn Randall's laboratory at the University of Chicago (Chicago, IL) where she will study hepatitis C virus entry and assembly.